AD NUMBER

AD894198

LIMITATION CHANGES

TO:

Approved for public release; distribution is unlimited.

FROM:

Distribution authorized to U.S. Gov't. agencies only; Test and Evaluation; MAY 1972. Other requests shall be referred to Air Force Armament Lab., Eglin AFB, FL.

AUTHORITY

ADTC ltr 2 Mar 1979

AEDC-TR-72-68
AFATL-TR-72-85

cy 2

WIND TUNNEL INVESTIGATION OF THE TRANSONIC STATIC STABILITY CHARACTERISTICS OF A BLUFF BODY SHAPE WITH VARIOUS AFTERBODY-STABILIZER CONFIGURATIONS

G. R. Gomillion

ARO, Inc.

May 1972

PROPULSION WIND TUNNEL FACILITY
ARNOLD ENGINEERING DEVELOPMENT CENTER
AIR FORCE SYSTEMS COMMAND
ARNOLD AIR FORCE STATION, TENNESSEE

NOTICES

When U. S. Government drawings specifications, or other data are used for any purpose other than a definitely related Government procurement operation, the Government thereby incurs no responsibility nor any obligation whatsoever, and the fact that the Government may have formulated, furnished, or in any way supplied the said drawings, specifications, or other data, is not to be regarded by implication or otherwise, or in any manner licensing the holder or any other person or corporation, or conveying any rights or permission to manufacture, use, or sell any patented invention that may in any way be related thereto.

Qualified users may obtain copies of this report from the Defense Documentation Center.

References to named commercial products in this report are not to be considered in any sense as an endorsement of the product by the United States Air Force or the Government.

WIND TUNNEL INVESTIGATION OF THE TRANSONIC STATIC STABILITY CHARACTERISTICS OF A BLUFF BODY SHAPE WITH VARIOUS AFTERBODY-STABILIZER CONFIGURATIONS

G. R. Gomillion
ARO, Inc.

FOREWORD

The work reported herein was sponsored by the Air Force Armament Laboratory (DLGC/Mr. C. Butler), Air Force Systems Command (AFSC), Eglin Air Force Base, Florida, under Program Element 63601F, System 670A.

The test results presented were obtained by ARO, Inc. (a subsidiary of Sverdrup & Parcel and Associates, Inc.), contract operator of the Arnold Engineering Development Center (AEDC), AFSC, Arnold Air Force Station, Tennessee, under Contract F40600-72-C-0003. The test was conducted from February 16 to 17, 1972, under ARO Project No. PT0258. The manuscript was submitted for publication on April 13, 1972.

This technical report has been reviewed and is approved.

George F. Garey
Lt Colonel, USAF
AF Representative, PWT
Directorate of Test

Frank J. Passarello
Colonel, USAF
Acting Director
Directorate of Test

ABSTRACT

An investigation was conducted in the Aerodynamic Wind Tunnel (4T) to obtain the static stability characteristics of a bluff body shape with various afterbody-stabilizer configurations. Data are presented for a Mach number range from 0.6 to 1.3 over an angle-of-attack range from -2 to 28 deg. For all configurations tested, it was found that the static margin was greatest for the configurations having the largest span swept and unswept blade-type fins.

CONTENTS

APPENDIX
ILLUSTRATIONS

Figure

NOMENCLATURE

A_b	Model base area, ft^2
b	Fin span, ft
C_A	Axial-force coefficient, measured axial force/$q_\infty S$
$C_{A,b}$	Base axial-force coefficient, $(p_\infty - p_b)A_b/q_\infty S$
C_ℓ	Rolling-moment coefficient, rolling moment/$q_\infty SD$
C_m	Pitching-moment coefficient, pitching moment/$q_\infty SD$ (moment reference point is 3.00 in. aft of model nose)
C_N	Normal-force coefficient, normal force/$q_\infty S$
C_n	Yawing-moment coefficient, yawing moment/$q_\infty SD$
C_Y	Side-force coefficient, side force/$q_\infty S$
D	Model body diameter, 0.1000 ft
M_∞	Free-stream Mach number
p_b	Average static pressure at model base, psfa
p_∞	Free-stream static pressure, psfa
q_∞	Free-stream dynamic pressure, psf
Re	Reynolds number based on D
S	Reference area, 0.0079 ft^2
X_{cp}	Center-of-pressure location, C_m/C_N (body diameters from moment reference point, positive when forward of moment reference)
X_{np}	Neutral-point location, $(dC_m/dC_N)_{\alpha=0}$ (body diameters from moment reference point, positive when forward of moment reference)

SECTION I
INTRODUCTION

A wind tunnel investigation was conducted in the Aerodynamic Wind Tunnel (4T) to provide static stability characteristics of a bluff body shape with various afterbody-stabilizer configurations. This test is one of a series of tests that have been conducted at AEDC under the Modular Weapon Systems program (Refs. 1, 2, and 3). Tests were conducted for 17 afterbody-stabilizer configurations at Mach numbers from 0.6 to 1.3 for an angle-of-attack range from -2 to 28 deg. The purpose of this report is to document the test and to present the data for all configurations tested.

SECTION II
APPARATUS

2.1 TEST FACILITY

Tunnel 4T is a closed-loop, continuous flow, variable density tunnel in which the Mach number can be varied from 0.1 to 1.3. At all Mach numbers, the stagnation pressure can be varied from 300 to 3700 psfa. The test section is 4 ft square and 12.5 ft long with perforated, variable porosity (0.5- to 10-percent open) walls. It is completely enclosed in a plenum chamber from which the air can be evacuated, allowing part of the tunnel airflow to be removed through the perforated walls of the test section. A more thorough description of the tunnel may be found in Ref. 4.

The model support system consists of a pitch sector, boom, and sting which provide a pitch capability from -12 to 28 deg with respect to the tunnel centerline. The center of rotation is at station 108. In addition, a remote-controlled roll mechanism allows roll angle variations of ±180 deg. A schematic of the test section showing the location of the test model is shown in Fig. 1 (Appendix). A photograph of the model installation is shown in Fig. 2.

2.2 TEST ARTICLES

All of the model configurations have a body maximum diameter of 0.100 ft and a length of 6.83 cal (0.683 ft), with the exception of configuration N10M5A17, which has a length of 7 cal (0.700 ft). Also, all model configurations consist of three components that are shown in Figs. 3 and 4 and which include the afterbody-stabilizer component, the afterbody component, and the nose component. The afterbody-stabilizer component has 17 configurations that are identified in Figs. 3a and 4a. The afterbody-stabilizer configurations have various fin-span-to-body diameter ratios, b/D, that vary from 1.00 to 4.00 cal. The fins of the afterbody-stabilizer configurations with four fins are oriented ±45 deg relative to the pitch plane of the model. The fins of the afterbody-stabilizer configurations with eight fins are symmetrically oriented about the vertical plane such that two fins are located on the top and the bottom of the model. Also, certain afterbody-stabilizer configurations have a 1.00-cal length and the others have a 1.83-cal length. There are two midsection configurations, M4 and M5, which utilize the centerbodies shown in Figs. 3b and 4b. For the M4 configuration, a 4.00-cal length centerbody is used with the 1.83-cal afterbody-stabilizer configurations and a 4.83-cal centerbody is used

with the 1.00-cal afterbody-stabilizer configurations. A 5.00-cal centerbody is used for the M5 configuration. Also shown in Figs. 3b and 4b is the only nose configuration tested (N10) which is a 1.00-cal-length hemisphere-cylinder shape.

2.3 INSTRUMENTATION

In order to accommodate various model base internal diameters and model loads, two different six-component, internal, strain-gage balances were used to measure the overall aerodynamic loads on the model. The largest diameter balance, 0.75 in., was used with the A1, A6, A17, A18, A23, and A24 afterbody-stabilizer configurations, and the 0.40-in.-diam balance was used with the A19, A20, A21, and A22 afterbody-stabilizer configurations. The balance outputs were recorded on an oscillograph for monitoring of model dynamics.

Static pressures on the model base were measured with differential pressure transducers. The base pressure was defined as the average of two pressures measured near the model base at two points located 180 deg apart on the sting.

The model angle of attack was measured with the pitch sector angle-of-attack indicator. These measurements were corrected for support system and balance deflections, resulting from aerodynamic forces and moments, to obtain true model orientation. These measurements were not corrected for any possible flow angularity. Electrical signals from the balances, pressure transducers, and standard tunnel instrumentation systems were processed by the PWT data acquisition system and digital computer for on-line data reduction.

SECTION III
TEST PROCEDURES

3.1 TEST DESCRIPTION

Steady-state force and moment data were obtained in Tunnel 4T at Mach numbers from 0.6 to 1.3. For all data presented the total pressure was held constant at approximately 2050 psfa with an approximate 100 psf tolerance, and the nominal variation of Reynolds number and dynamic pressure with Mach number is shown in Fig. 5. Also, for all data presented the tunnel total temperature was held above 100°F. Tunnel conditions were held constant at each Mach number while pitch angle varied, and data were recorded at each selected angle. The pitch range was from -2 to 28 deg. The models were tested with free transition throughout the test program.

3.2 PRECISION OF MEASUREMENTS

The estimated uncertainties associated with tunnel conditions and measured coefficients are as follows:

	M_∞ = 0.6	M_∞ = 0.8	M_∞ = 1.0	M_∞ = 1.2	M_∞ = 1.3
ΔM_∞	±0.0021	±0.0023	±0.0039	±0.0095	±0.0144
Δq_∞	±2.2	±2.2	±2.6	±3.1	±4.5
$\Delta C_{A,b}$	±0.010	±0.007	±0.008	±0.015	±0.020
			0.75-in.-diam balance		
ΔC_N	±0.032	±0.022	±0.024	±0.026	±0.018
ΔC_A	±0.026	±0.017	±0.013	±0.012	±0.012
ΔC_m	±0.084	±0.056	±0.054	±0.050	±0.042
ΔC_Y	±0.015	±0.009	±0.006	±0.005	±0.005
ΔC_n	±0.058	±0.039	±0.030	±0.026	±0.026
ΔC_ℓ	±0.006	±0.004	±0.003	±0.003	±0.003
			0.40-in.-diam balance		
ΔC_N	±0.028	±0.019	±0.019	±0.015	±0.013
ΔC_A	±0.074	±0.050	±0.040	±0.035	±0.034
ΔC_m	±0.051	±0.034	±0.026	±0.023	±0.022
ΔC_Y	±0.012	±0.009	±0.005	±0.004	±0.004
ΔC_n	±0.023	±0.016	±0.010	±0.009	±0.009
ΔC_ℓ	±0.011	±0.007	±0.006	±0.005	±0.005

The uncertainty quoted for Mach number relates to the variation of Mach number in the vicinity of the test article. The uncertainty for setting and maintaining Mach number during a pitch polar is approximately ±0.005 for all Mach numbers. The uncertainty in angle-of-attack measurements is ±0.1 deg. The estimated uncertainties in force and moment coefficients are based on 95-percent probability and include possible errors in balance calibration curve fits, and in the case of moment coefficients, transfer of force uncertainties from the balance force system center to the moment reference point (MRP) of the model.

SECTION IV
RESULTS AND DISCUSSION

The measured force and moment data presented have been reduced to coefficient form in the body axes system. The moment reference point (MRP) is located on the centerline 2.5 cal from the model nose. The variations of C_N, X_{cp}, C_A, $C_{A,b}$, C_Y, C_n, and C_ℓ with α are presented in Figs. 6 through 11 for each model configuration tested. Also, all $C_{A,b}$ for all model configurations presented in this report are calculated for the values of A_b shown in Fig. 4.

A comparison of the aerodynamic characteristics of the configurations with drag plates, N10M4A19 and N10M4A20, is presented in Fig. 6. In general, both configurations produce similar variations in normal-force coefficients for all Mach numbers and angles of attack except for $\alpha > 20$ deg and $M_\infty = 0.6$ and 0.8, where the configuration N10M4A20 produces less normal force (Fig. 6a). Figure 6b indicates that the static margin of both

configurations is greatest at $M_\infty < 1.0$ and that the stability of both configurations is reduced for $M_\infty \geq 1.0$ with the neutral-point and the center-of-pressure locations moving near or forward of the MRP. The axial-force coefficients are similar for both drag plate configurations with configuration N10M4A20 generally producing the larger values (Fig. 6c). Below $\alpha = 15$ deg there is no significant side-force coefficient produced by either configuration (Fig. 6e), but for $\alpha > 16$ deg and particularly for $M_\infty = 0.6$ and 0.8 there is a very significant side-force coefficient for both configurations that is apparently attributable to an unsymmetrical arrangement of vortices trailing from the model. Also for $\alpha > 16$ deg the yawing-moment coefficients are significantly affected (Fig. 6f) with the rolling-moment coefficients showing some effect (Fig. 6g).

A comparison for the bomb configurations with different span star fins (N10M4A21, b/D = 1.00 and 1.10) and configuration N10M4A22 is presented in Fig. 7. For all Mach numbers and angles of attack presented the larger span star fin produces the largest normal-force coefficients, the largest static margin, and, generally, slightly larger axial-force coefficients for the configurations compared (Figs. 7a, b, and c). Figure 7b shows that both spans of the star fins produce neutral-point and center-of-pressure locations that remain aft of the MRP for all Mach numbers and angles of attack. Also, Fig. 7b shows that configuration N10M4A22 is unstable except for high angles of attack with the neutral-point location and the center-of-pressure location for low angles of attack well forward of the MRP at all Mach numbers. The apparent unsymmetrical trailing vortex effect is shown in Fig. 7e for $\alpha > 15$ deg where there is a large and erratic side force for all configurations, particularly at Mach numbers from 0.6 through 1.0. Also, both the yawing-moment coefficient and rolling-moment coefficient are noticeably affected (Figs. 7f and g).

The effects of span on configuration N10M4A18 (Fig. 8), configuration N10M4A23 (Fig. 9), and configuration N10M4A24 (Fig. 10) are generally similar and these configurations are discussed as a single group. All configurations have tapered afterbodies and the blade-type fins. The A18 configurations have swept fins, but configurations A23 and A24 have unswept fins. For all Mach numbers and angles of attack presented, increasing the fin span increases the normal-force coefficient (Figs. 8a, 9a, and 10a), the static margin (Figs. 8b, 9b, and 10b); and the axial-force coefficient (Figs. 8c, 9c, and 10c). The erratic behavior of X_{cp} at small α for configuration N10M4A24, b/D = 4.00 (Fig. 10b) is attributed to bending of the fins. A significant permanent set in these fins was produced by aerodynamic loads during testing. Figures 8b, 9b, and 10b show that all neutral-point locations and, with the noted exception, all center-of-pressure locations are well aft of the MRP and generally the X_{cp} moves forward with increasing angle of attack. The fins of the largest span (b/D = 3.46) of configuration N10M4A18 were also observed to have been slightly bent after being tested, and the side force at $\alpha = 0$ deg shown in Fig. 8e is the apparent result. Also the significantly bent fins of the largest span (b/D = 4.00) of configuration N10M4A24 produce a side force at $\alpha = 0$ deg (Fig. 10e). With the exception of configuration N10M4A18, b/D = 2.88, there is a very large side force for $\alpha > 16$ deg at $M_\infty = 0.6$ and 0.8, and this is again attributable to the unsymmetrical trailing vortices (Figs. 8e, 9e, and 10e). The trends in side force at high α are generally also reflected in the yawing-moment and rolling-moment coefficients.

A comparison for two finned configurations (N10M4A1 and N10M4A6) and a finless configuration N10M5A17 is presented in Fig. 11. As expected configuration N10M5A17 produces less normal-force coefficient (Fig. 11a) and is less stable than either finned configuration (Fig. 11b). Also configuration N10M4A1 produces more normal force and static margin than configuration N10M4A6 (Figs. 11a and b). In general the variations in axial-force coefficients (Fig. 11c) are similar for all configurations, and a measurable increase in axial force is produced by the fins. Figures 11e, f, and g show that for $\alpha > 15$ deg at $M_\infty = 0.6$ and 0.8, significant side force, yawing moment, and rolling moment are evident for configurations N10M4A1 and N10M4A6, but not for N10M5A17. This suggests that an interaction between the previously mentioned vortices and the fins is responsible.

REFERENCES

1. Caldwell, R. L. and Gomillion, G. R. "Wind Tunnel Investigation of the Transonic Static Stability Characteristics and Scale Effects of Various Bomb Configurations." AEDC-TR-71-21 (AD880562L), February 1971.

2. Caldwell, R. L. "Static and Dynamic Stability Investigation of Bombs for the Modular Weapon System at Transonic Mach Numbers." AEDC-TR-71-65 (AD882494L), April 1971.

3. Anderson, C. F. and Henson, J. R. "Aerodynamic Characteristics of Several Bluff Bodies of Revolution at Mach Numbers from 0.6 to 1.5." AEDC-TR-71-130 (AD885911), AFATL-TR-71-82, July 1971.

4. Test Facilities Handbook (Ninth Edition). "Propulsion Wind Tunnel Facility, Vol. 4." Arnold Engineering Development Center, July 1971.

APPENDIX
ILLUSTRATIONS

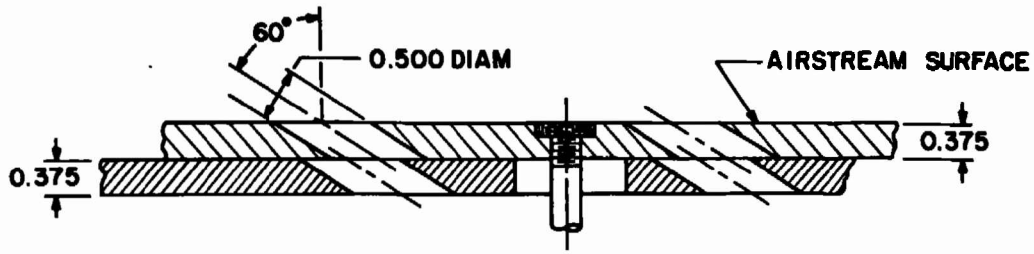

TYPICAL PERFORATED WALL CROSS SECTION

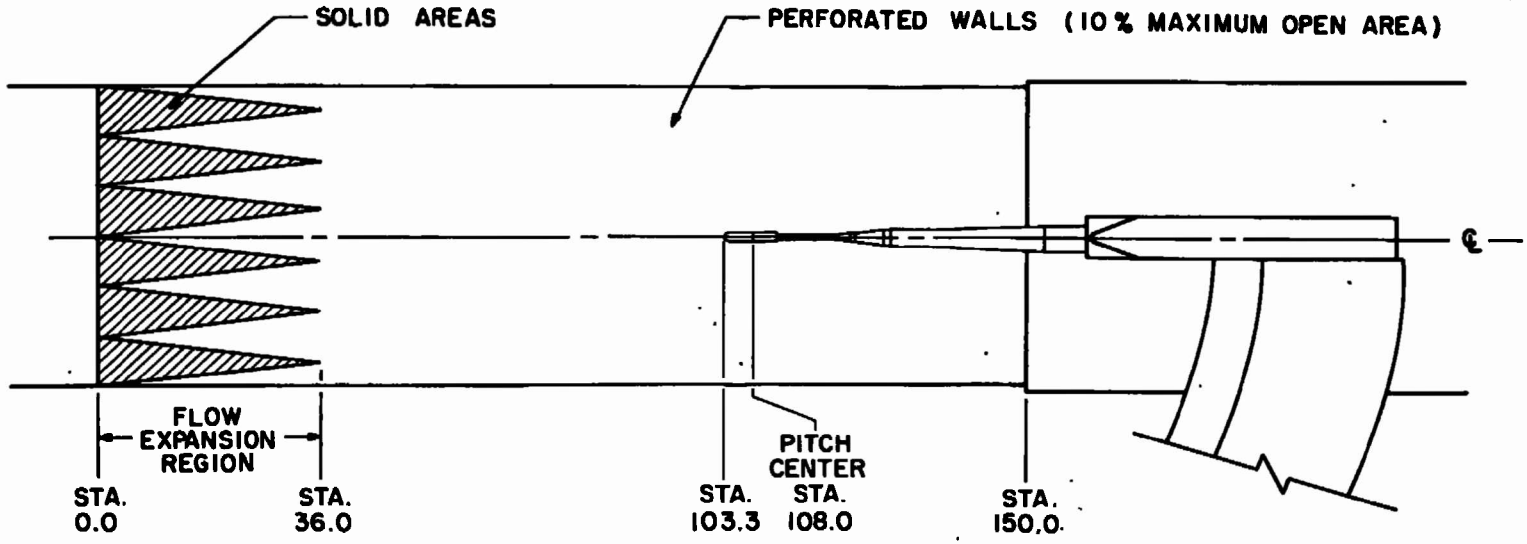

TUNNEL STATIONS AND DIMENSIONS IN INCHES

Fig. 1 Sketch of Model Installation

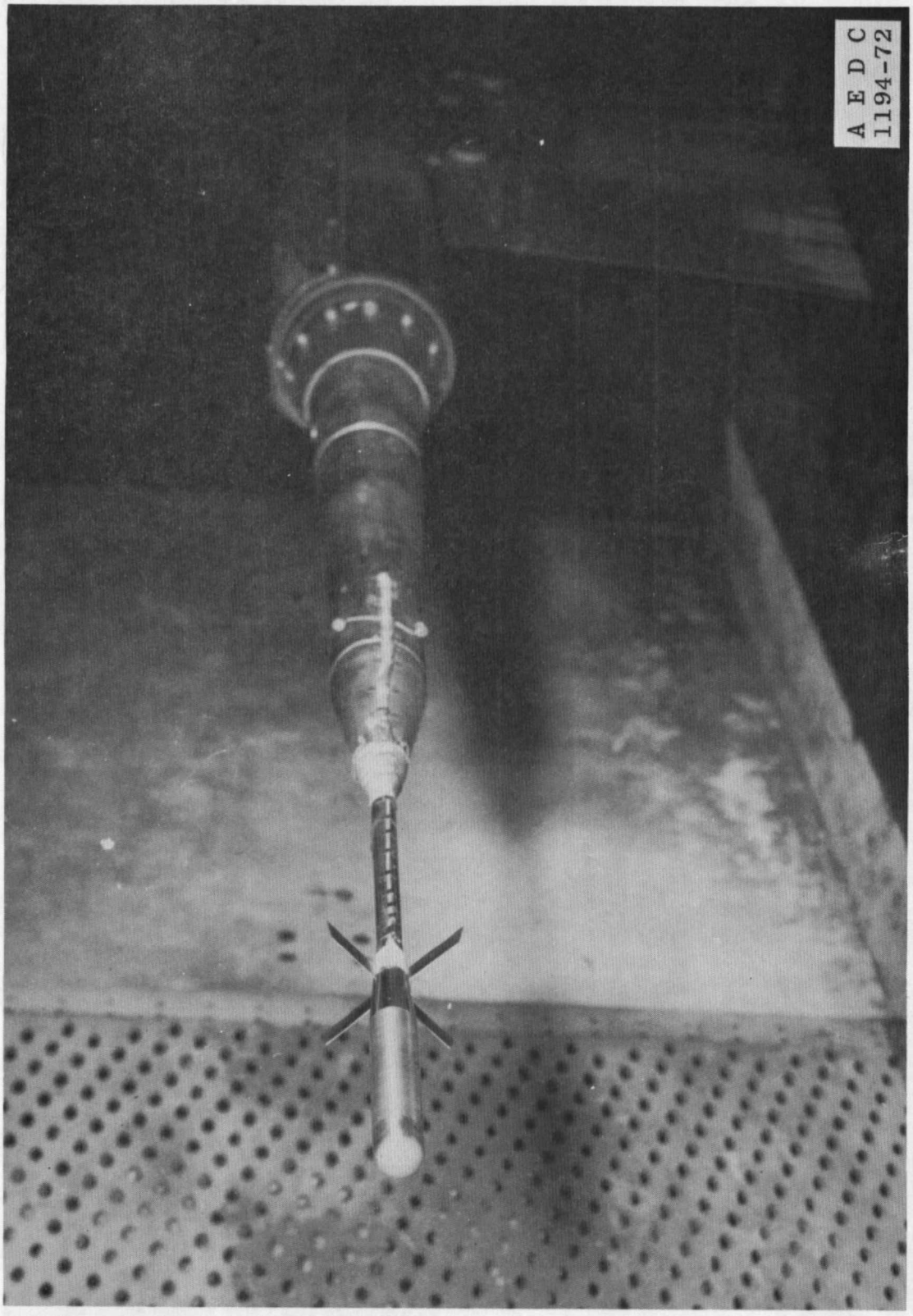

Fig. 2 Photograph of Model Installation

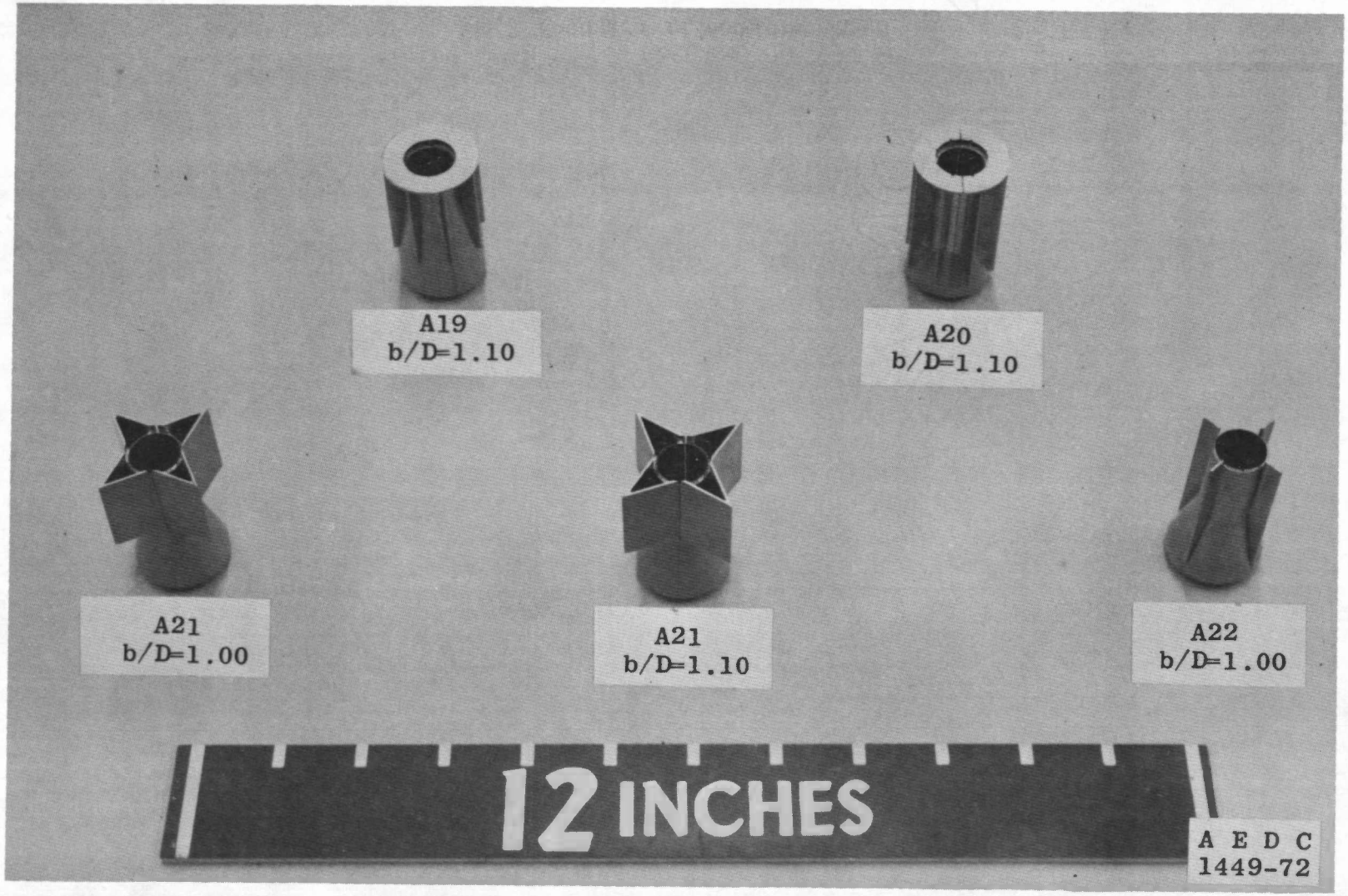

a. Afterbody-Stabilizer Components

Fig. 3 Photographs of Model Components

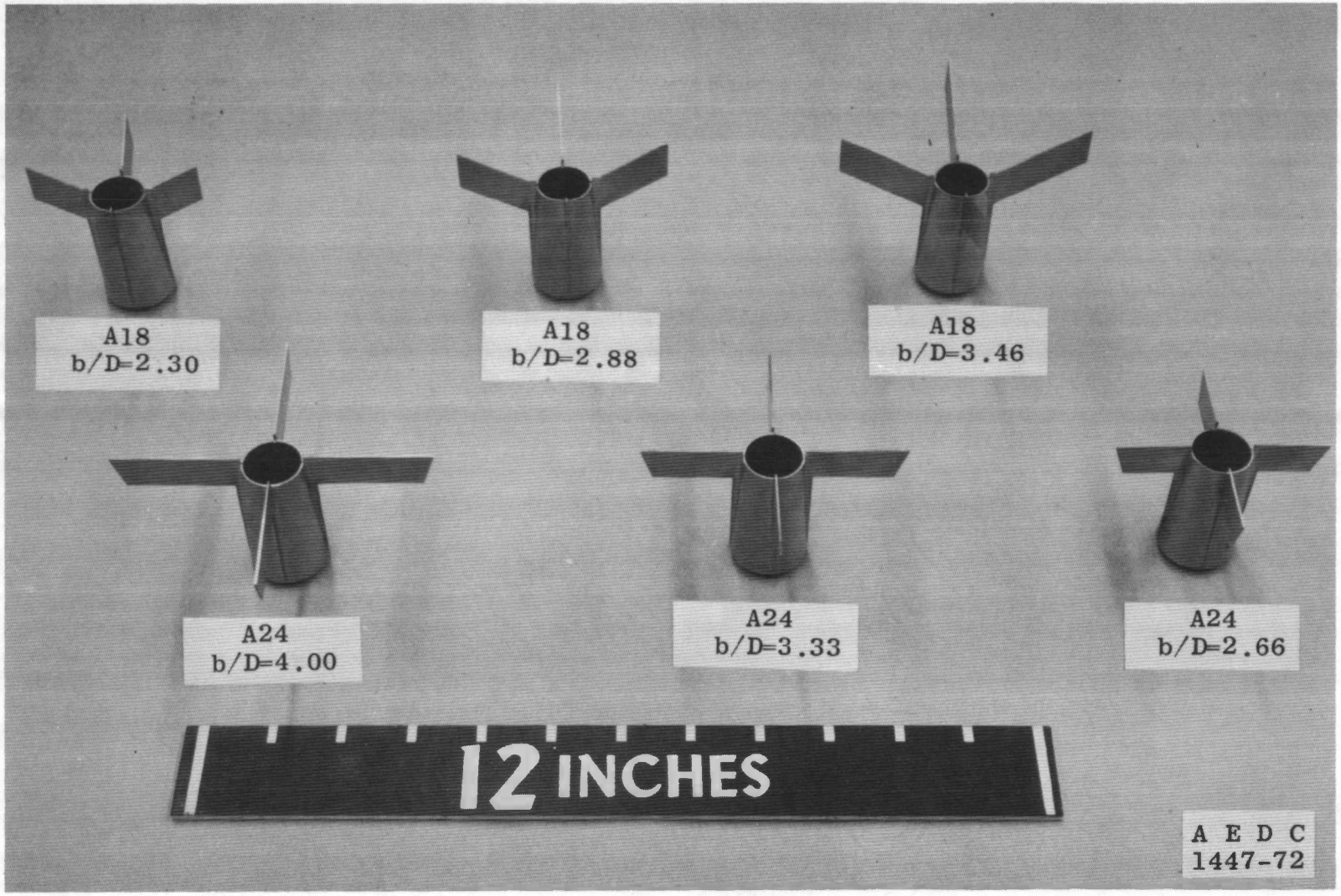

a. Continued

Fig. 3 Continued

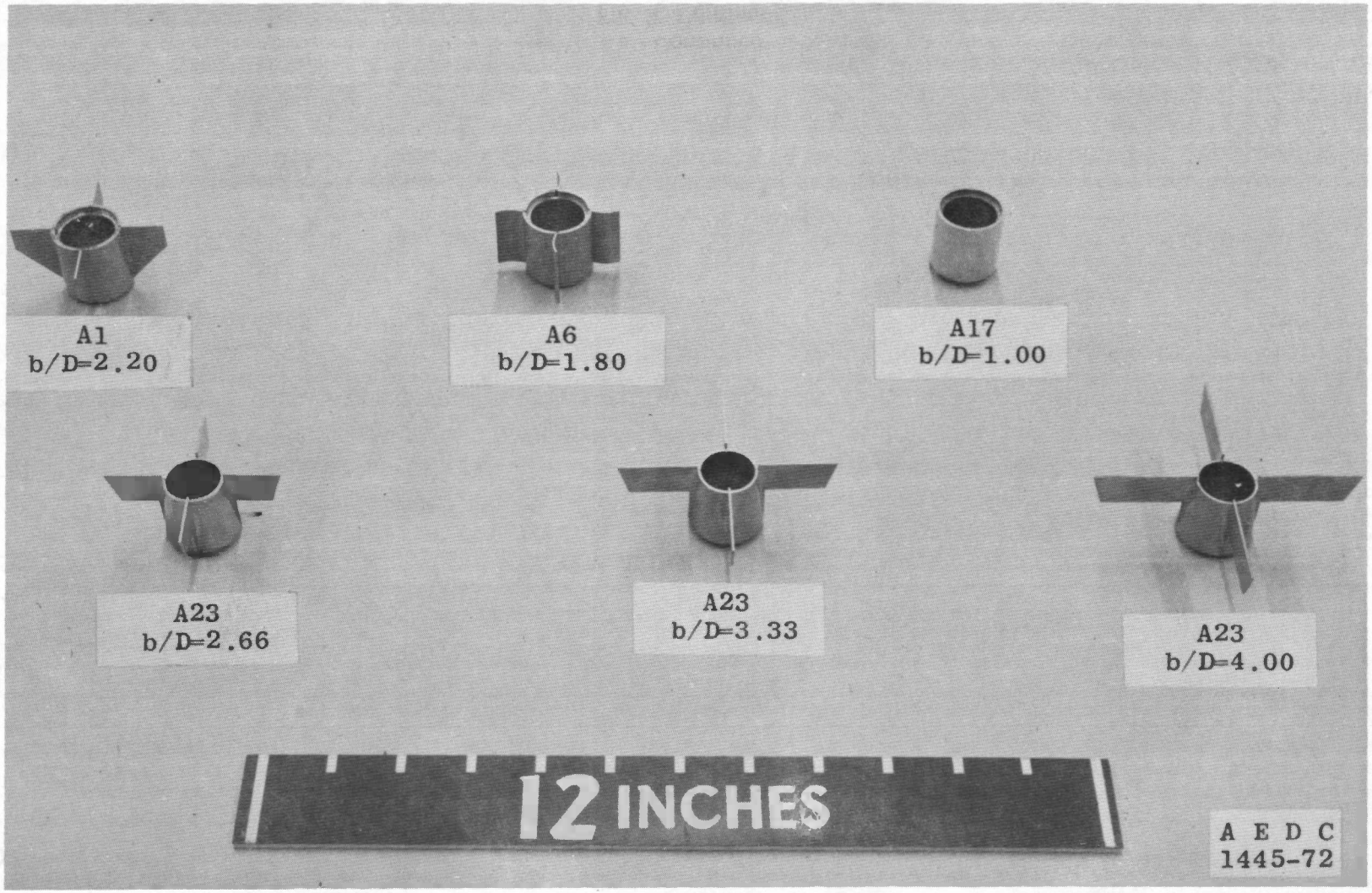

a. Concluded
Fig. 3 Continued

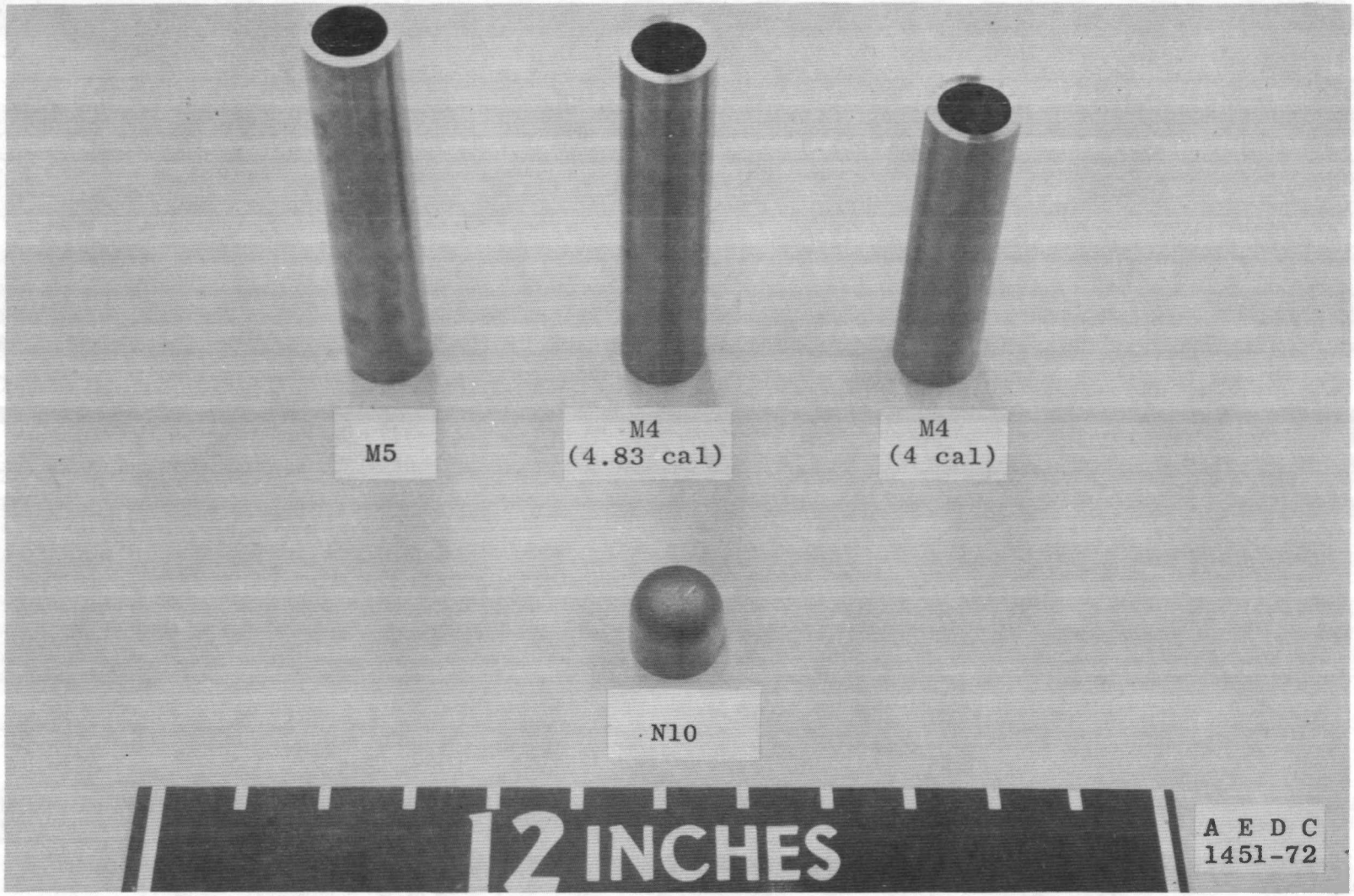

b. Nose and Centerbody Components
Fig. 3 Concluded

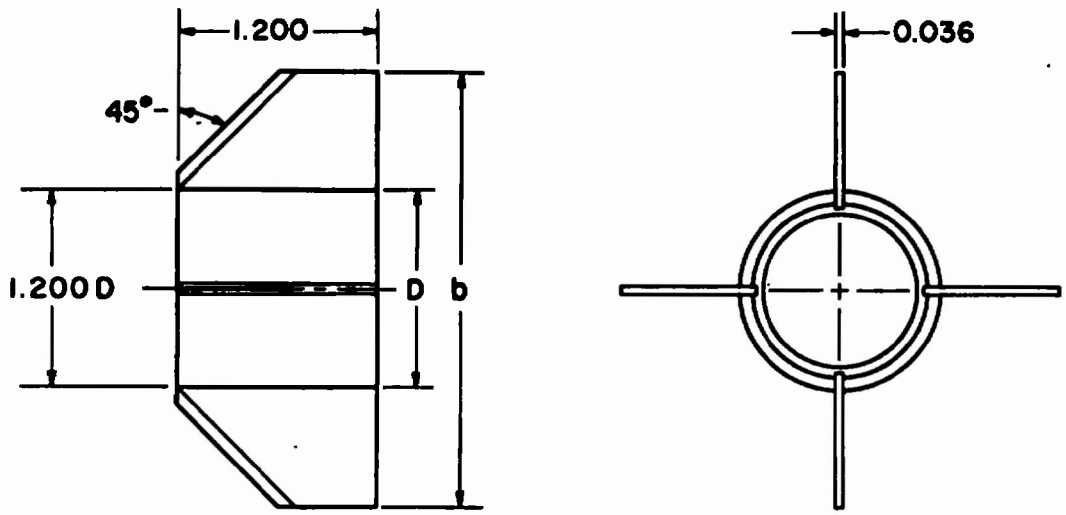

$b/D = 2.20 \quad A_b = 0.0079\ ft^2$

A1

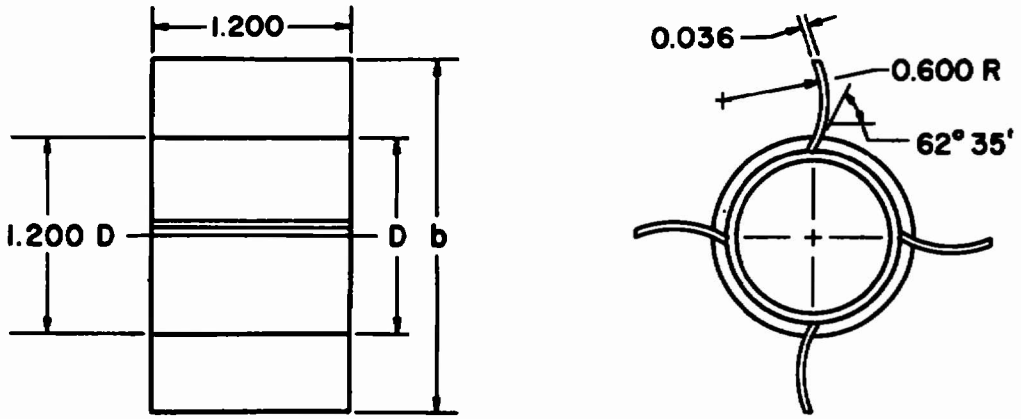

$b/D = 1.80 \quad A_b = 0.0079\ ft^2$

A6

DIMENSIONS IN INCHES

a. Afterbody-Stabilizer Components

Fig. 4 Dimensional Sketches of Model Components

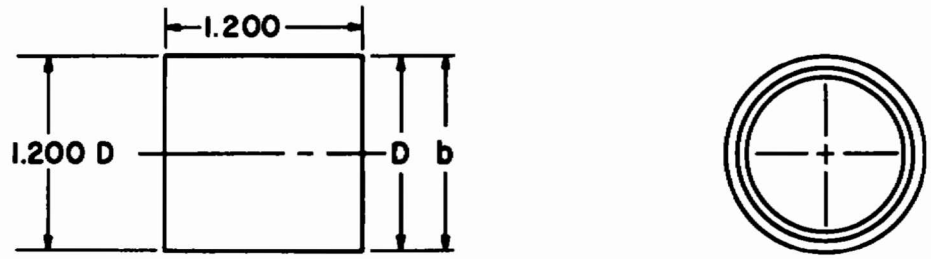

$b/D = 1.00 \quad A_b = 0.0079\ ft^2$

A17

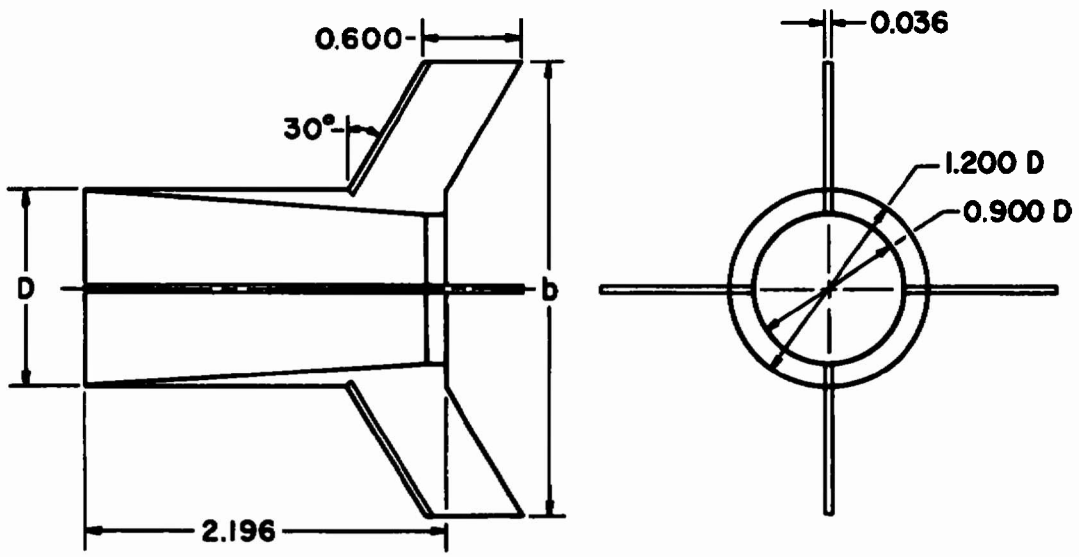

$b/D = 2.30, 2.88, 3.46 \quad A_b = 0.0044\ ft^2$

A18

DIMENSIONS IN INCHES

a. Continued
Fig. 4 Continued

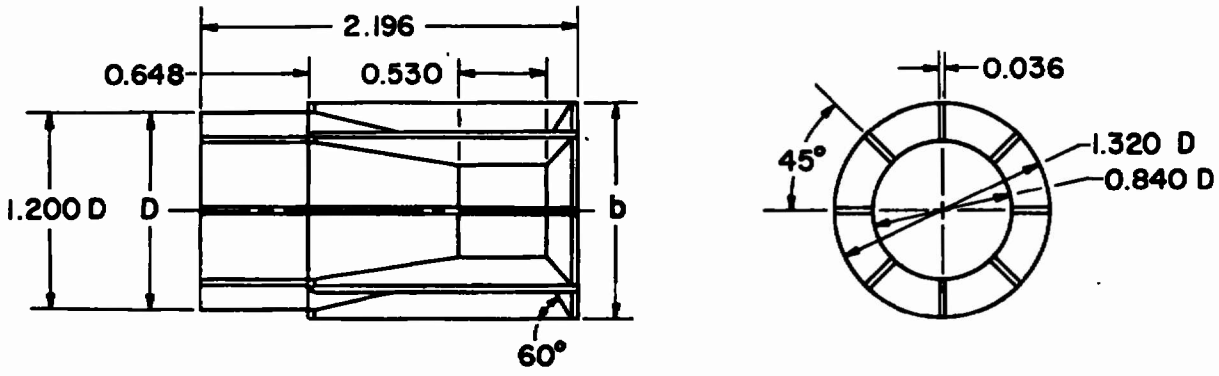

$b/D = 1.10$ $A_b = 0.0095\ ft^2$

A19

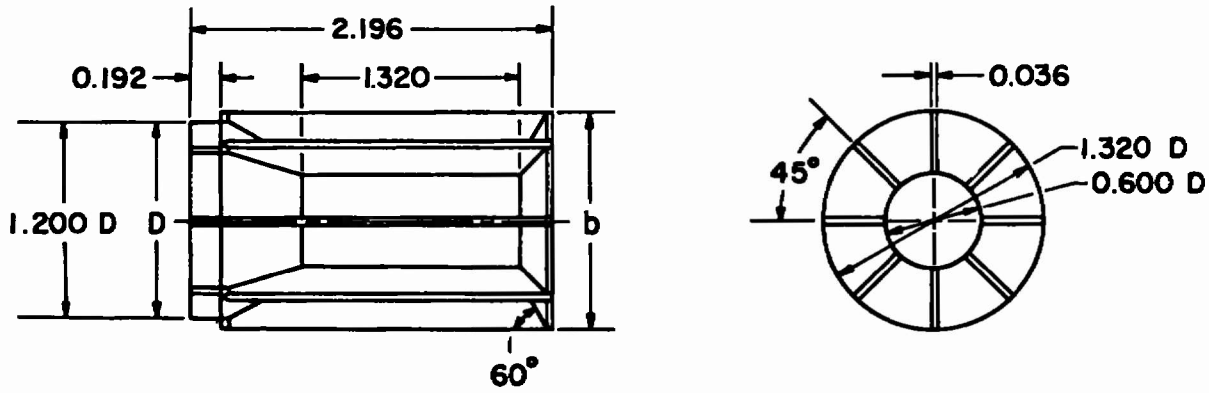

$b/D = 1.10$ $A_b = 0.0095\ ft^2$

A20

DIMENSIONS IN INCHES

a. Continued
Fig. 4 Continued

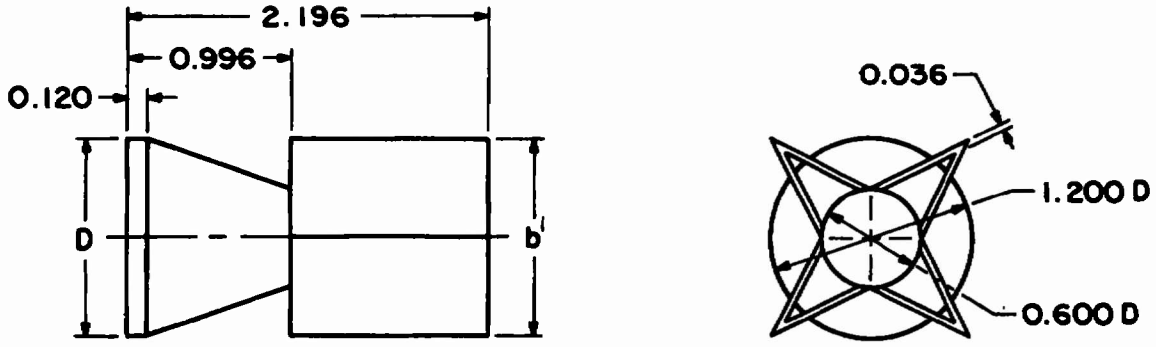

$b/D = 1.00, 1.10$ $A_b = 0.0026\ ft^2$

A21

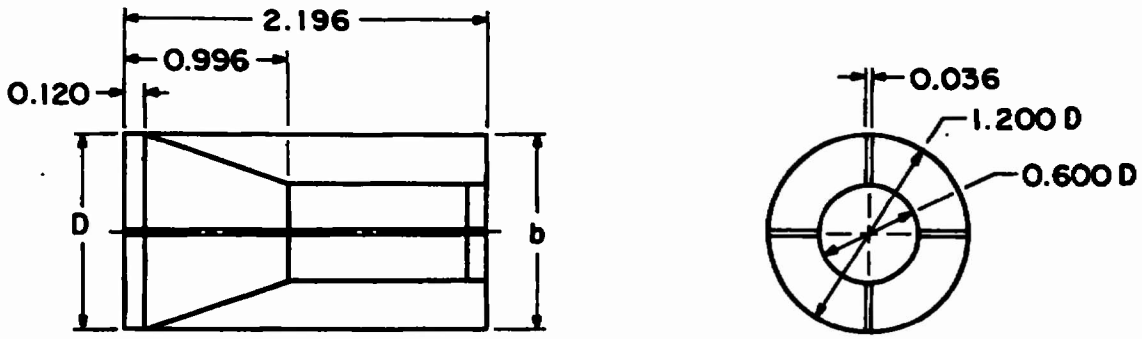

$b/D = 1.00$ $A_b = 0.0026\ ft^2$

A22

DIMENSIONS IN INCHES

a. Continued

Fig. 4 Continued

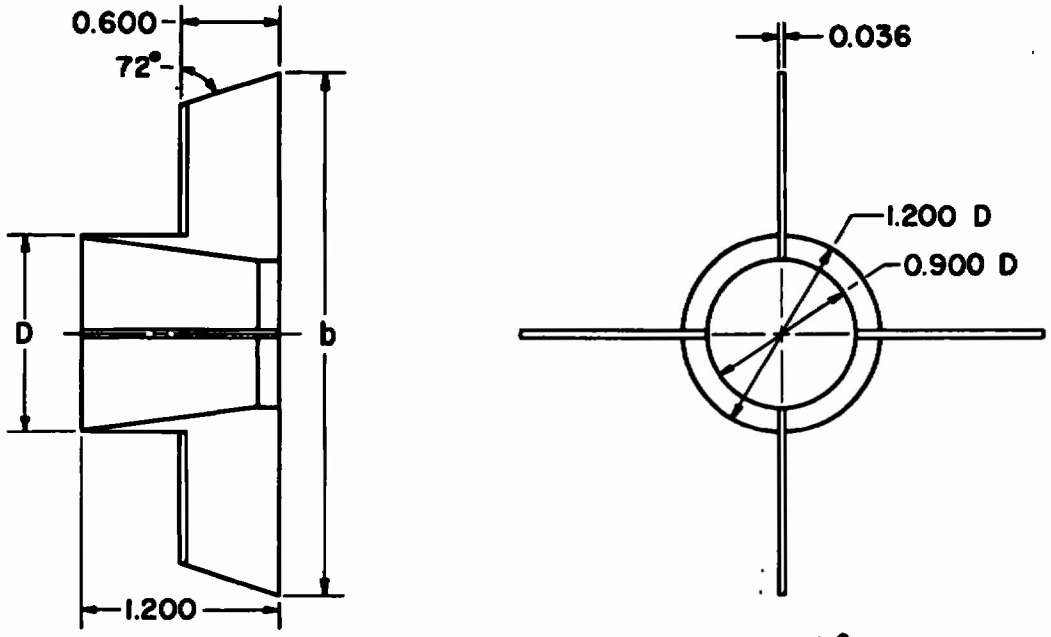

$b/D = 2.66, 3.33, 4.00 \quad A_b = 0.0044\ ft^2$

A23

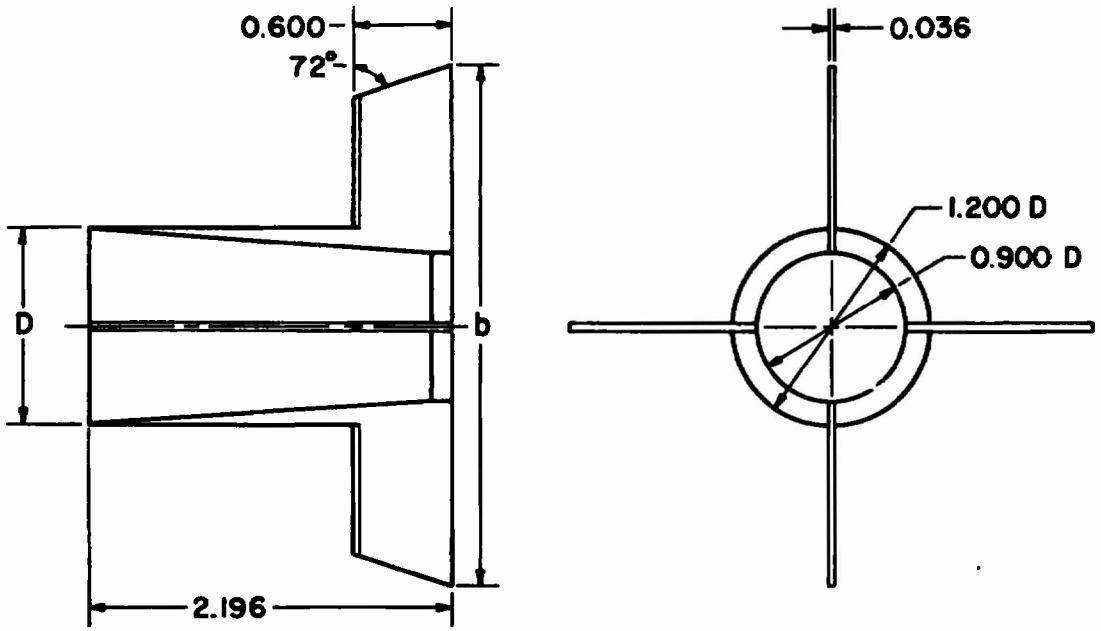

$b/D = 2.66, 3.33, 4.00 \quad A_b = 0.0044\ ft^2$

A24

DIMENSIONS IN INCHES

a. Concluded
Fig. 4 Continued

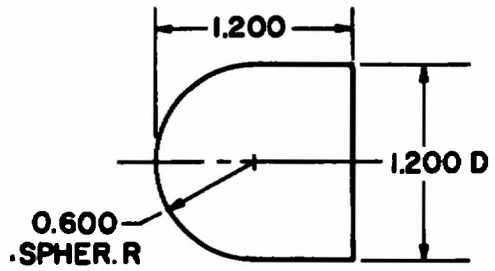

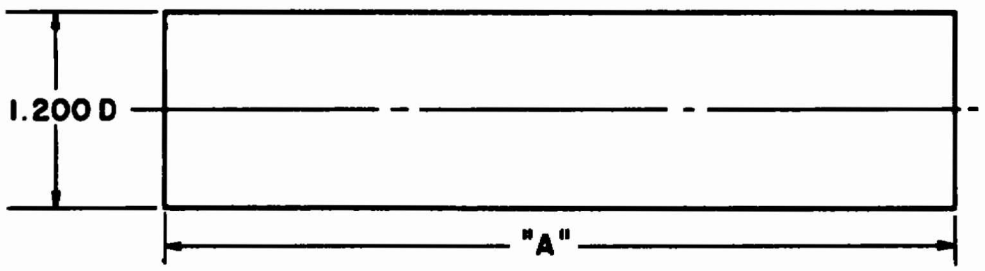

MIDSECTION	AFTERBODIES	"A"
M4	A18, A19, A20, A21, A22, A24	4.800
M4	A1, A6, A23	5.976
M5	A17	6.000

ALL DIMENSIONS IN INCHES

b. Nose and Centerbody Components
Fig. 4 Concluded

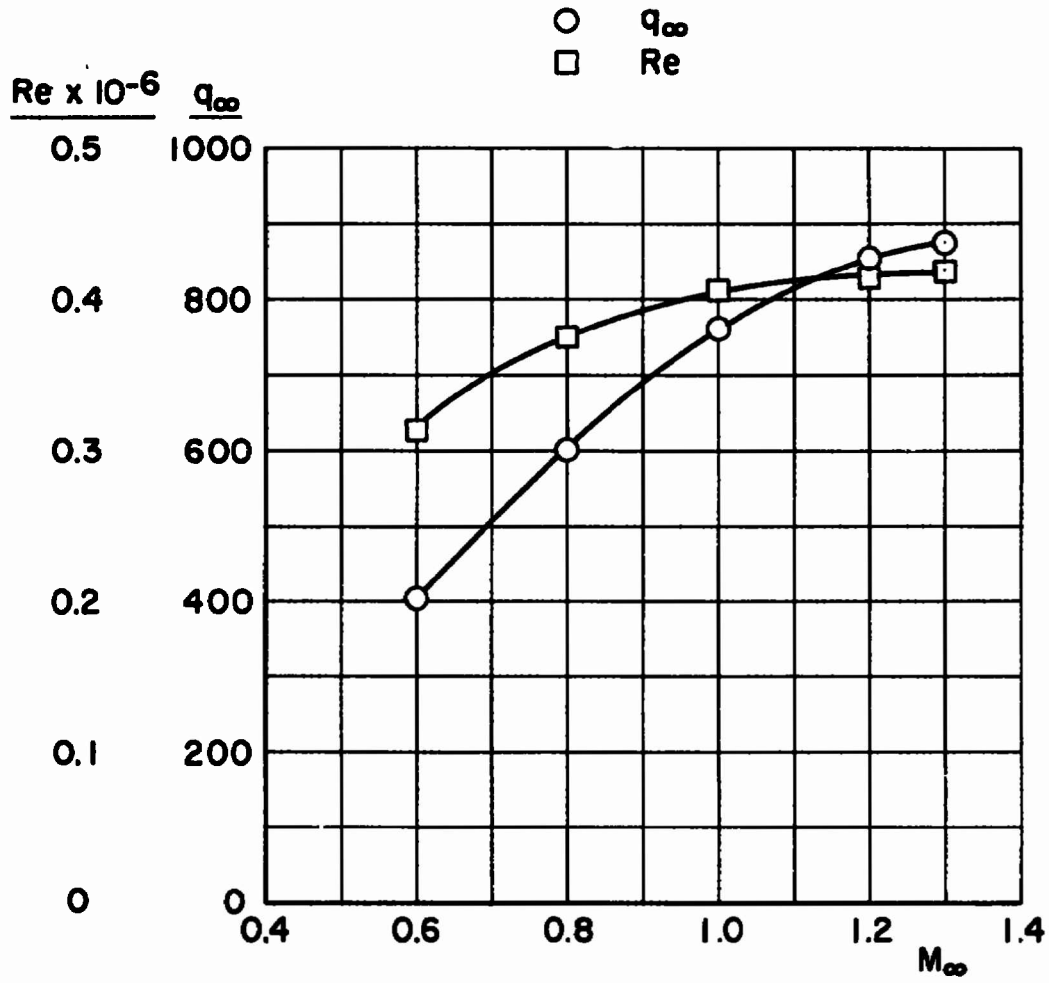

Fig. 5 Nominal Variation of Reynolds Number and Dynamic Pressure with Mach Number

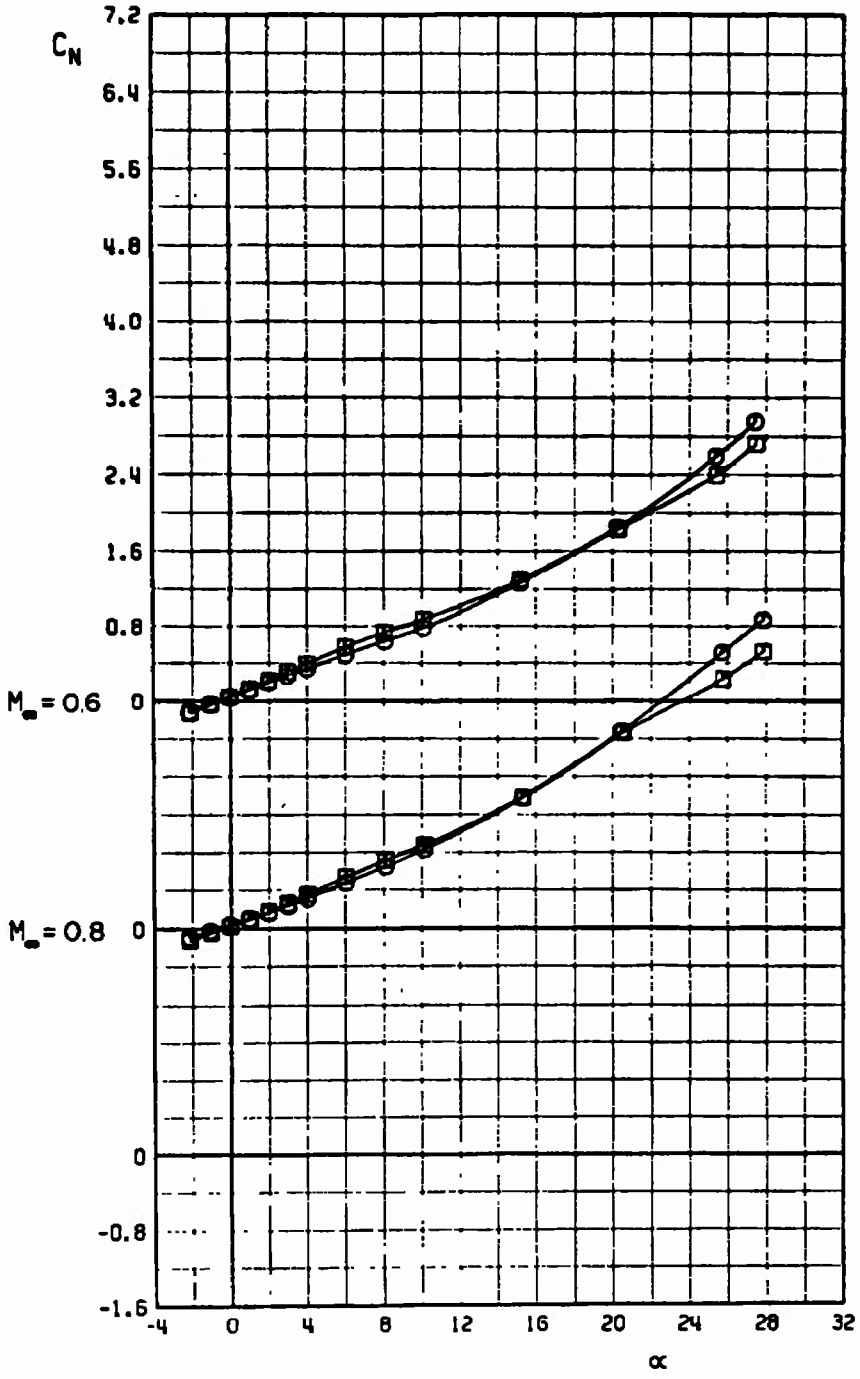

a. C_N versus α

Fig. 6 Aerodynamic Coefficients of Configurations N10M4A19, b/D = 1.10 and N10M4A20, b/D = 1.10

	CONFIGURATION	b/D
⊙	N10 M4 A19	1.10
⊡	N10 M4 A20	1.10

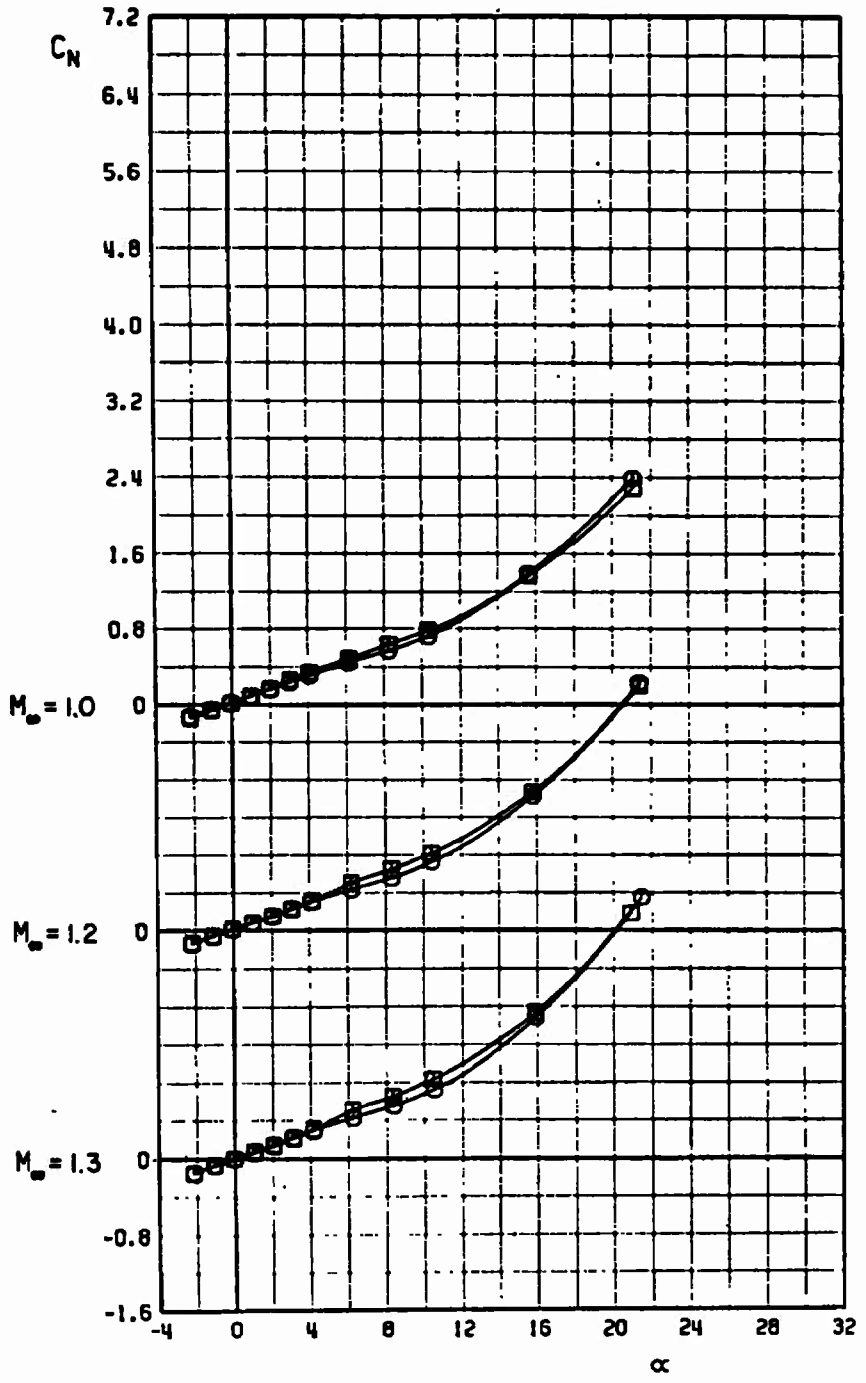

a. Concluded

Fig. 6 Continued

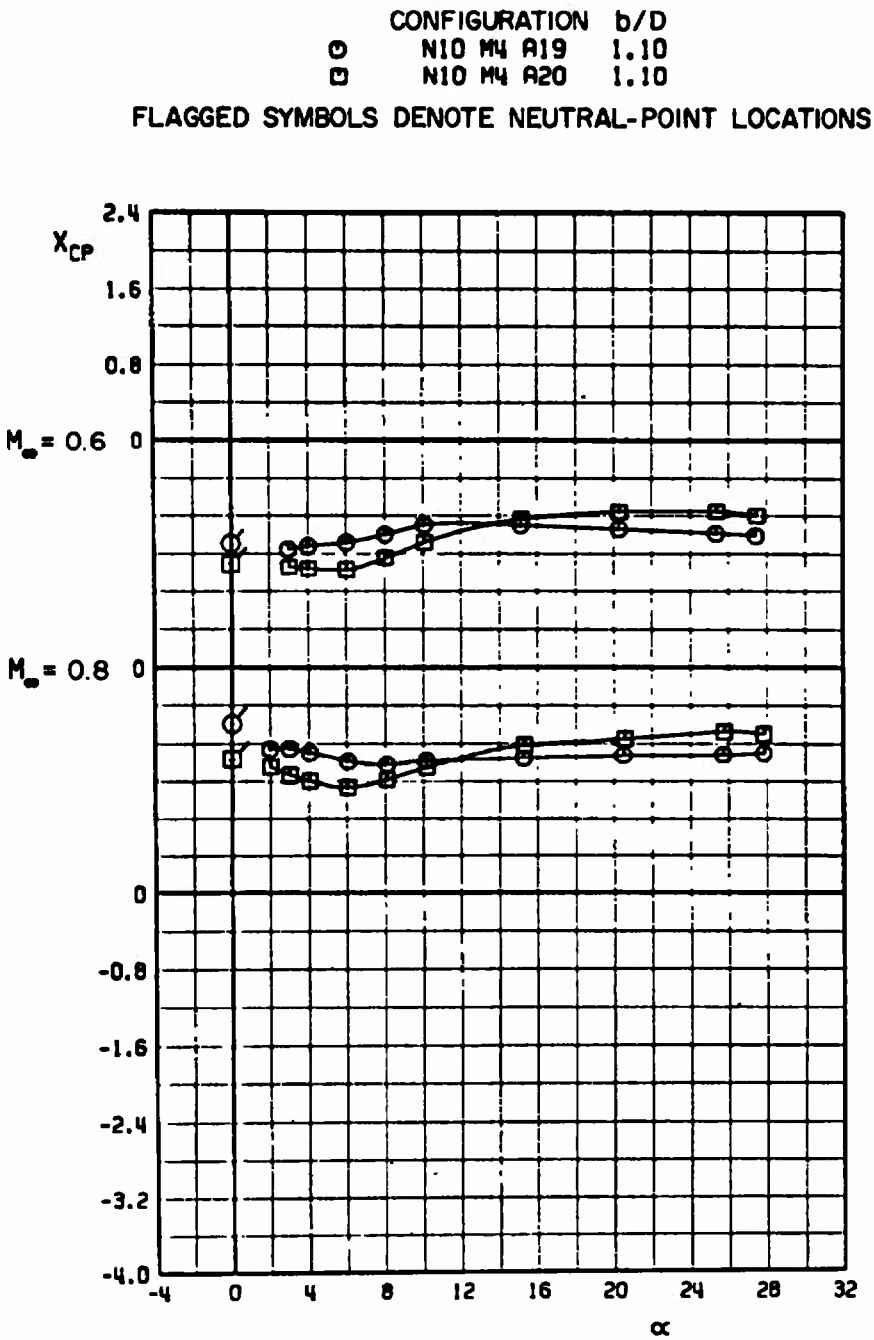

b. X_{cp} versus α
Fig. 6 Continued

	CONFIGURATION	b/D
⊙	N10 M4 A19	1.10
⊡	N10 M4 A20	1.10

FLAGGED SYMBOLS DENOTE NEUTRAL-POINT LOCATIONS

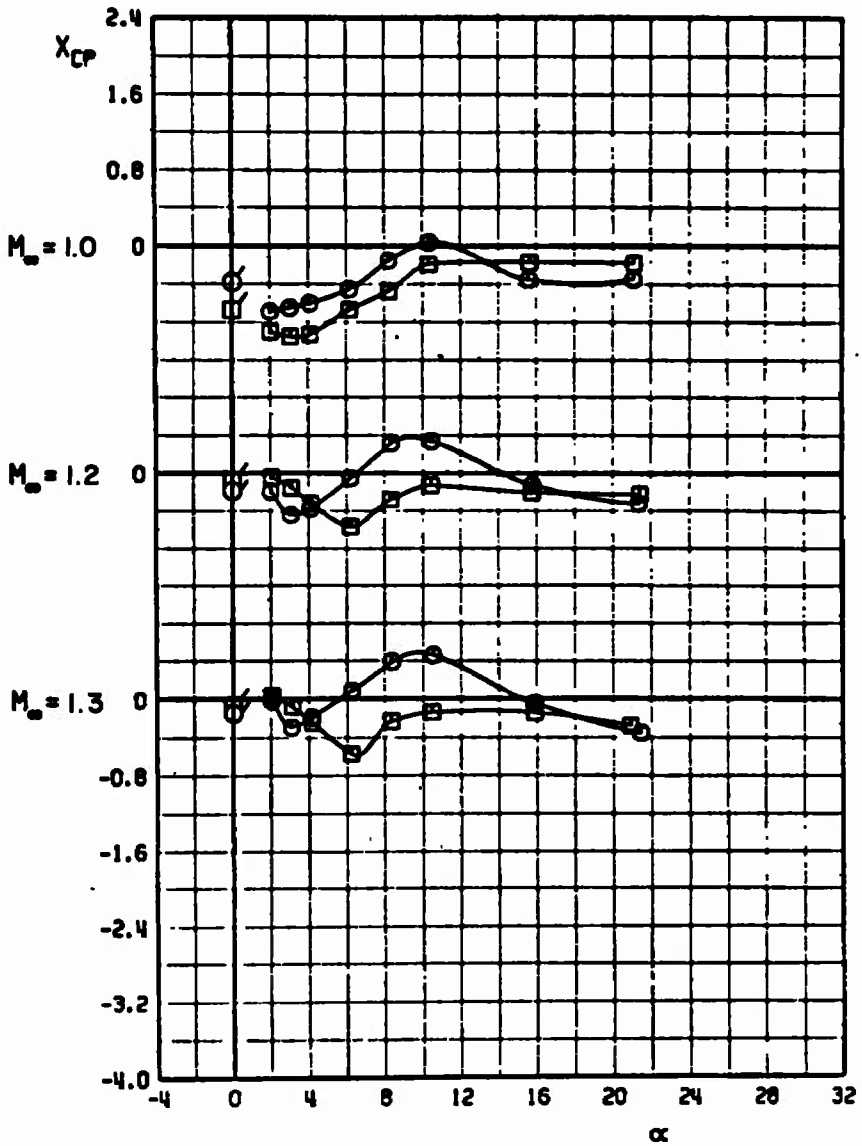

b. Concluded
Fig. 6 Continued

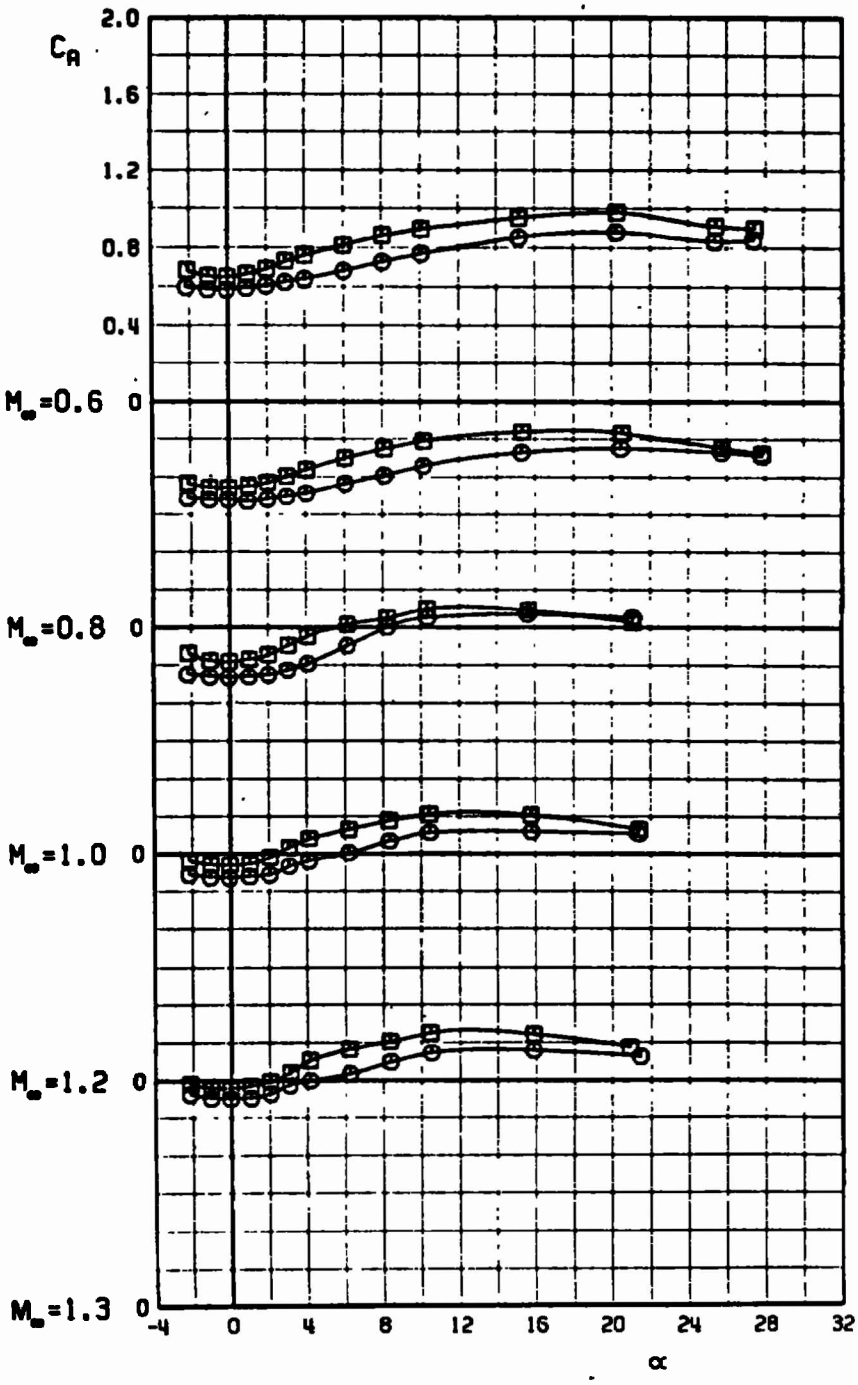

c. C_A versus α

Fig. 6 Continued

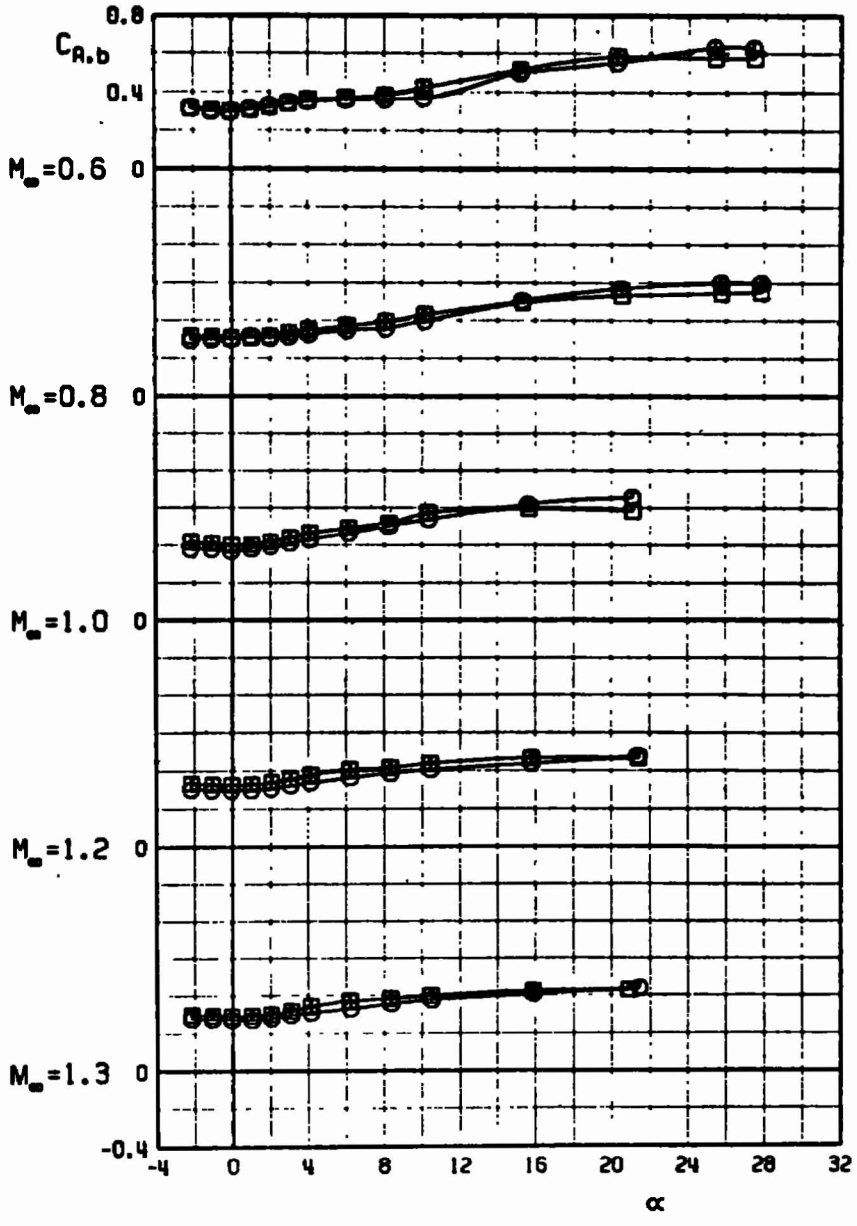

d. $C_{A,b}$ versus α
Fig. 6 Continued

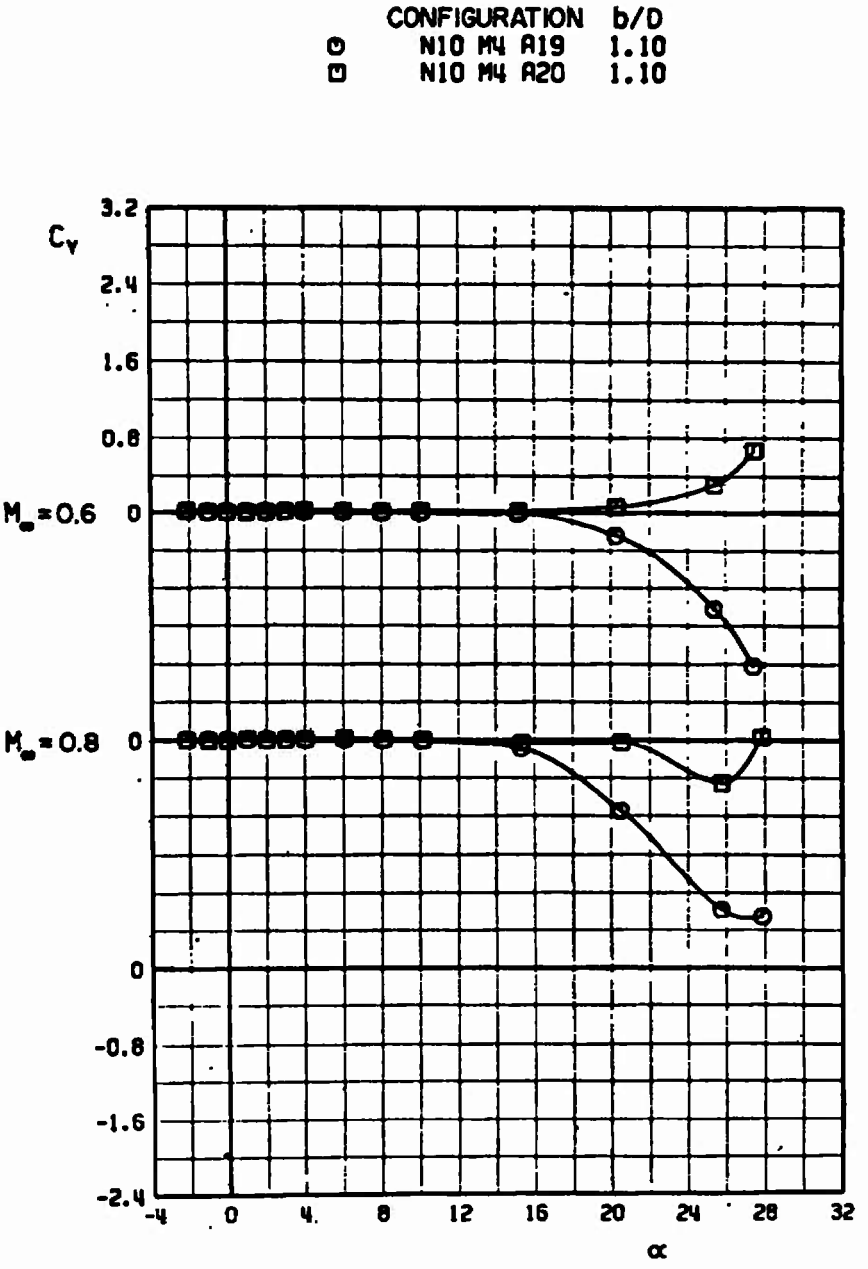

e. C_Y versus α
Fig. 6 Continued

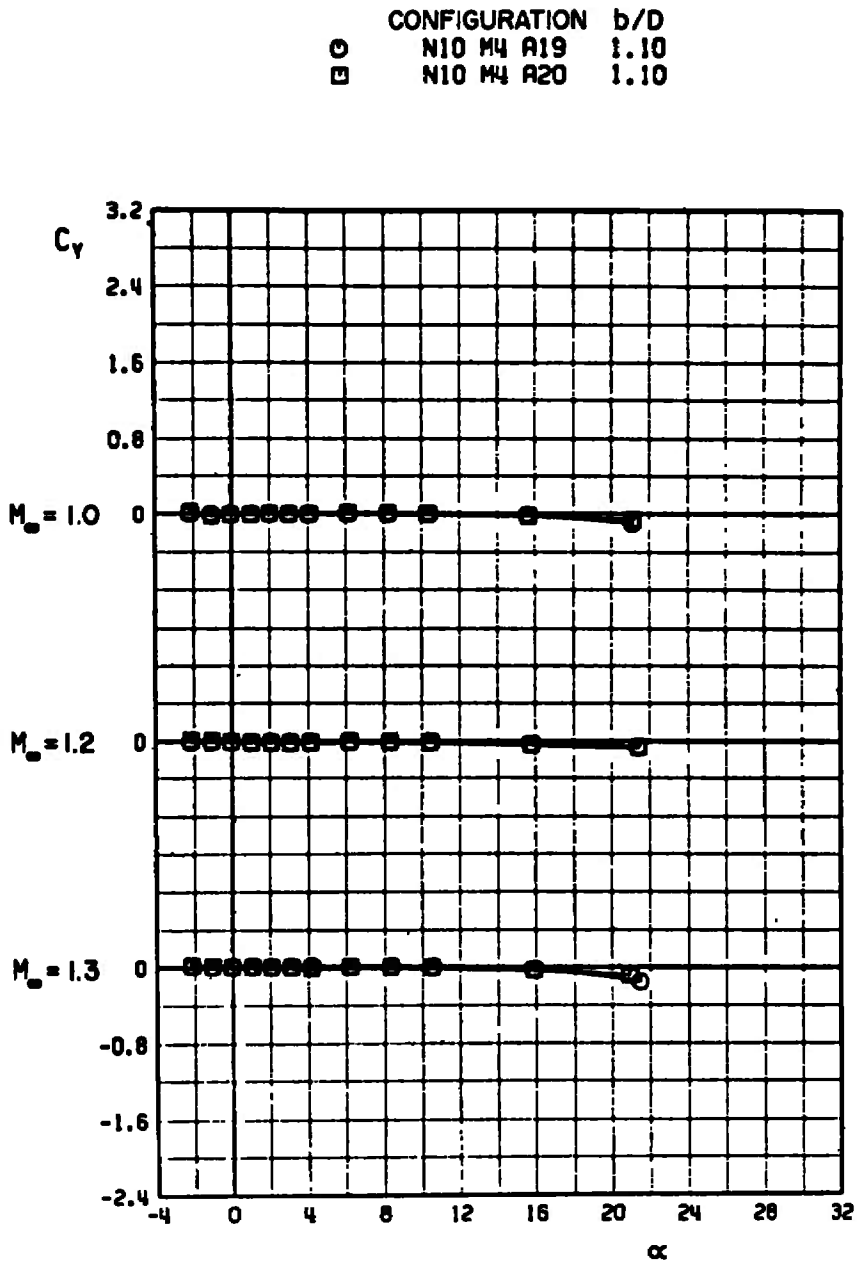

e. Concluded
Fig. 6 Continued

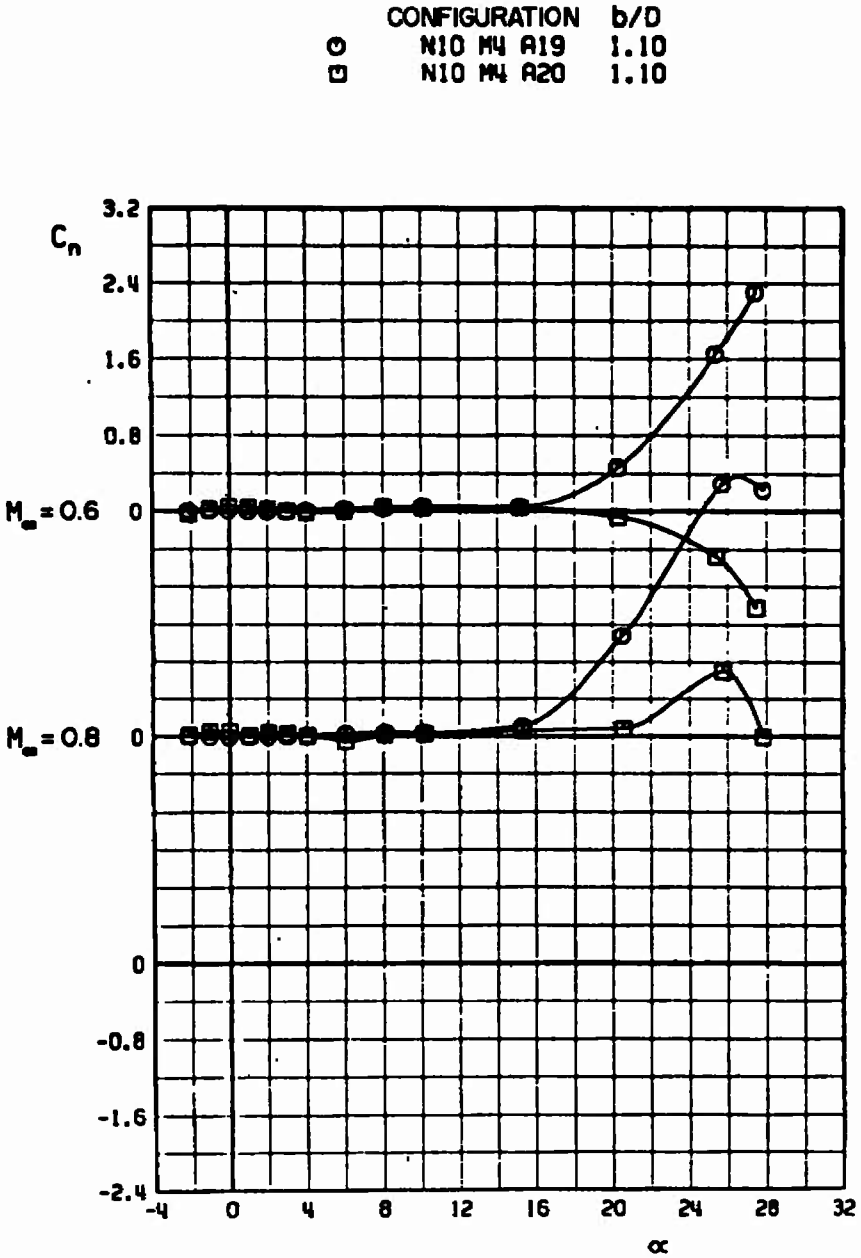

f. C_n versus α
Fig. 6 Continued

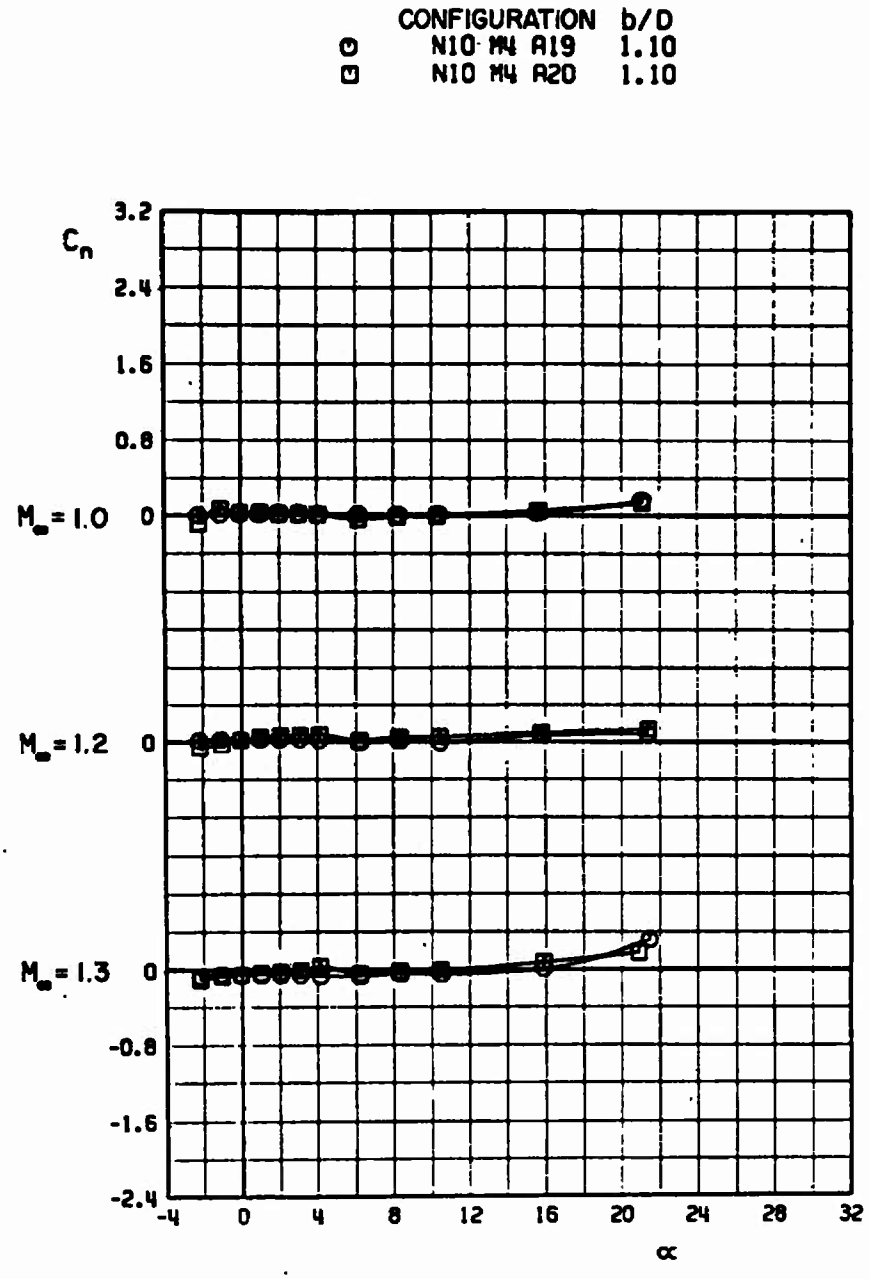

f. Concluded
Fig. 6 Continued

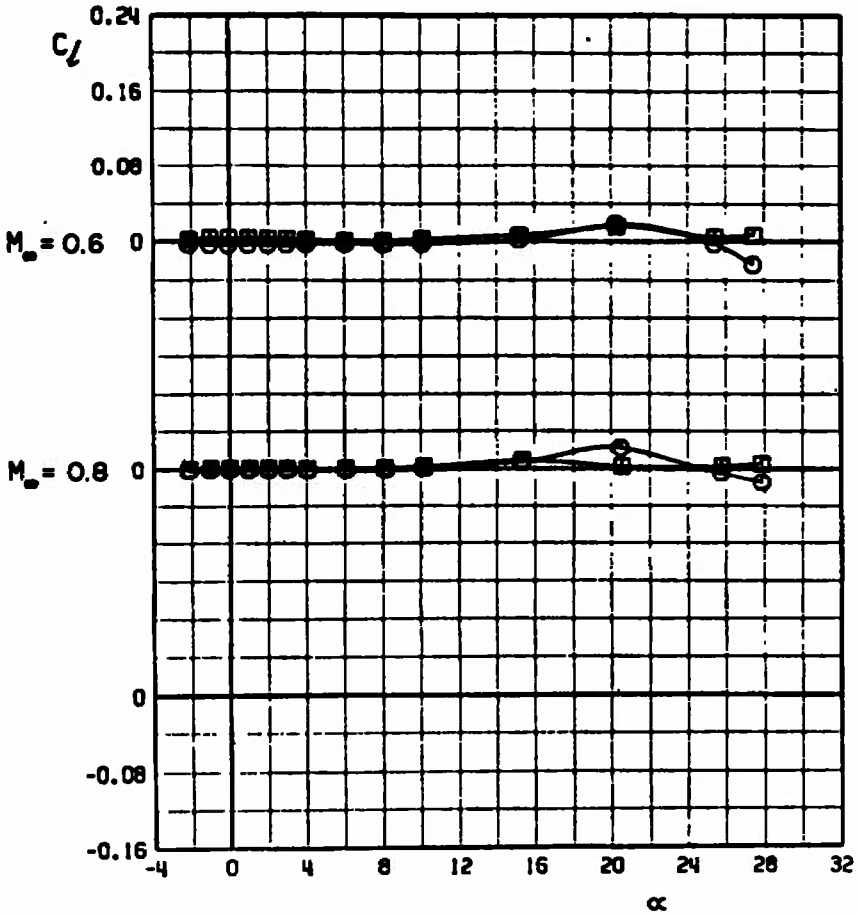

g. C_ℓ versus α
Fig. 6 Continued

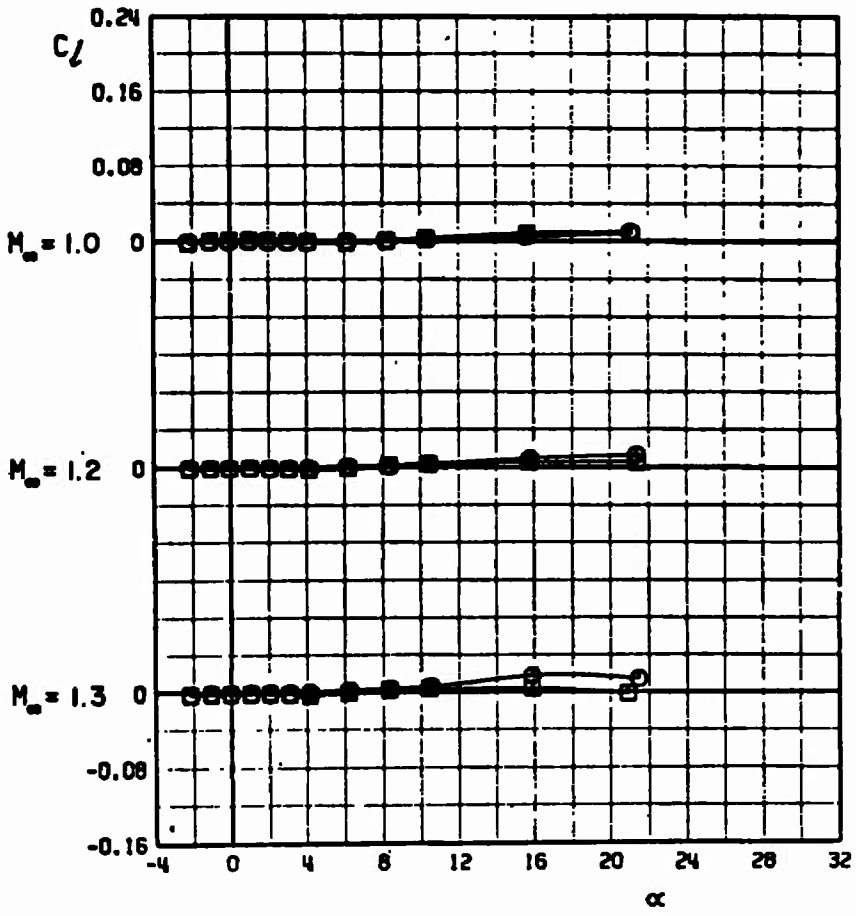

g. Concluded

Fig. 6 Concluded

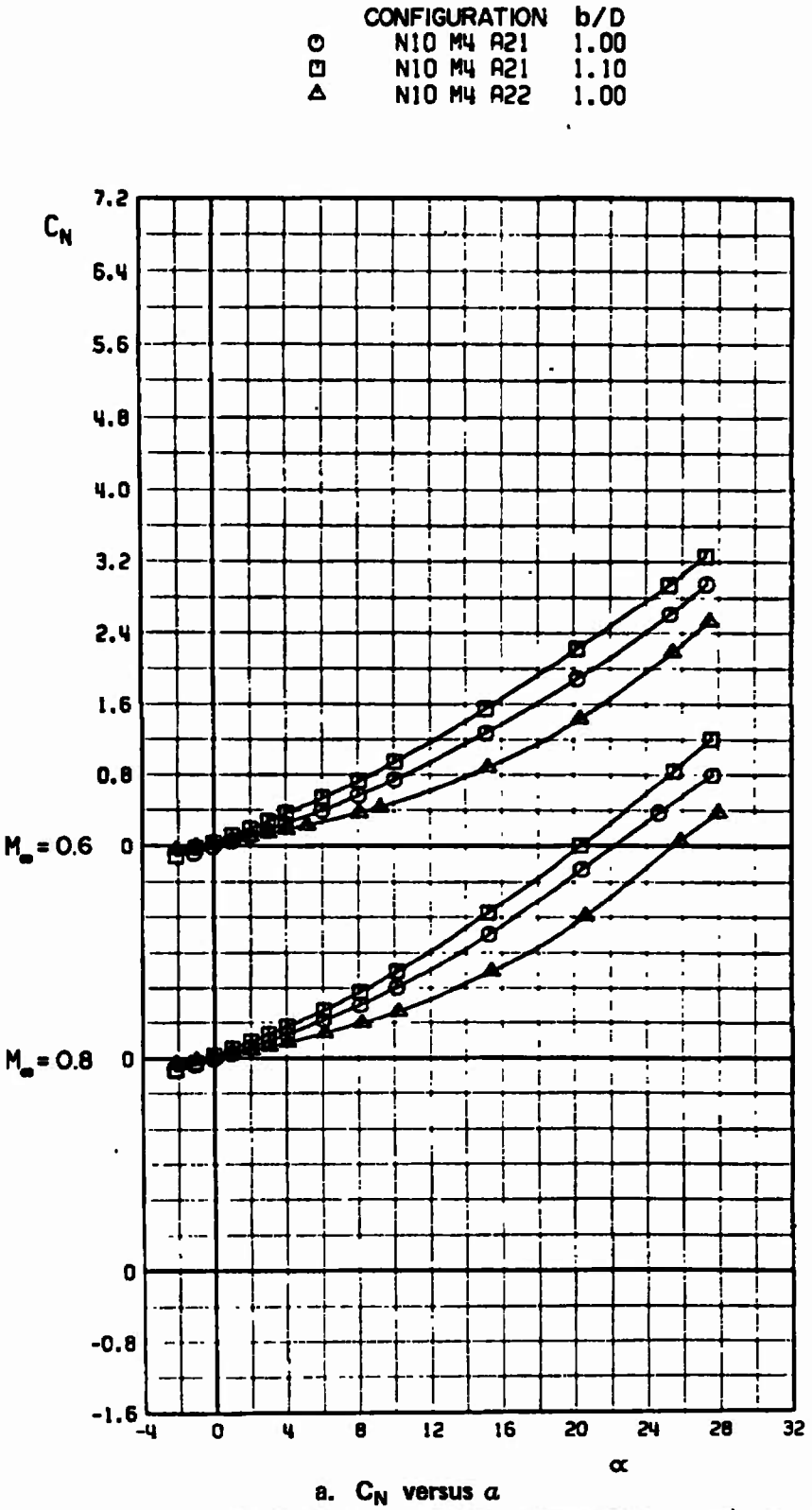

a. C_N versus α

Fig. 7 Aerodynamic Coefficients of Configurations N10M4A21, b/D = 1.00 and 1.10 and Configuration N10M4A22, b/D = 1.00

	CONFIGURATION	b/D
○	N10 M4 A21	1.00
□	N10 M4 A21	1.10
△	N10 M4 A22	1.00

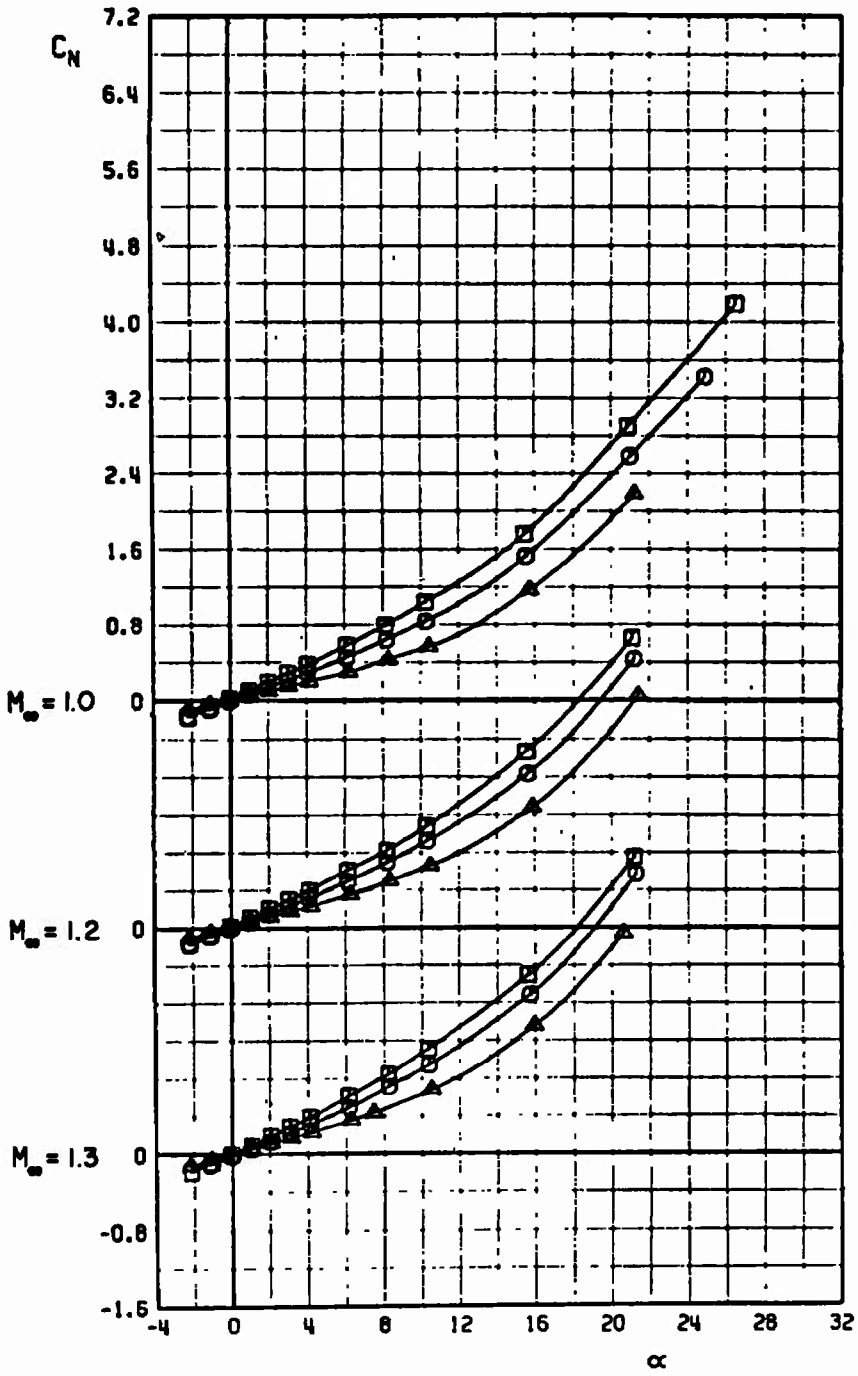

a. Concluded
Fig. 7 Continued

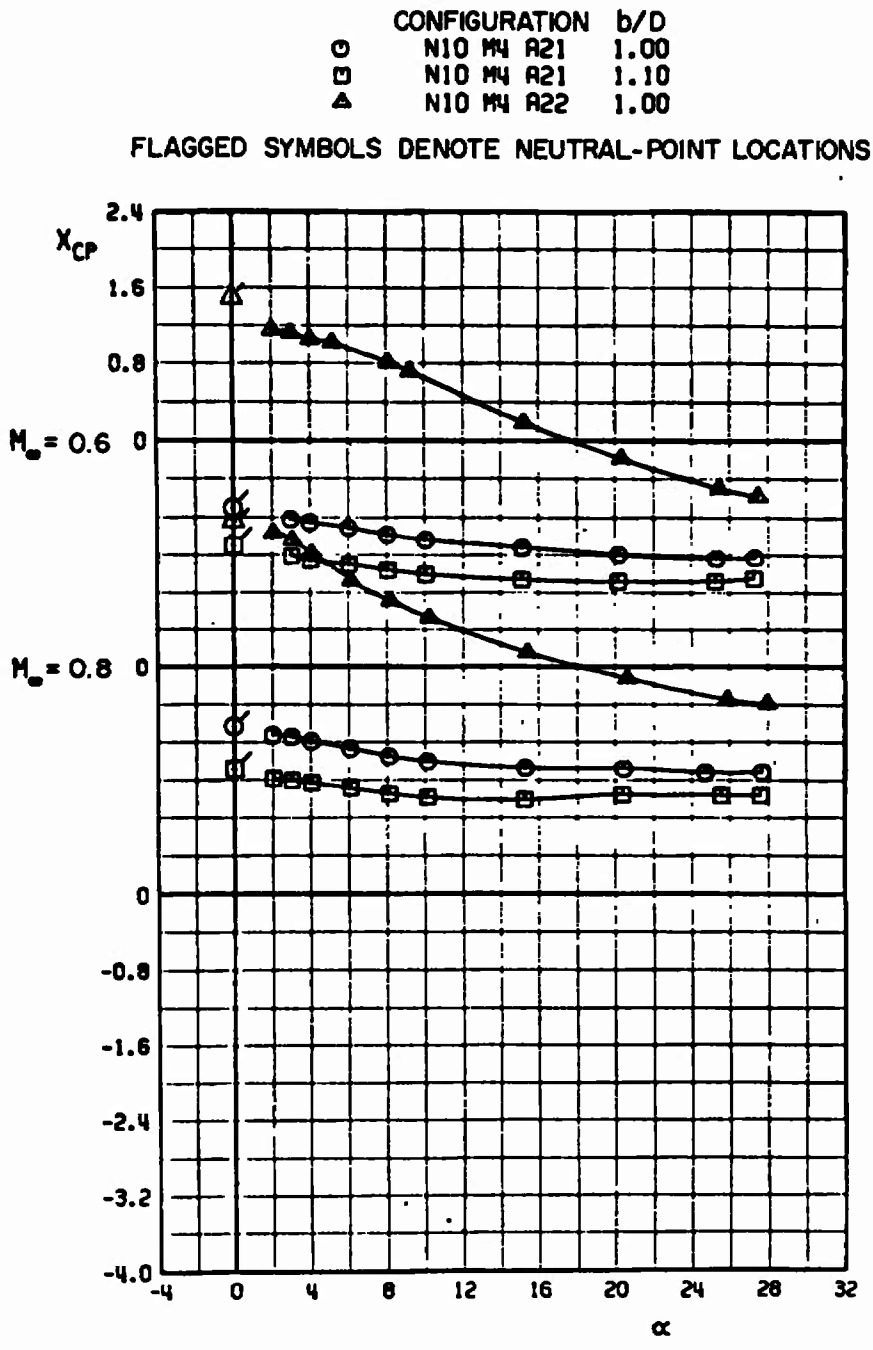

b. X_{cp} versus α
Fig. 7 Continued

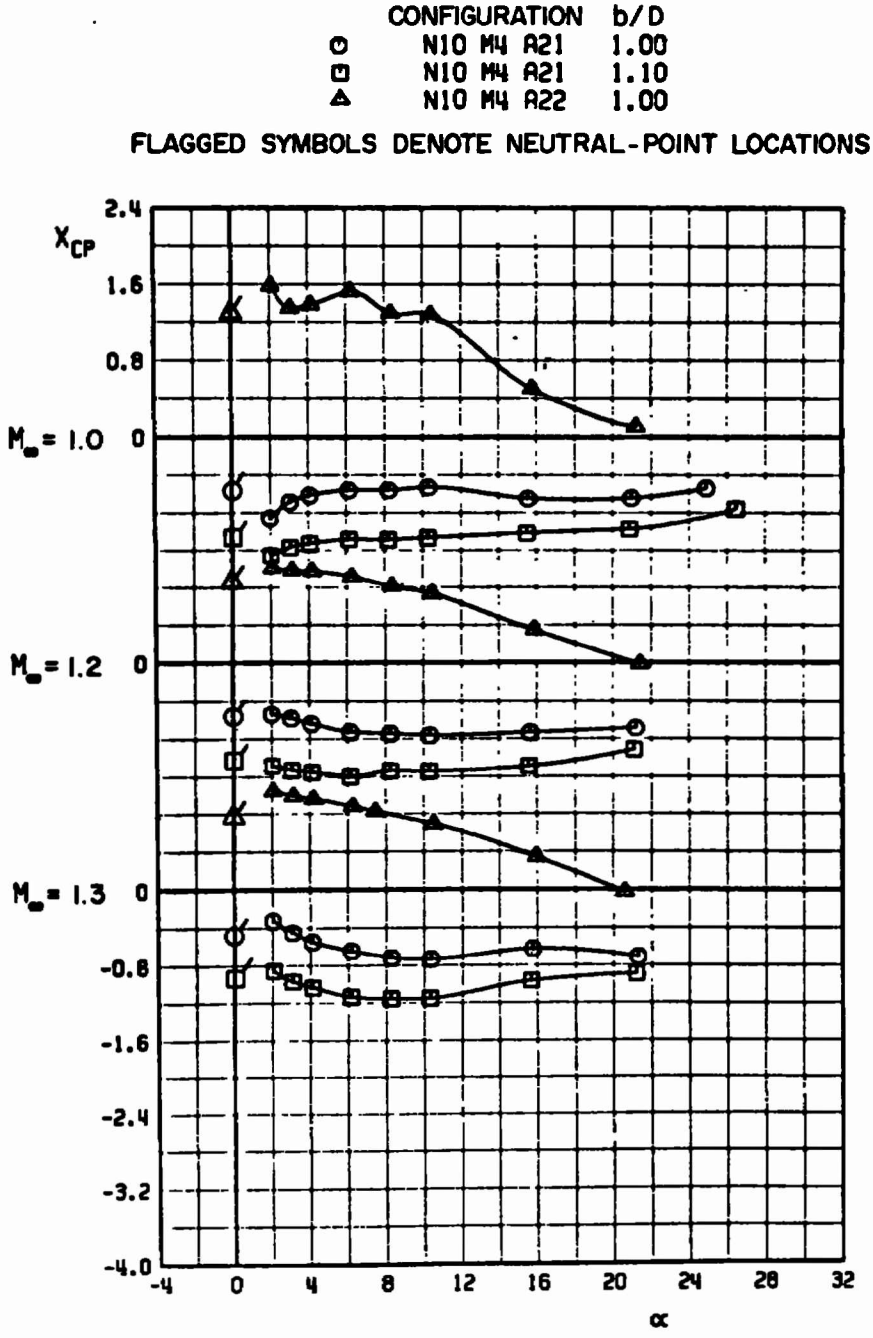

b. Concluded
Fig. 7 Continued

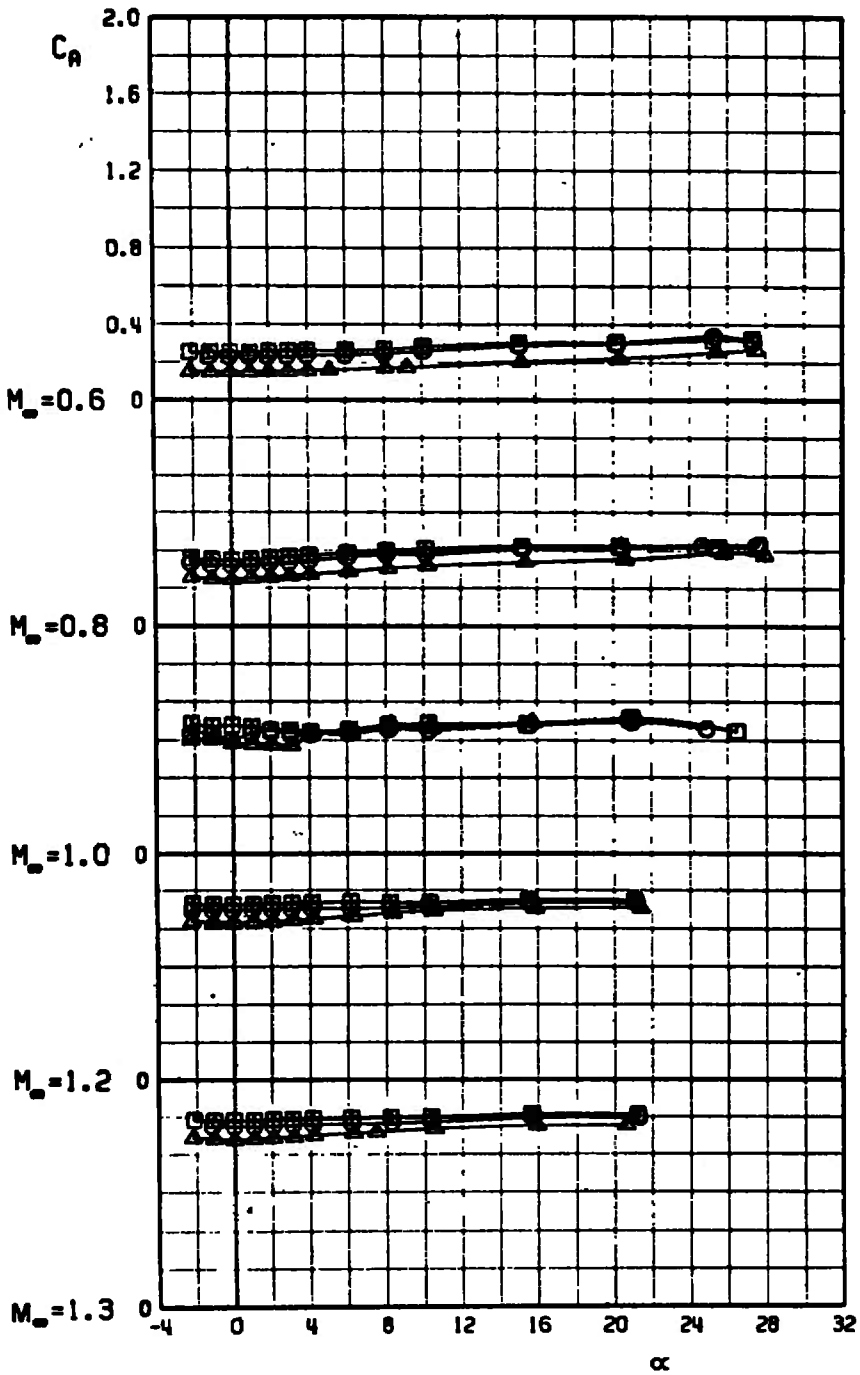

c. C_A versus α
Fig. 7 Continued

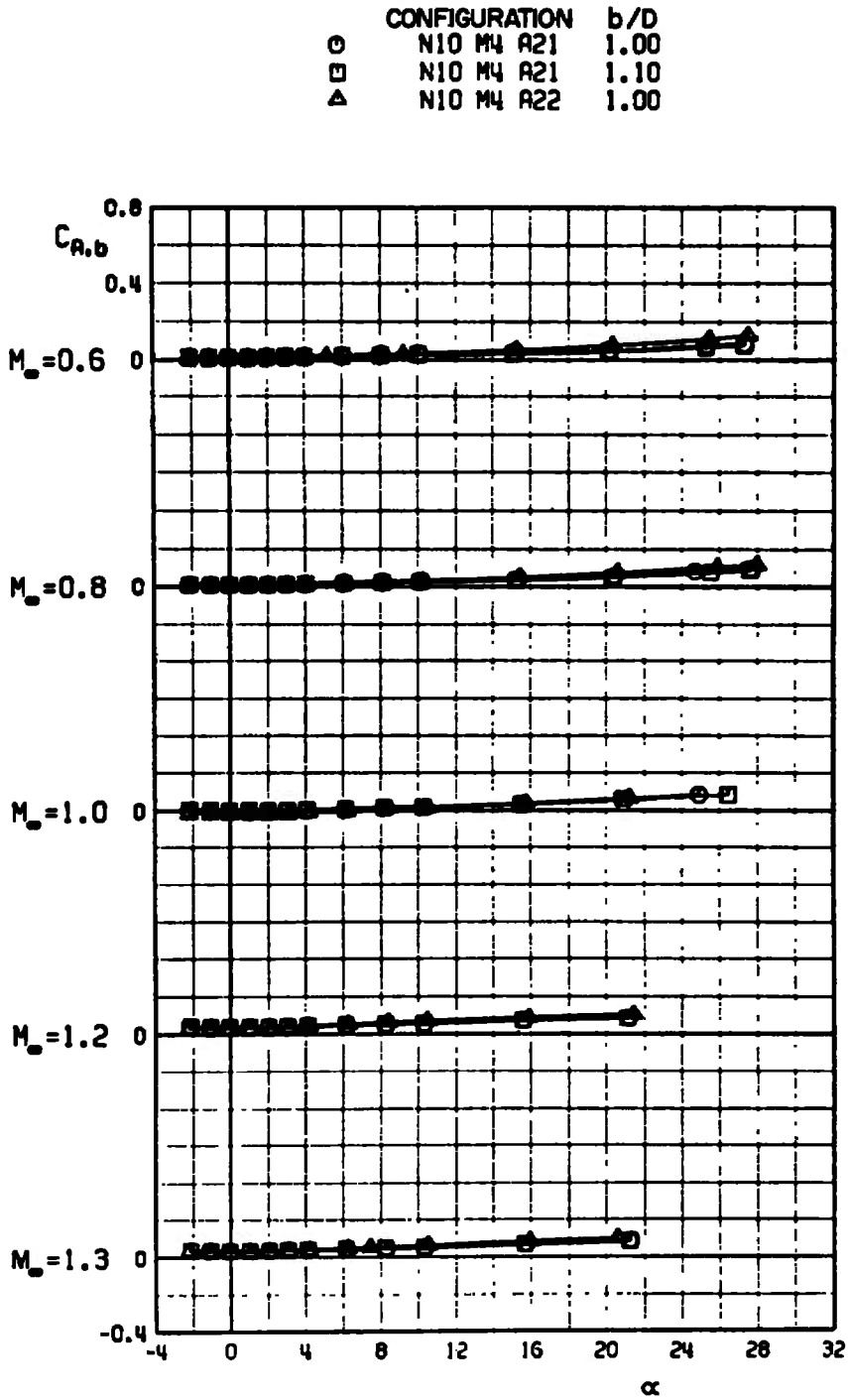

d. $C_{A,b}$ versus α
Fig. 7 Continued

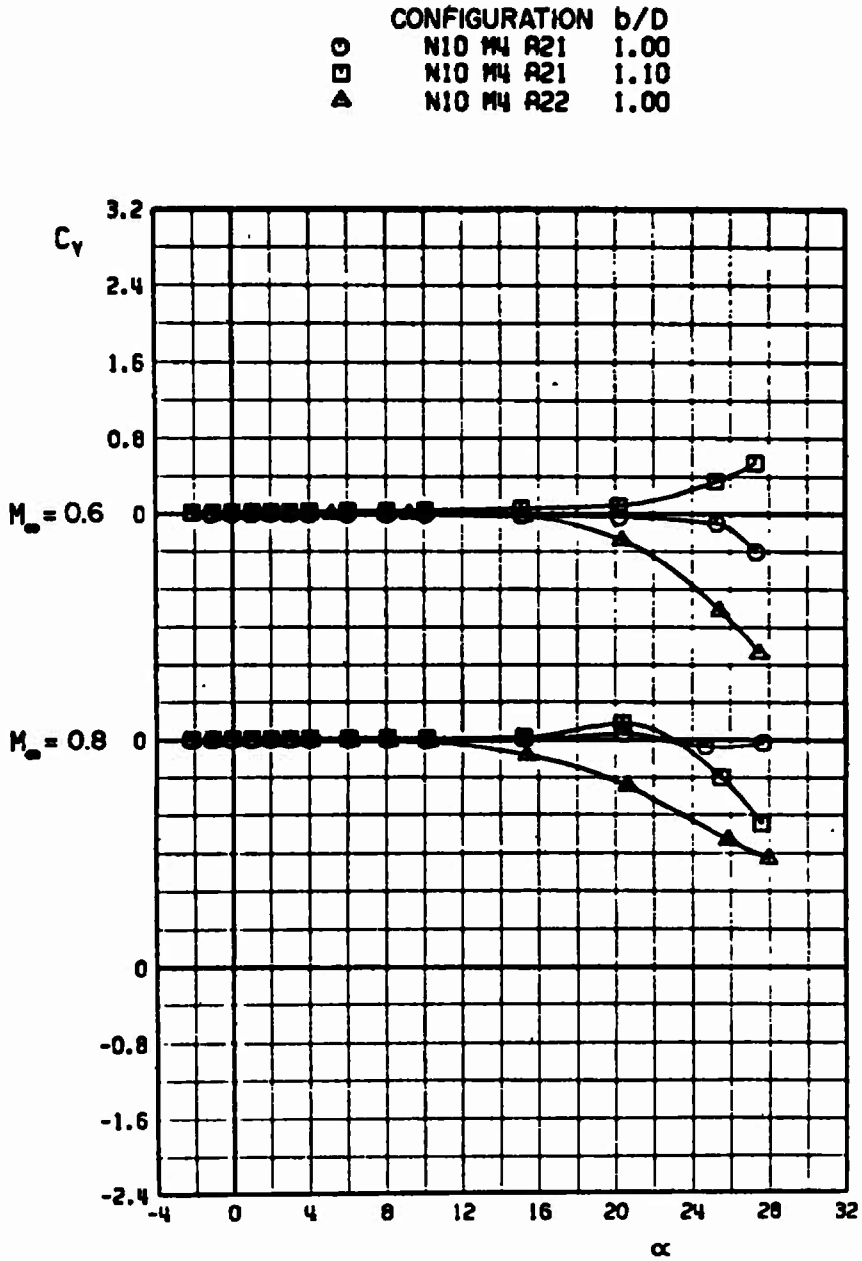

e. C_Y versus α
Fig. 7 Continued

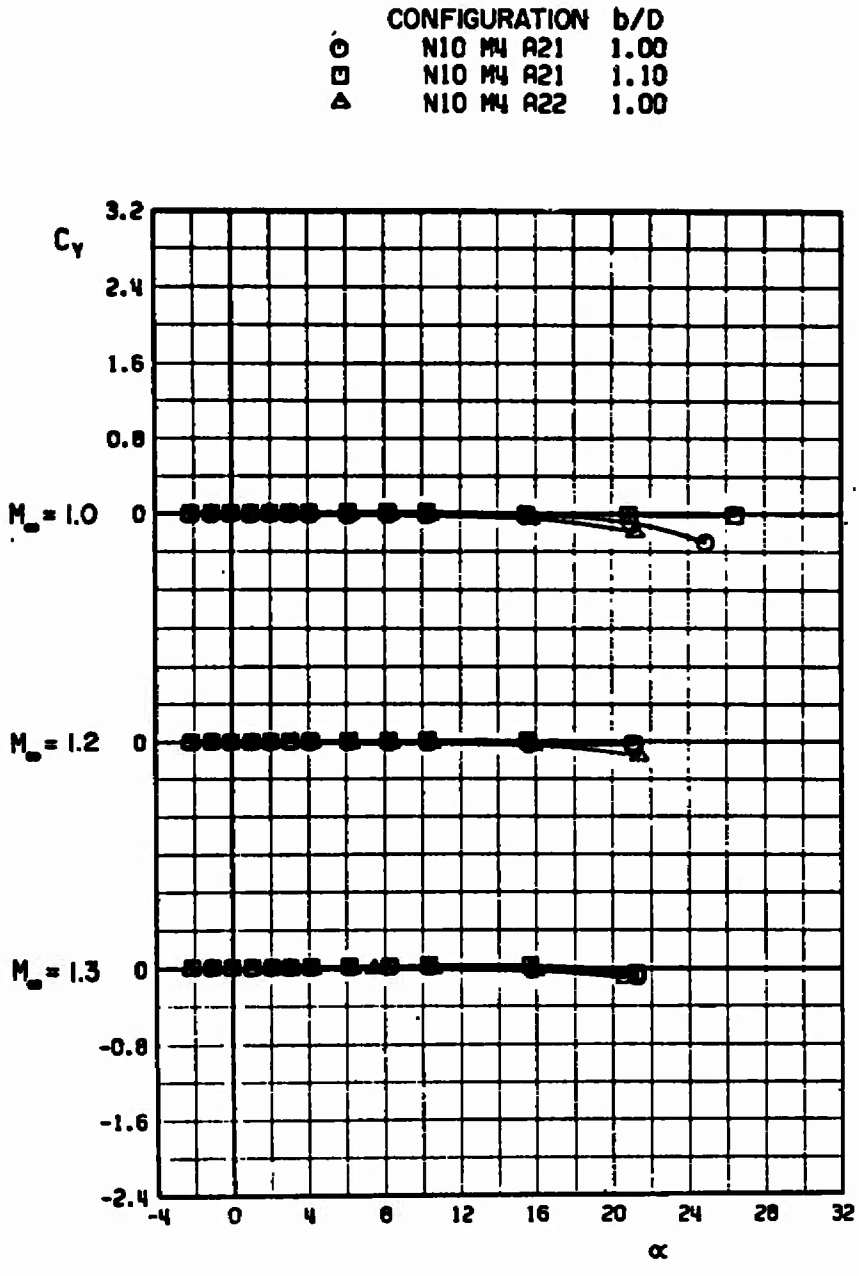

e. Concluded
Fig. 7 Continued

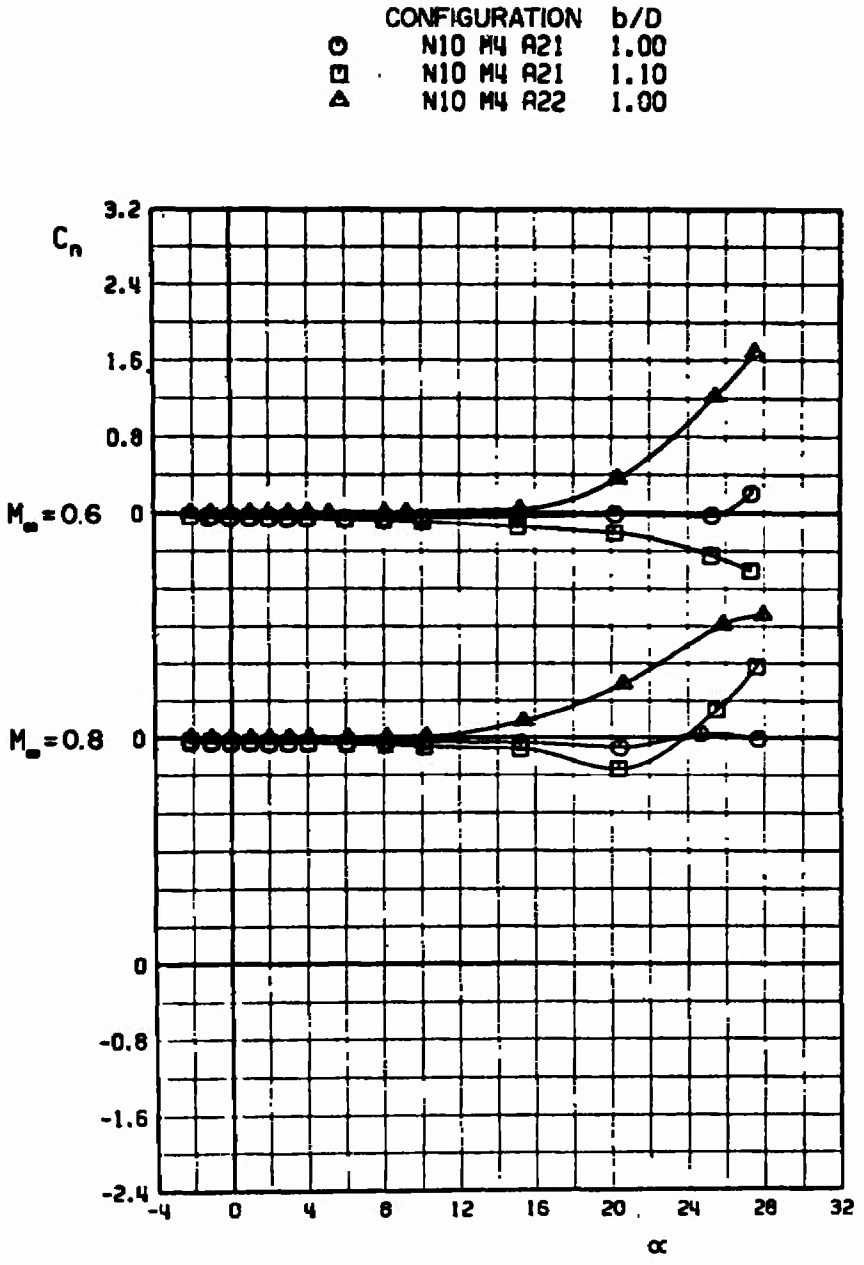

f. C_n versus α
Fig. 7 Continued

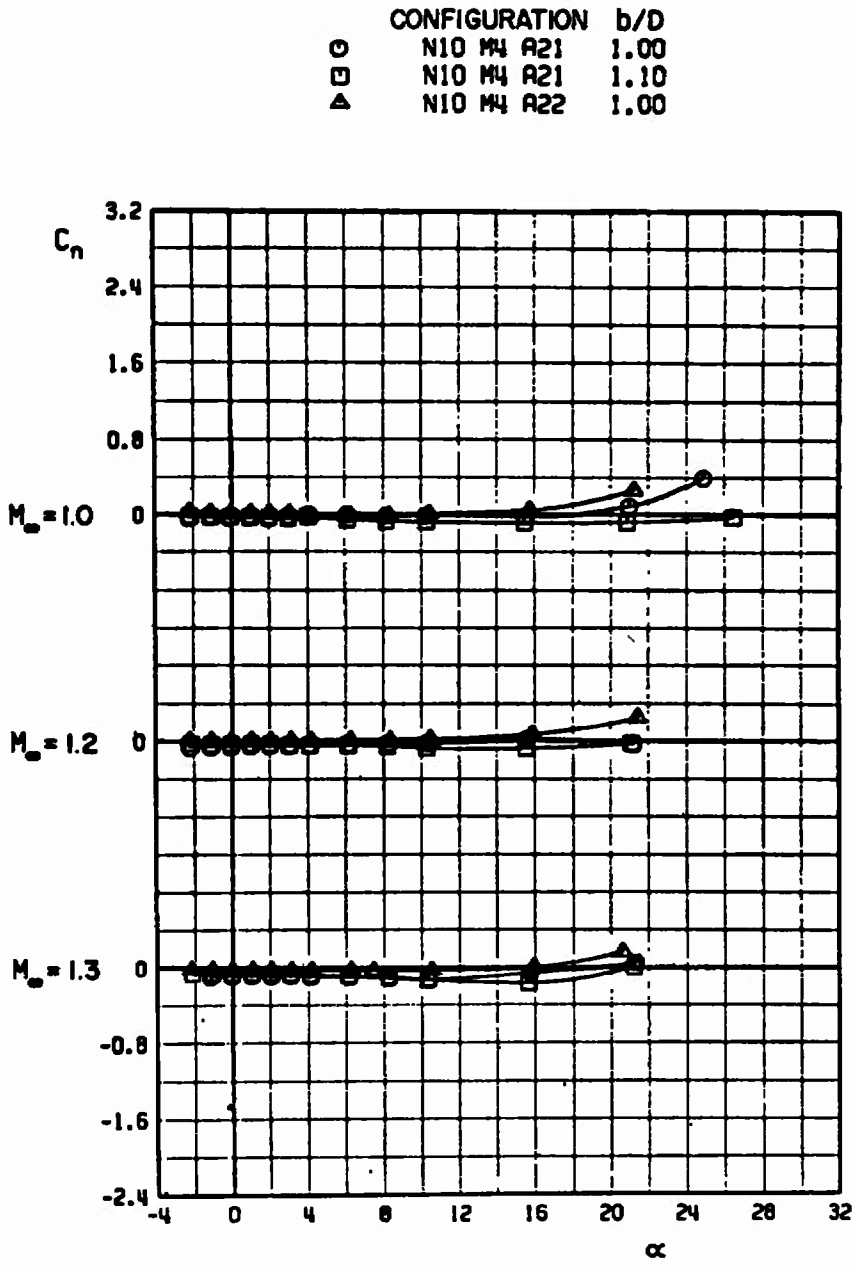

f. Concluded
Fig. 7 Continued

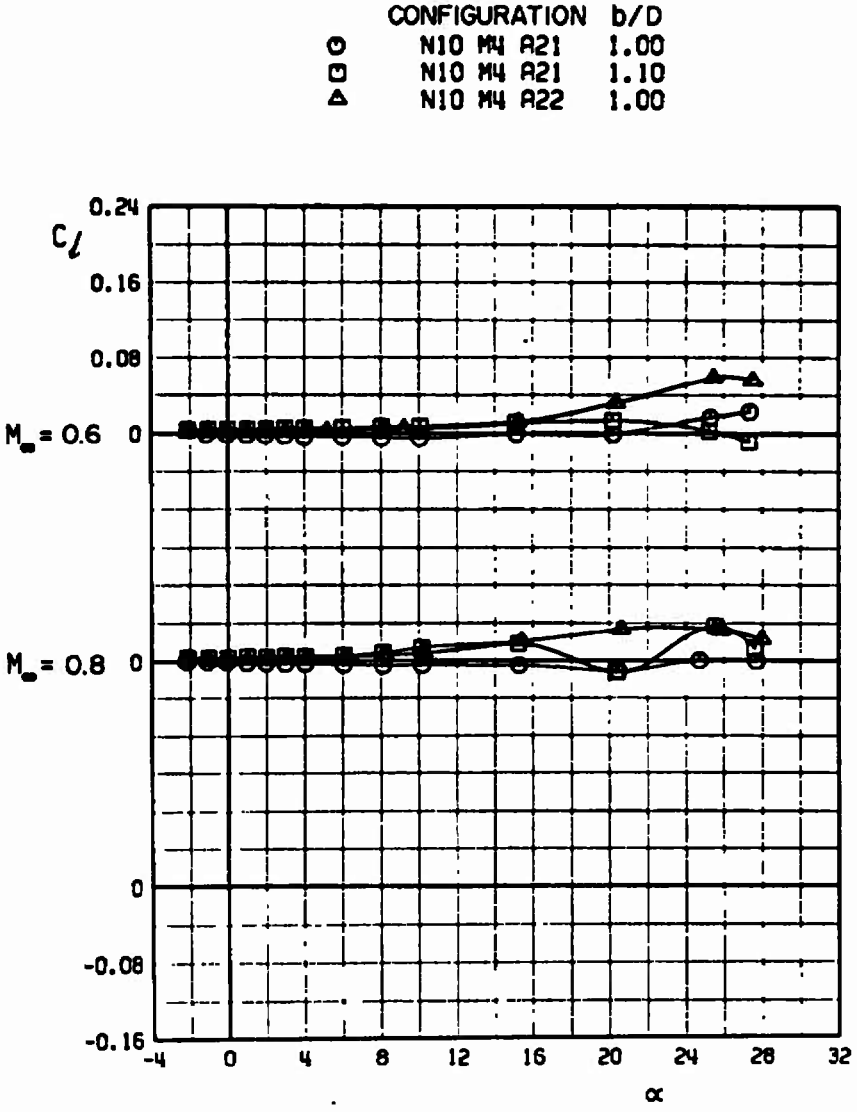

g. C_ℓ versus α
Fig. 7 Continued

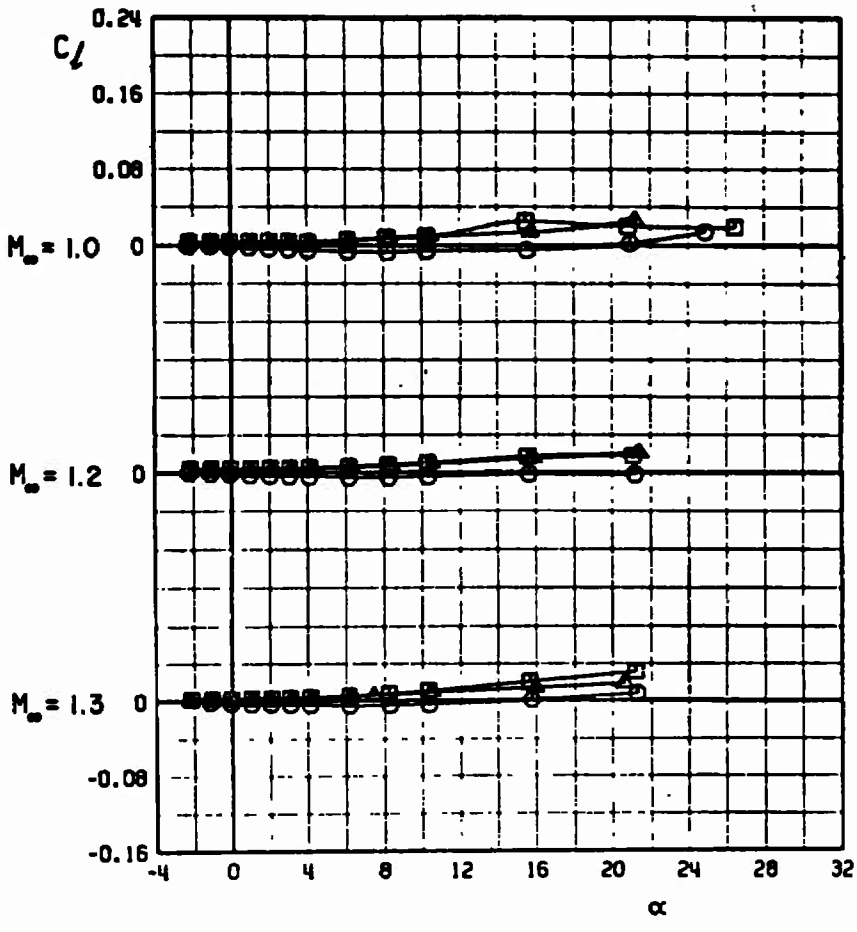

g. Concluded
Fig. 7 Concluded

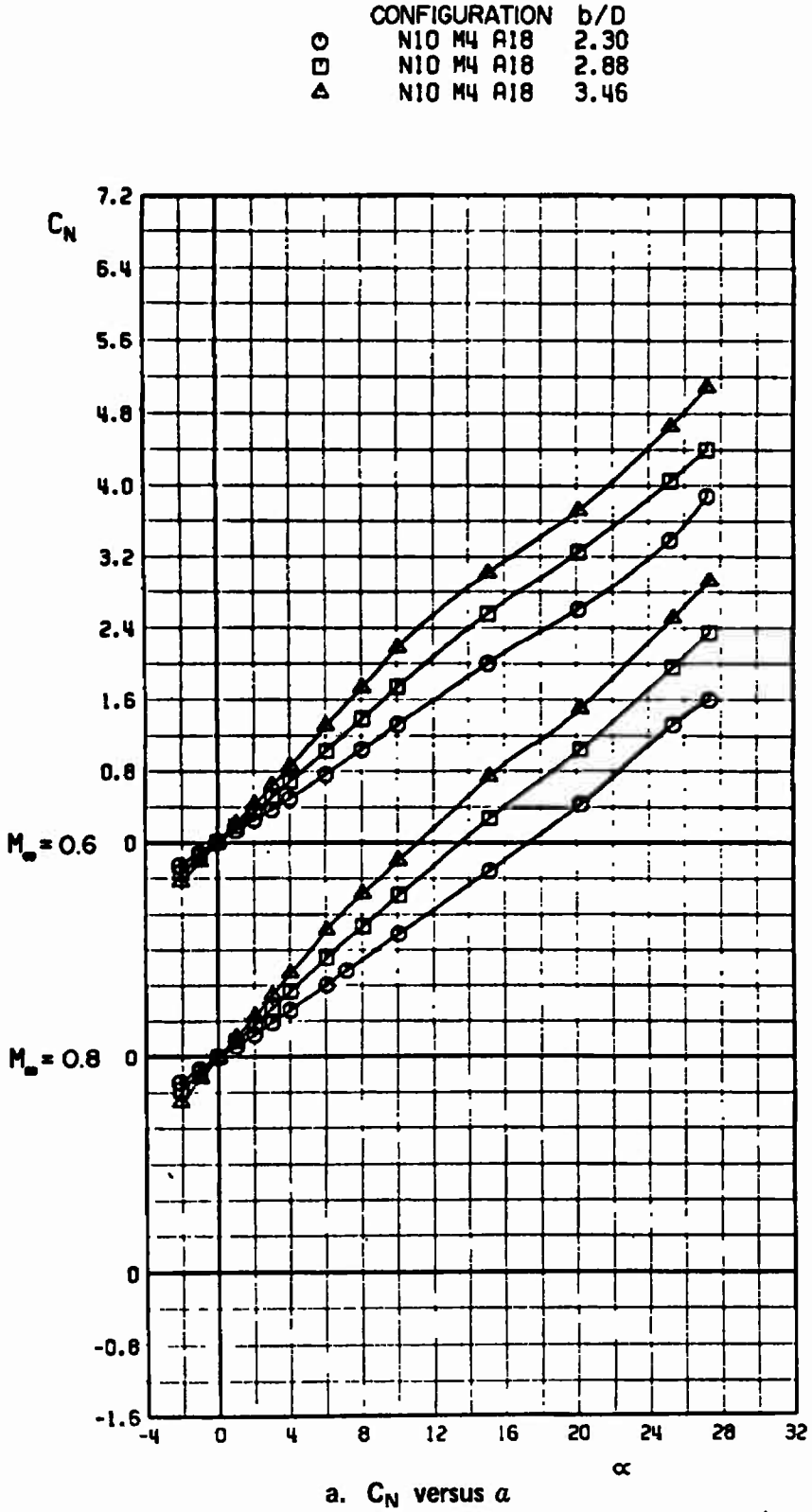

a. C_N versus α

Fig. 8 Aerodynamic Coefficients of Configurations N10M4A18, b/D = 2.30, 2.88 and 3.46

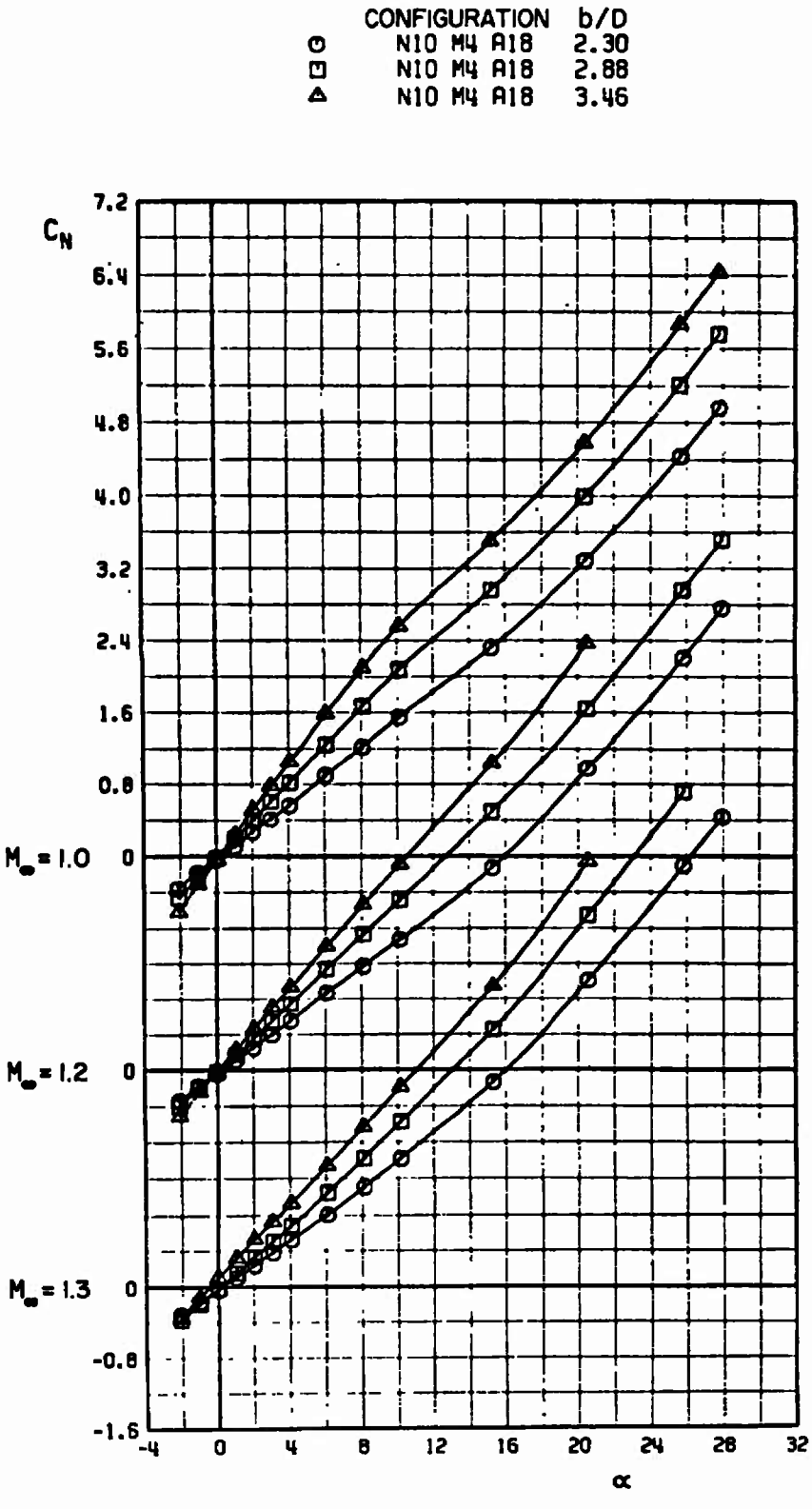

a. Concluded

Fig. 8 Continued

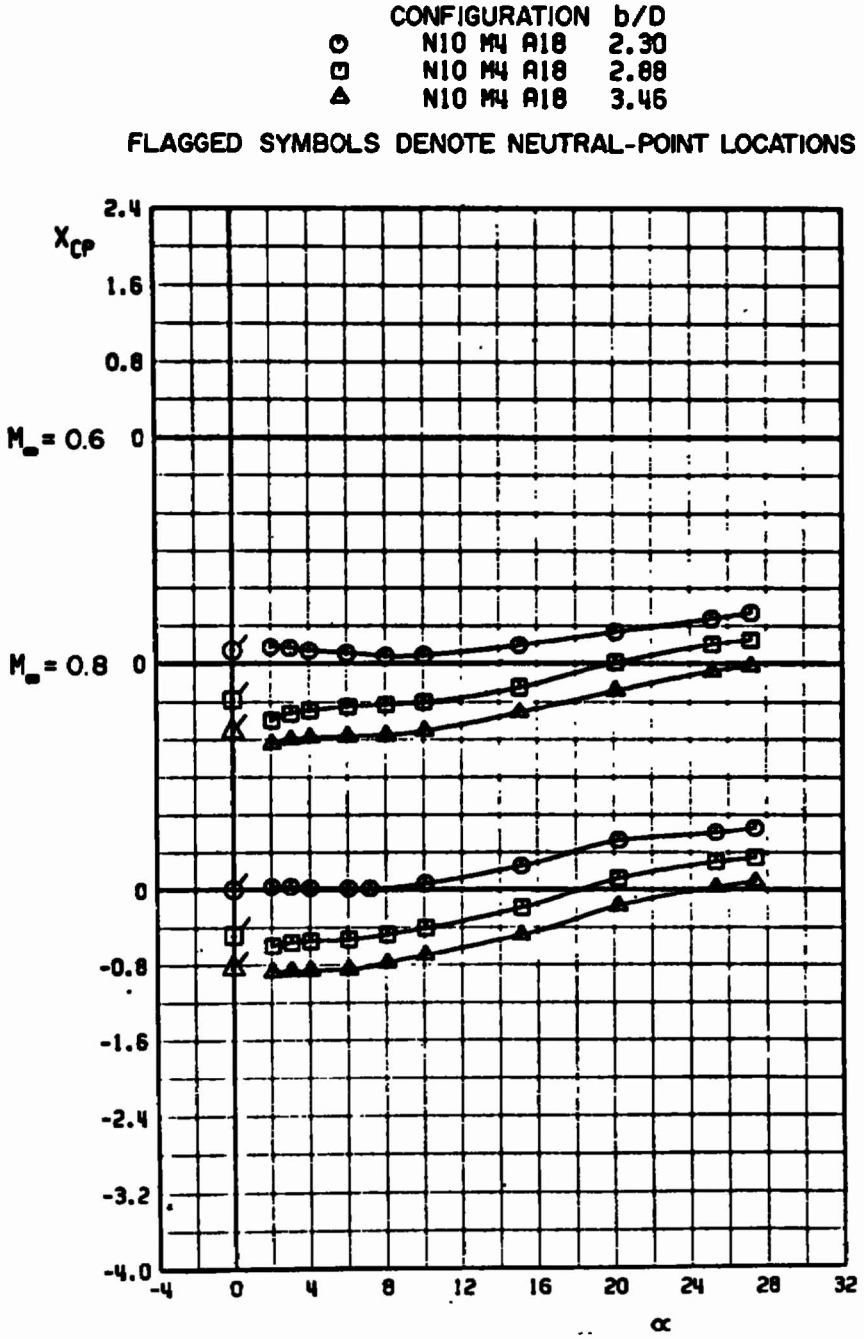

b. X_{cp} versus α
Fig. 8 Continued

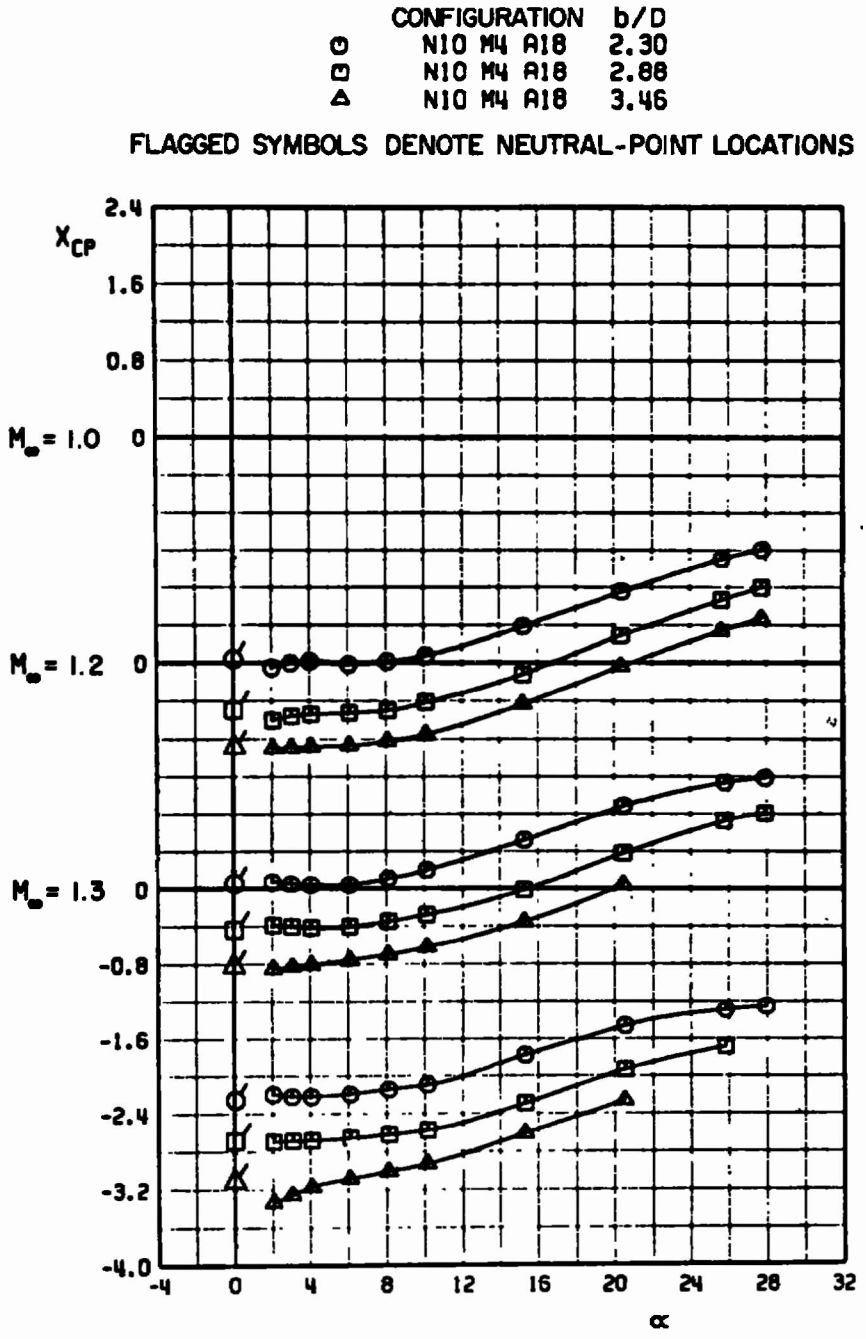

b. Concluded
Fig. 8 Continued

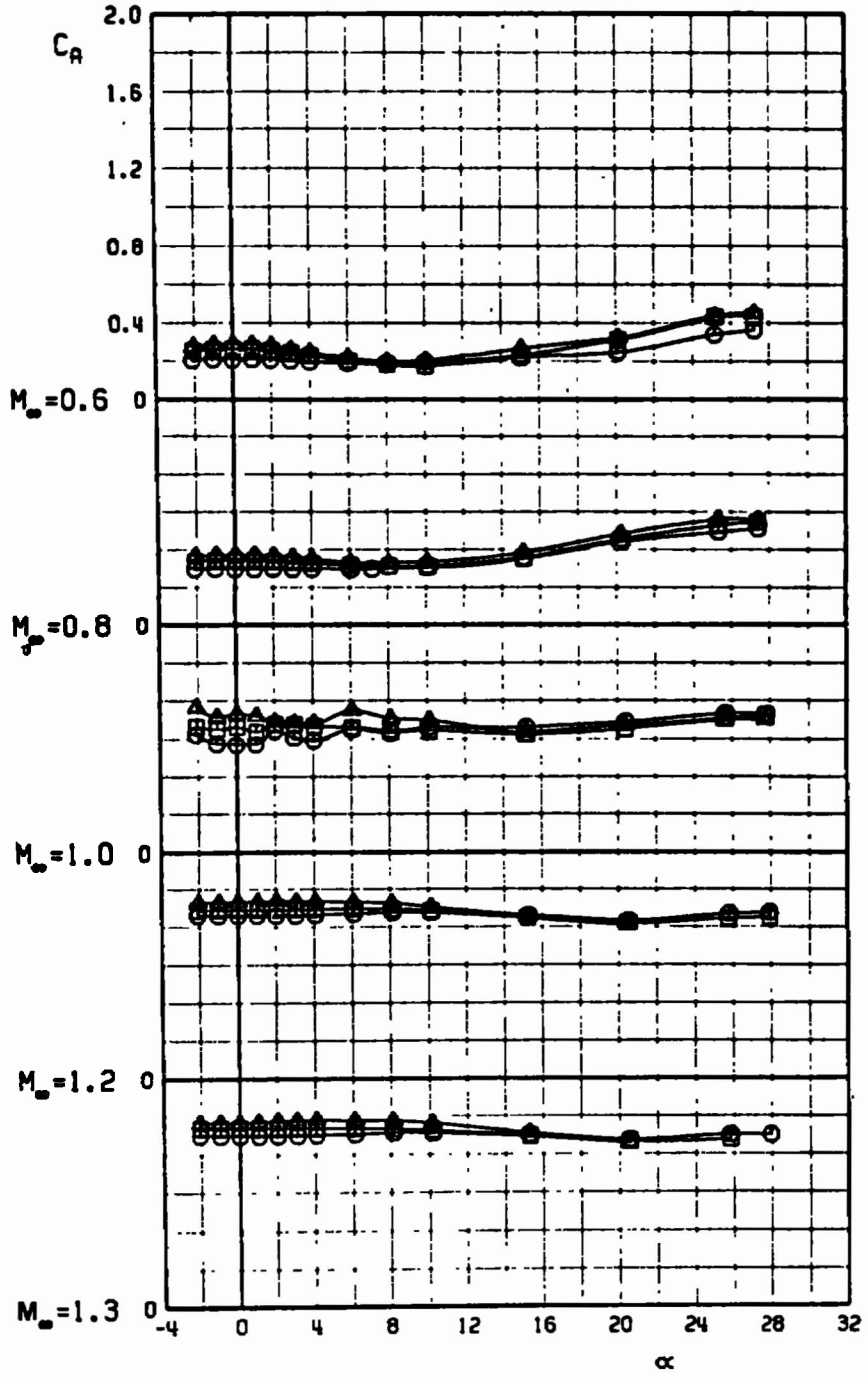

c. C_A versus α
Fig. 8 Continued

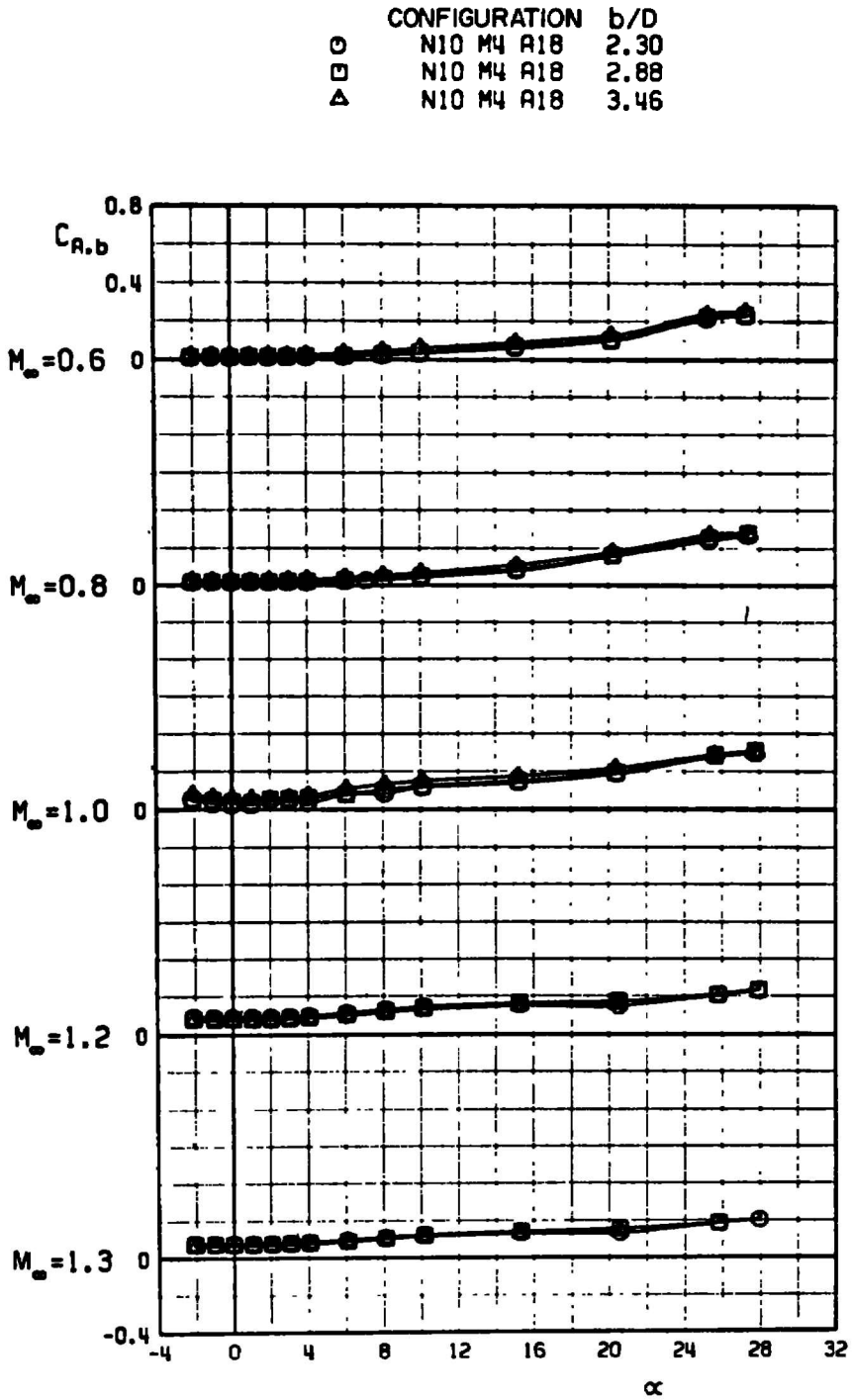

d. $C_{A,b}$ versus α
Fig. 8 Continued

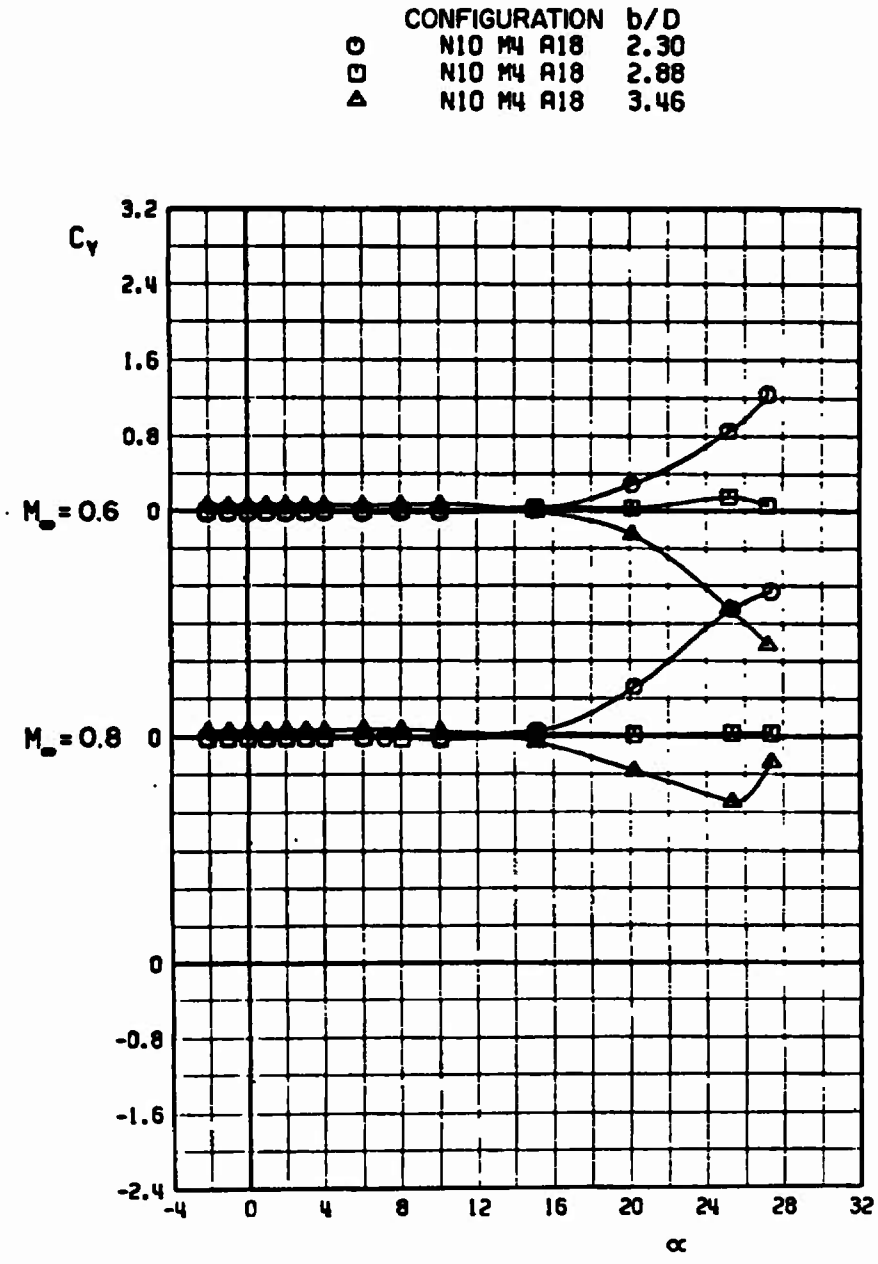

e. C_Y versus α

Fig. 8 Continued

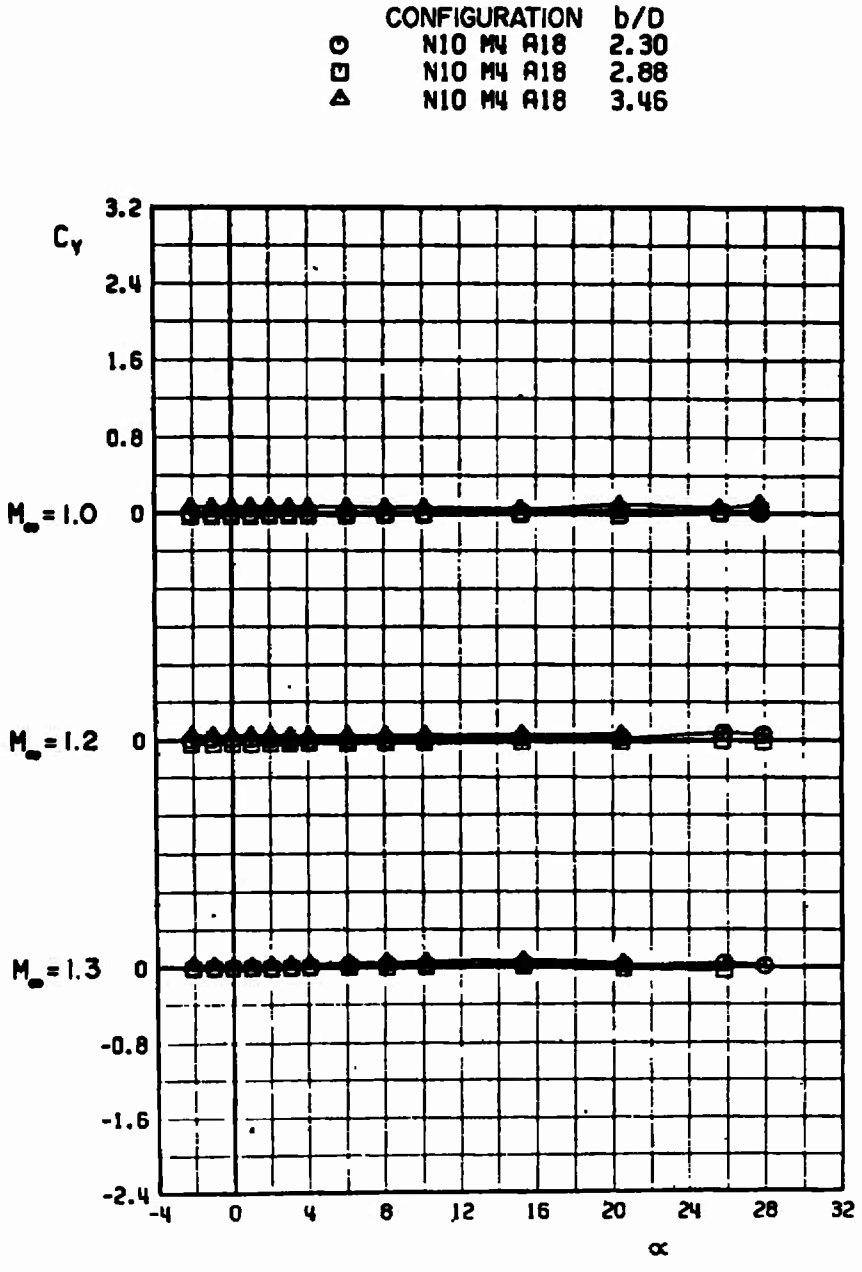

e. Concluded
Fig. 8 Continued

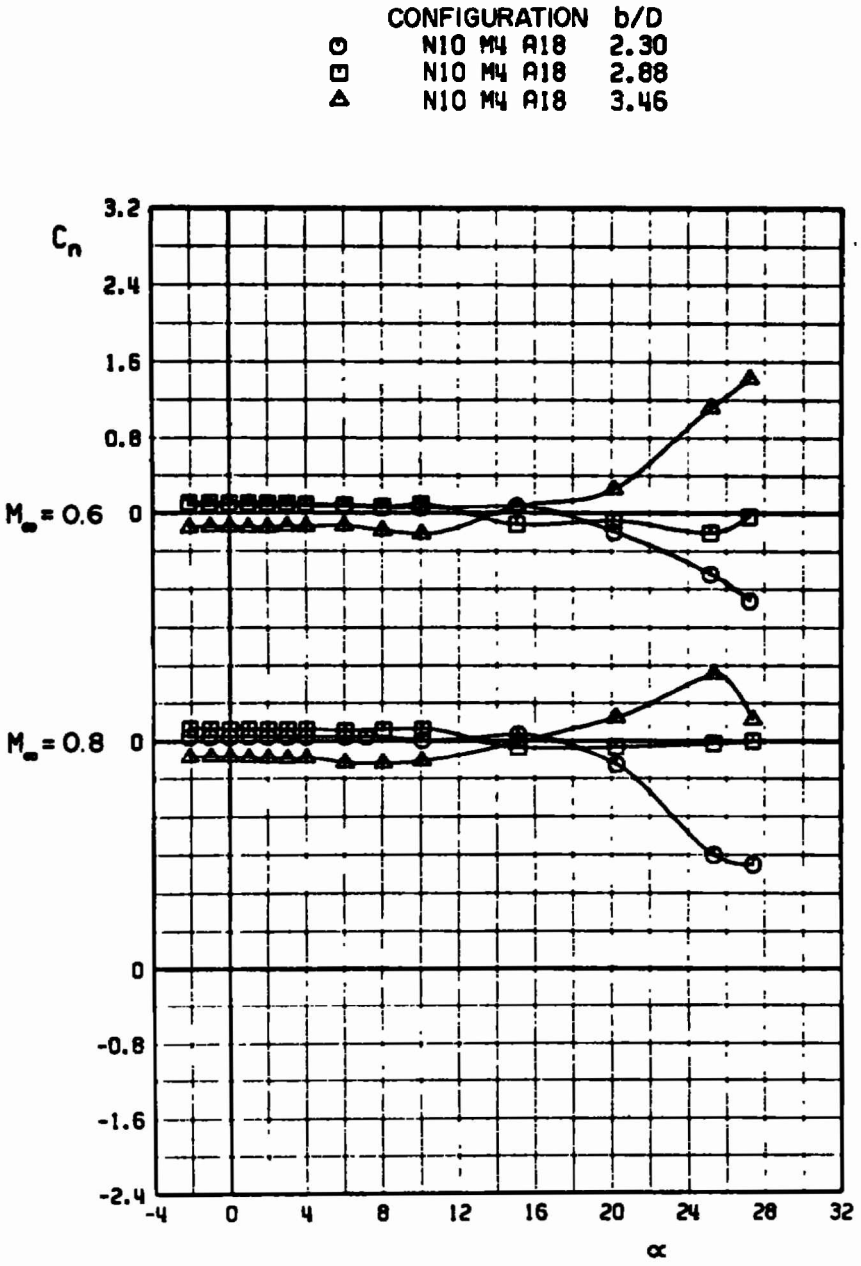

f. C_n versus α
Fig. 8 Continued

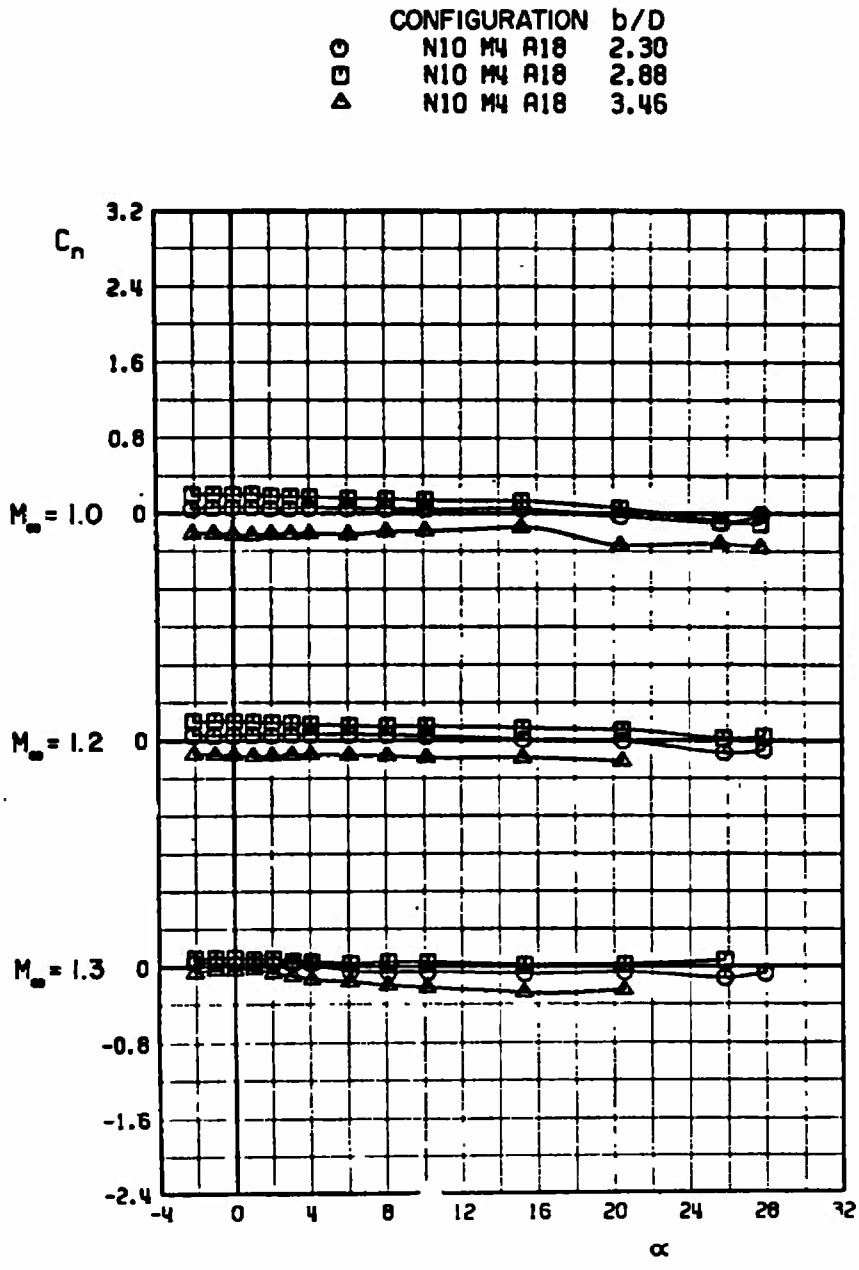

f. Concluded
Fig. 8 Continued

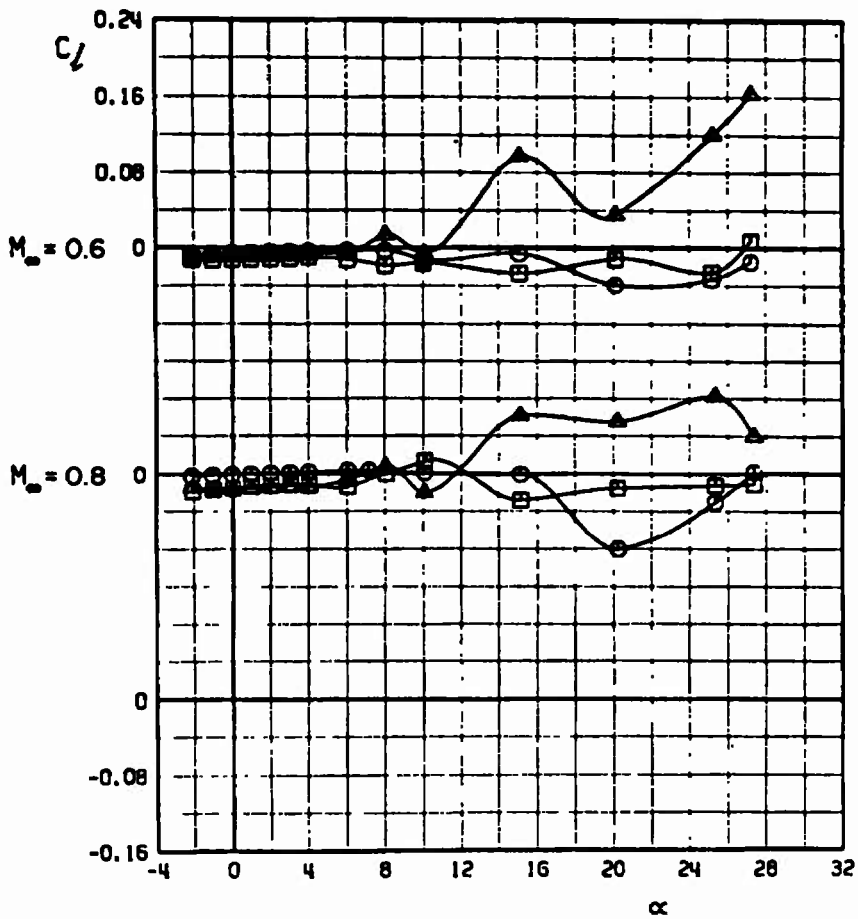

g. C_ℓ versus α

Fig. 8 Continued

	CONFIGURATION	b/D
○	N10 M4 A18	2.30
□	N10 M4 A18	2.88
△	N10 M4 A18	3.46

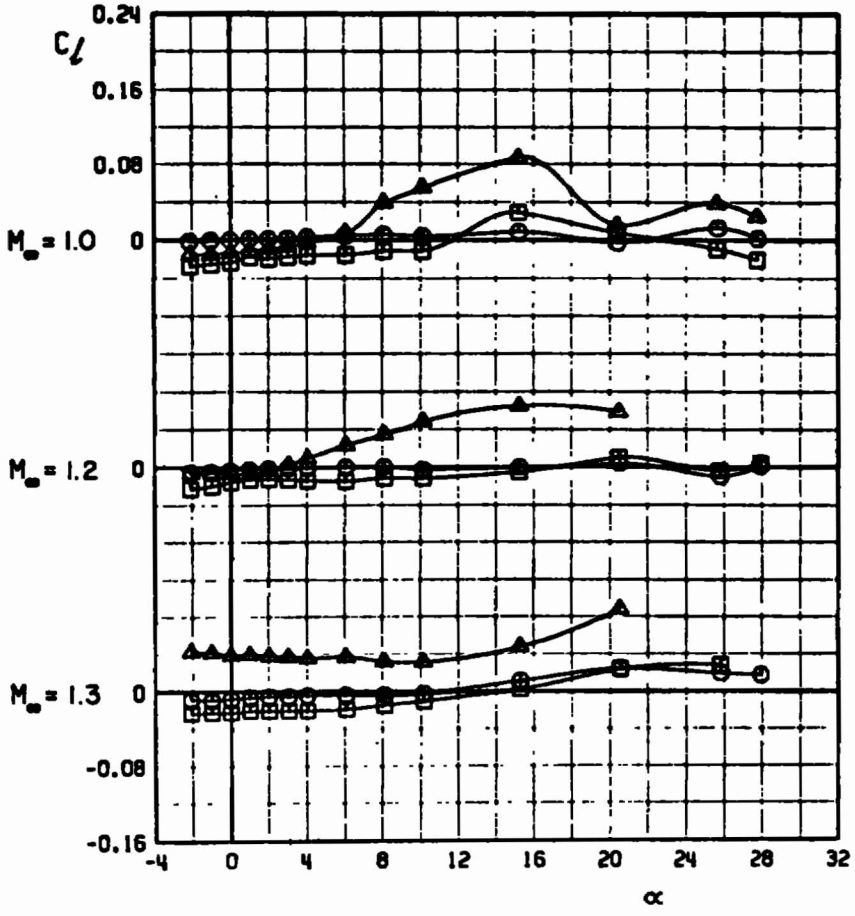

g. Concluded
Fig. 8 Concluded

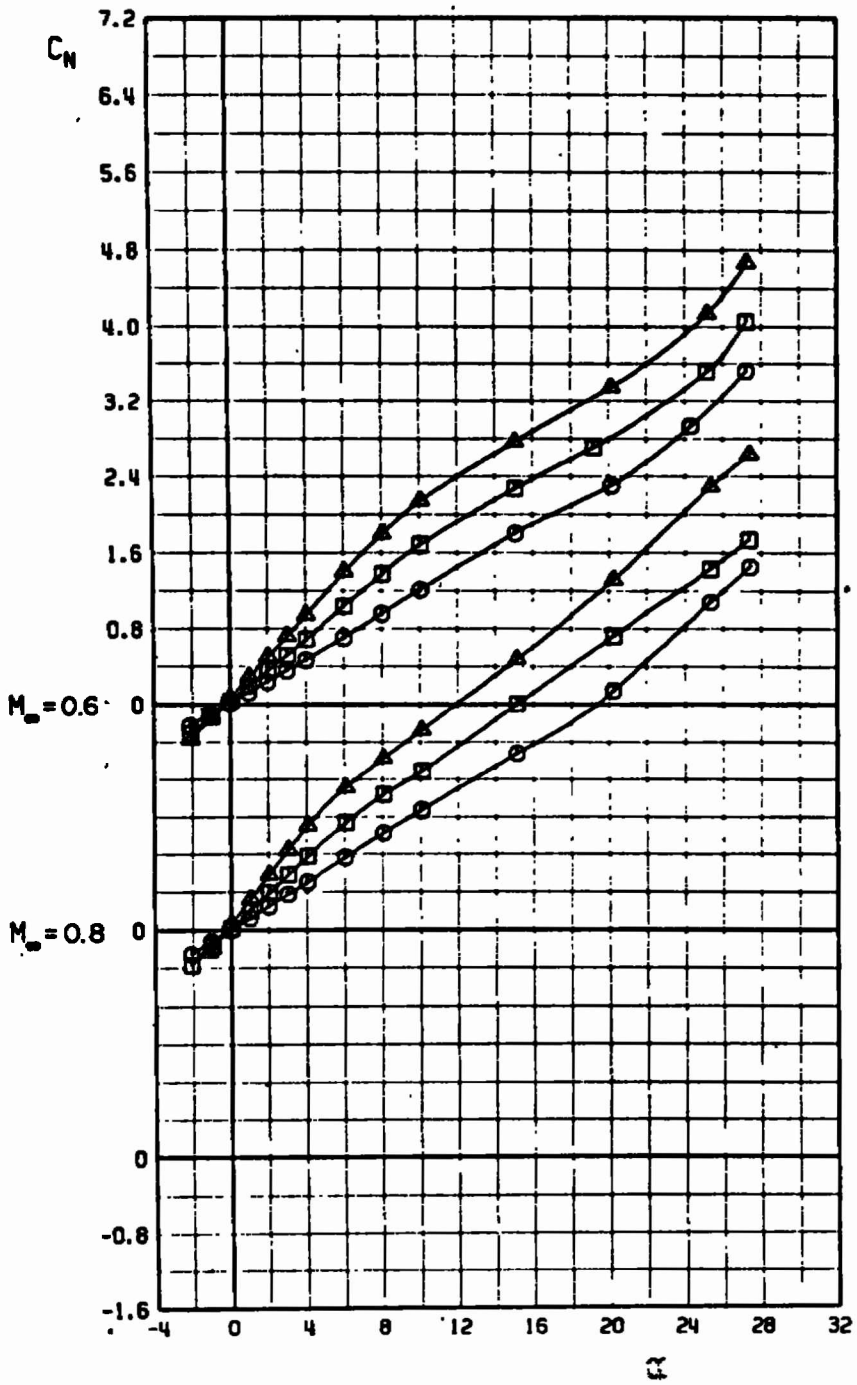

a. C_N versus α

Fig. 9 Aerodynamic Coefficients of Configurations N10M4A23, b/D = 2.66, 3.33, and 4.00

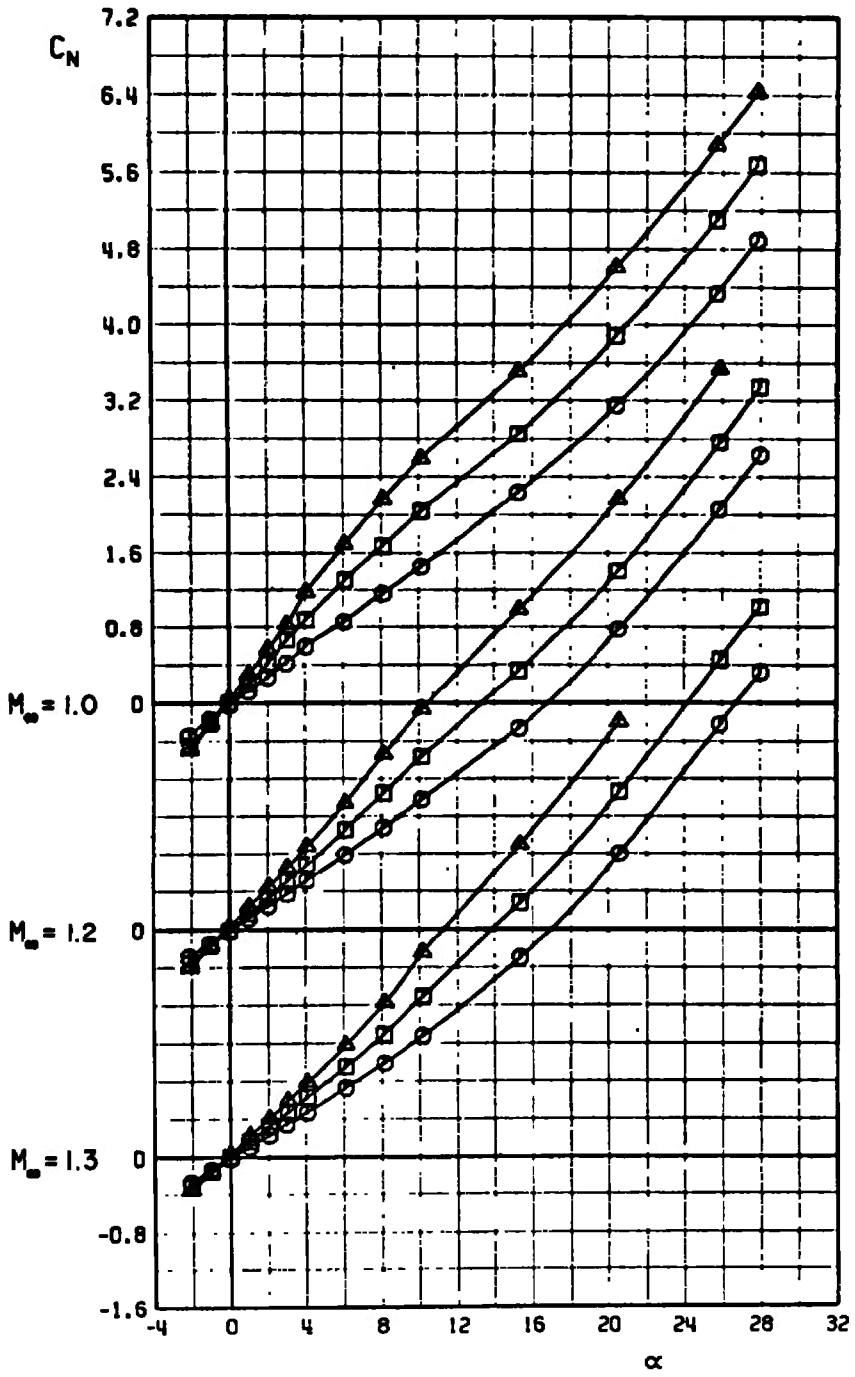

a. Concluded

Fig. 9 Continued

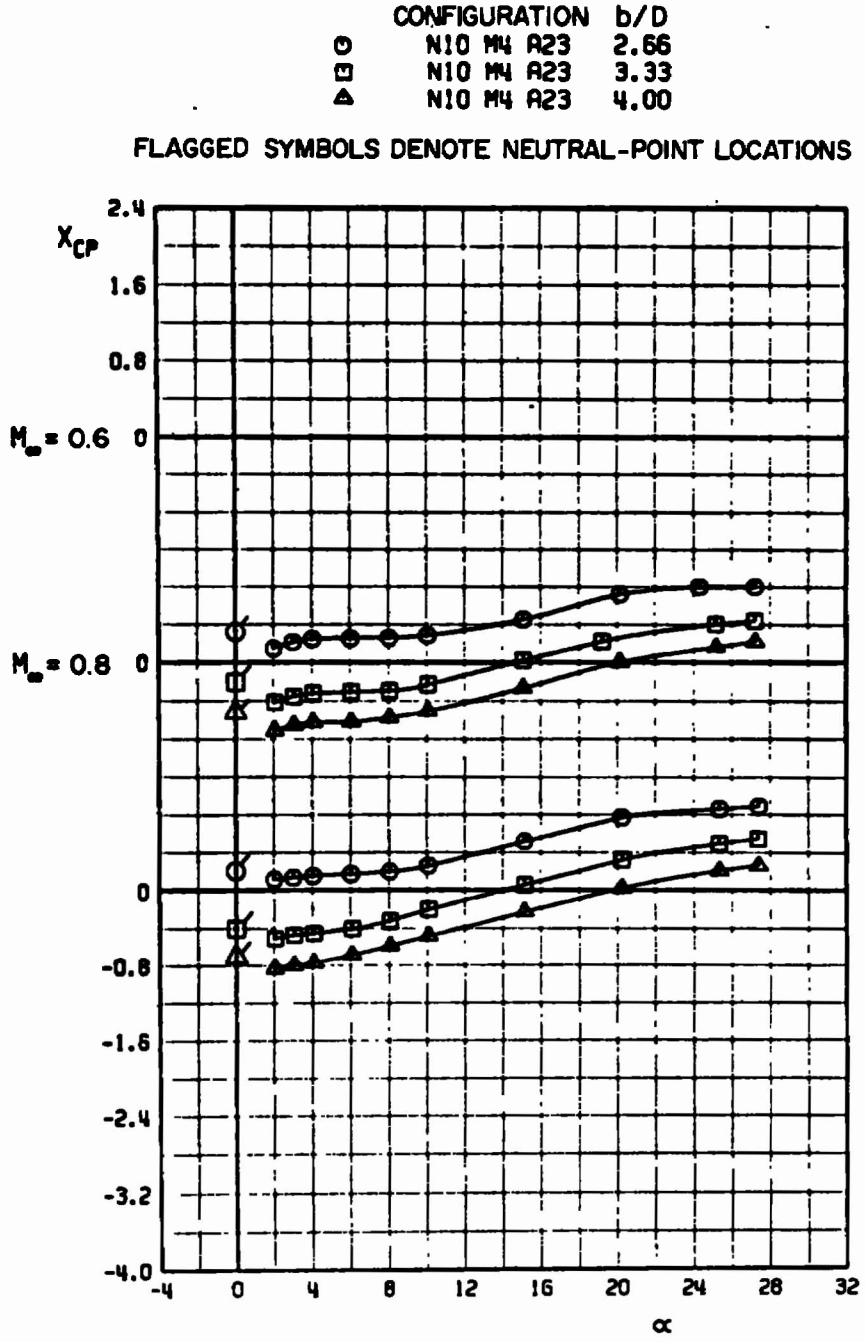

b. X_{cp} versus α

Fig. 9 Continued

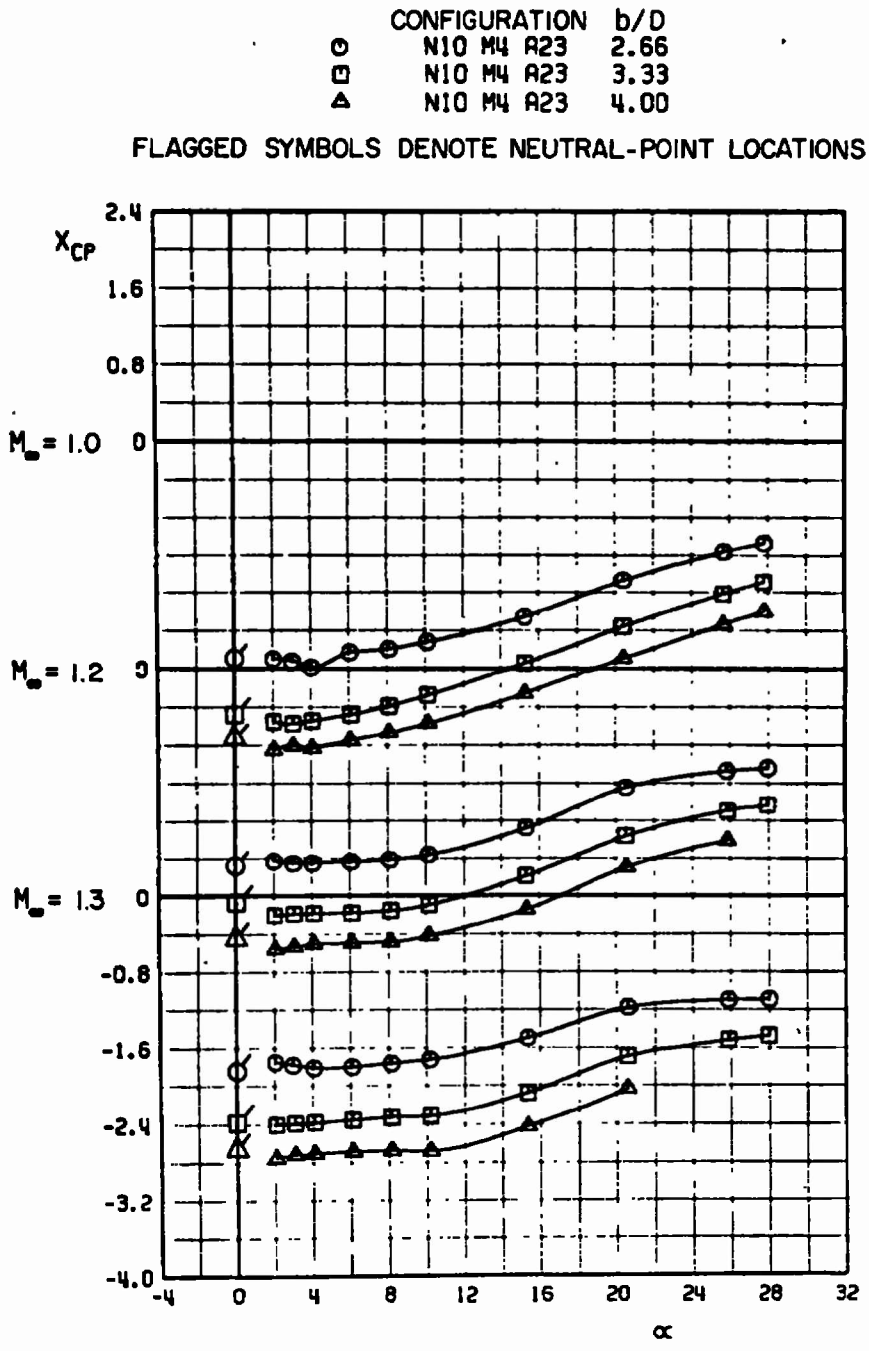

b. Concluded
Fig. 9 Continued

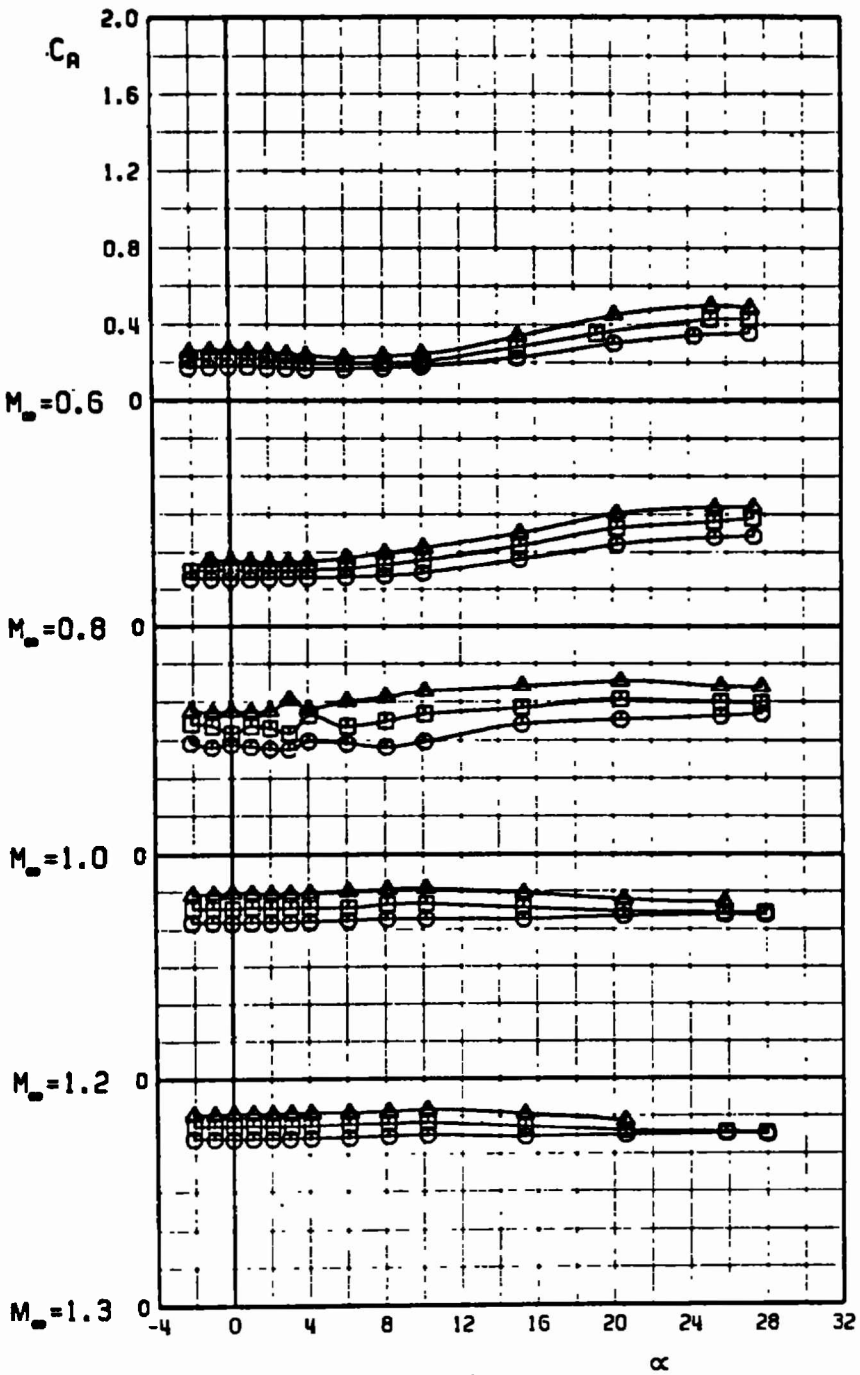

c. C_A versus α
Fig. 9 Continued

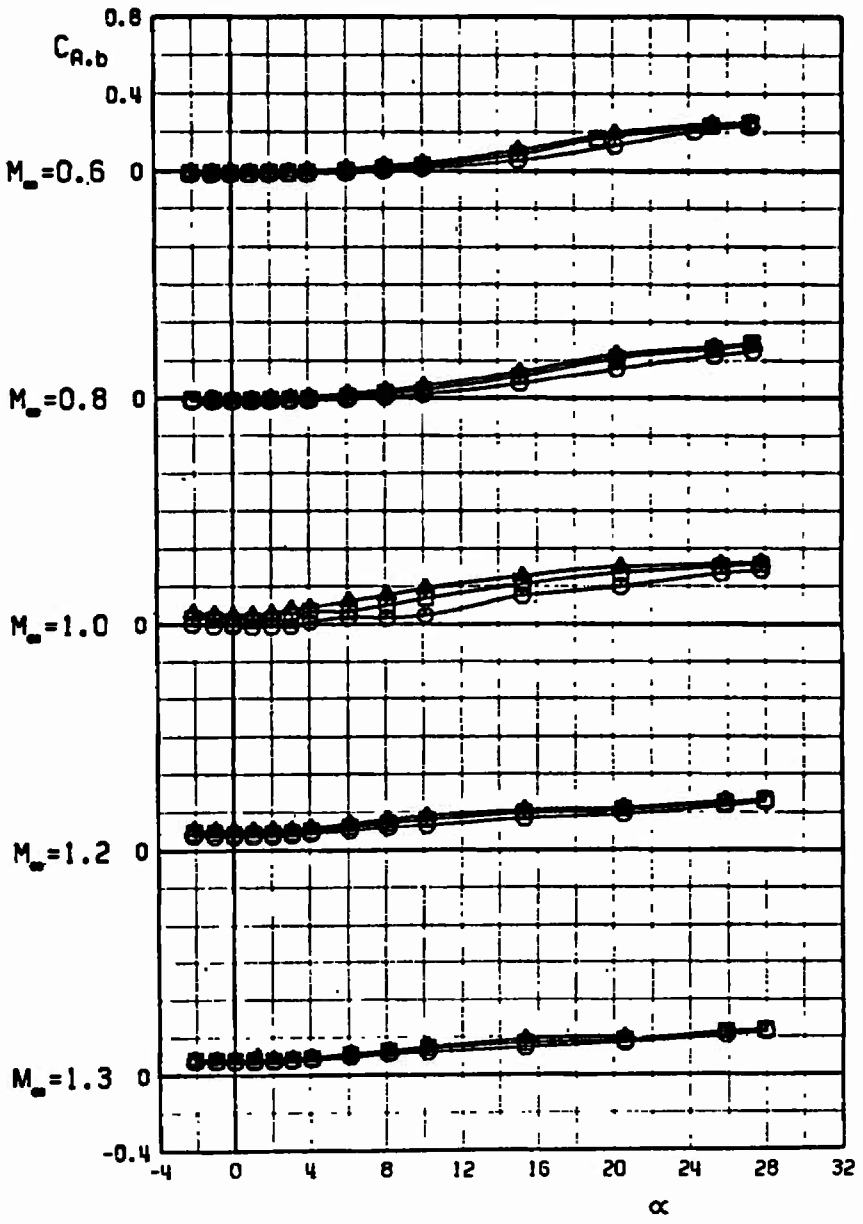

d. $C_{A,b}$ versus α
Fig. 9 Continued

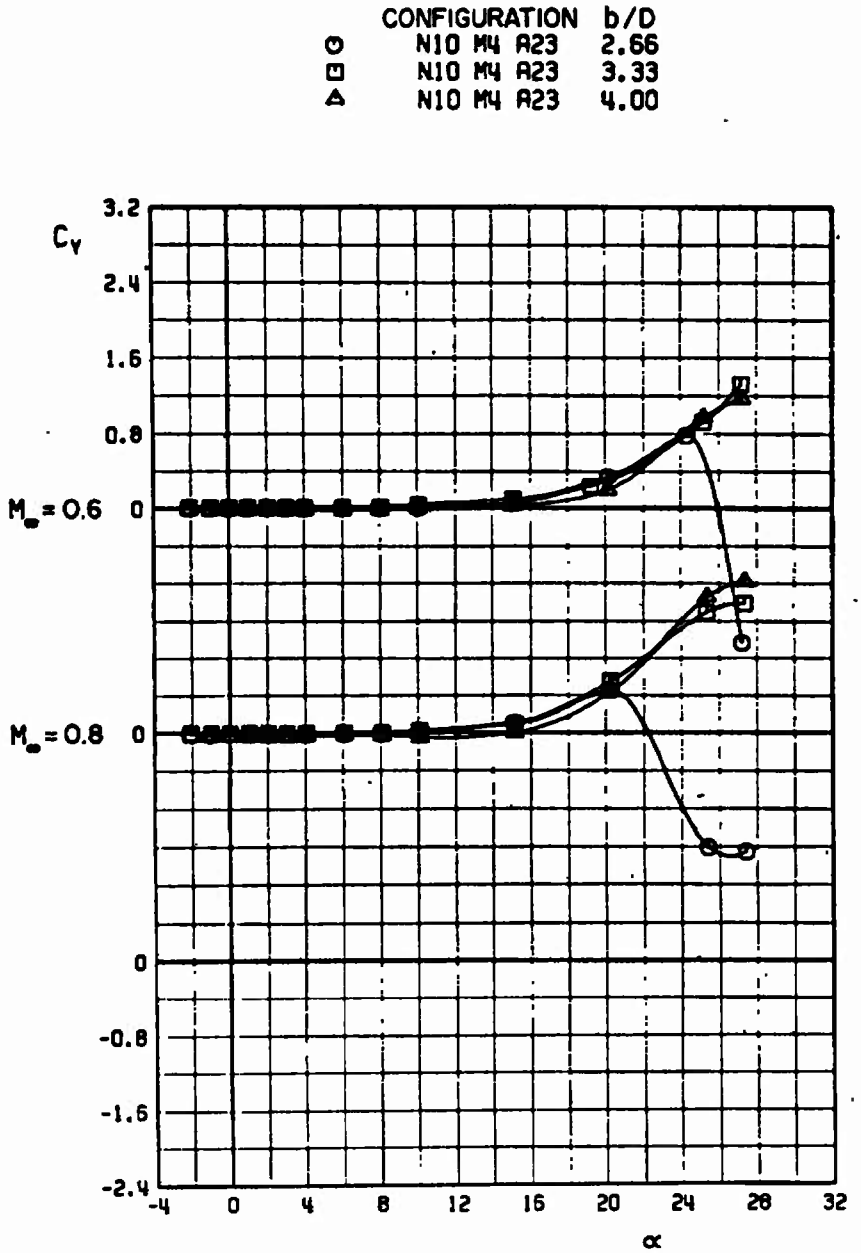

e. C_Y versus α

Fig. 9 Continued

	CONFIGURATION	b/D
⊙	N10 M4 A23	2.66
⊡	N10 M4 A23	3.33
△	N10 M4 A23	4.00

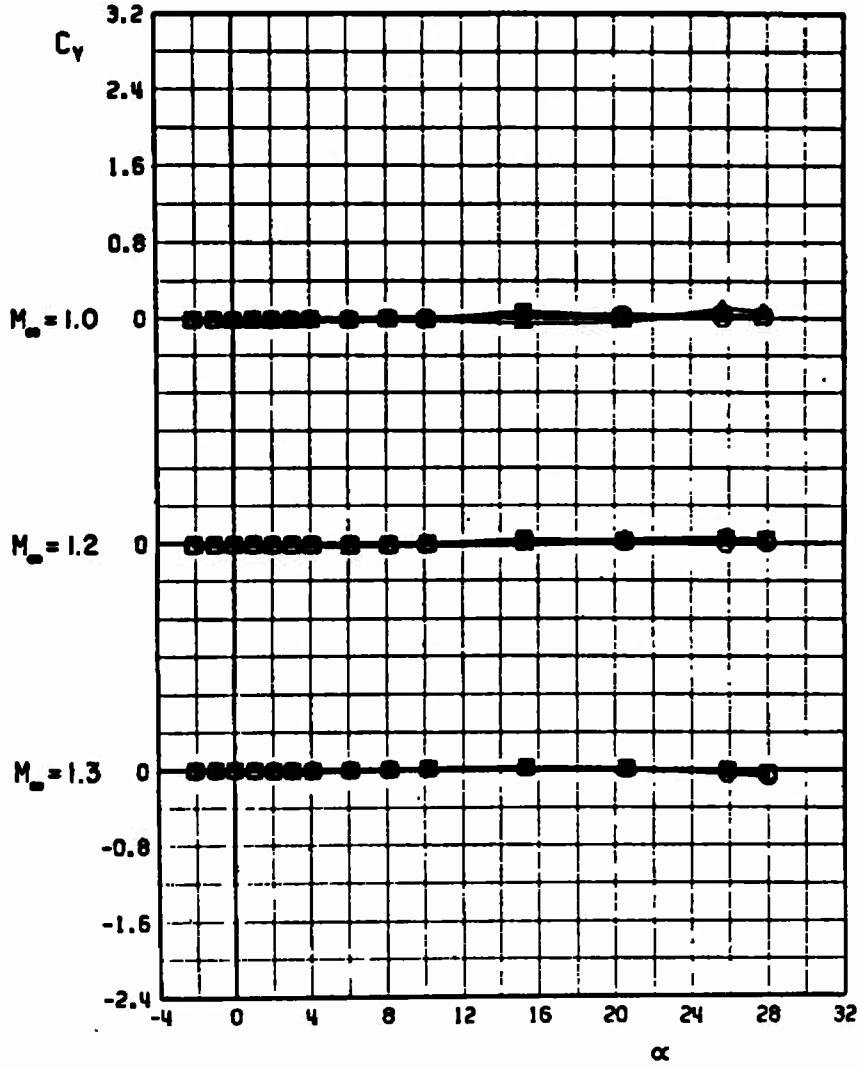

e. Concluded

Fig. 9 Continued

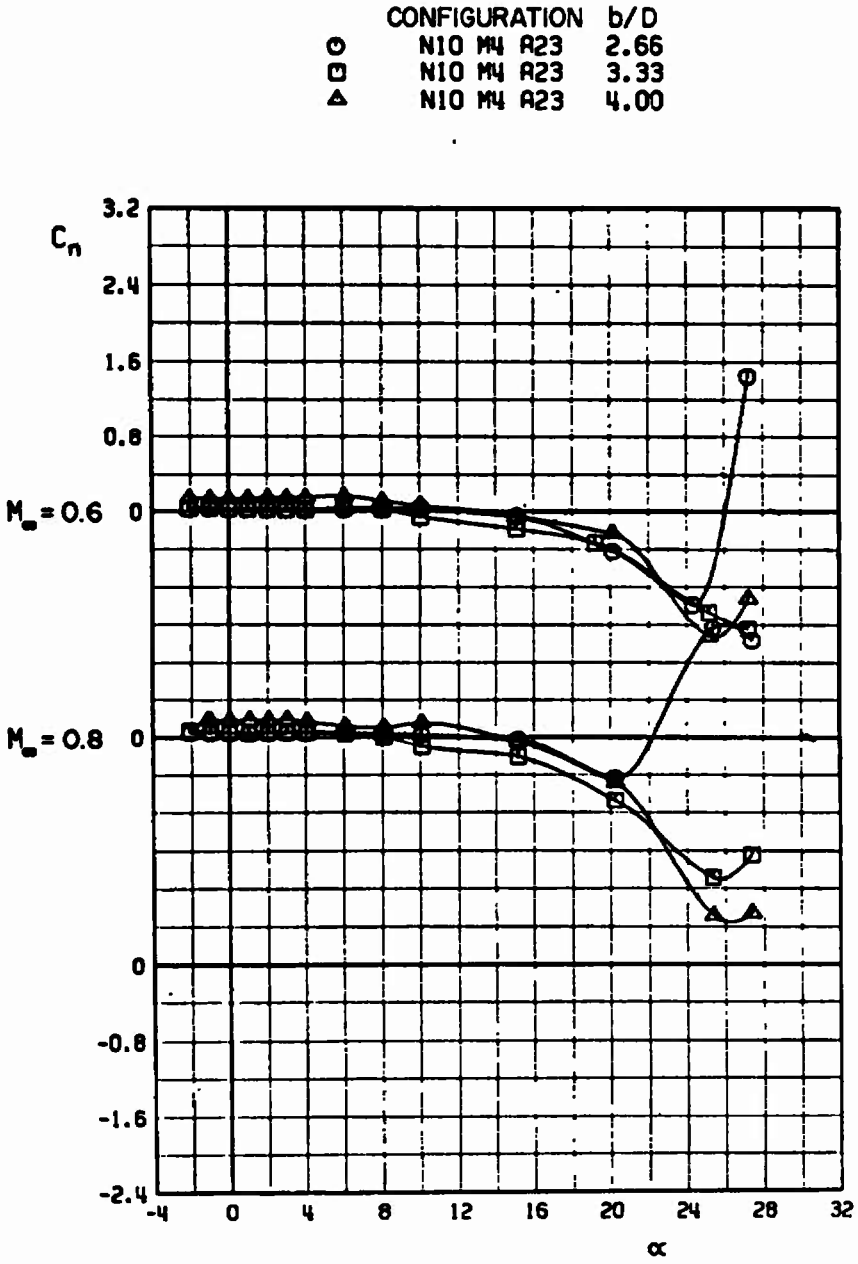

f. C_n versus α

Fig. 9 Continued

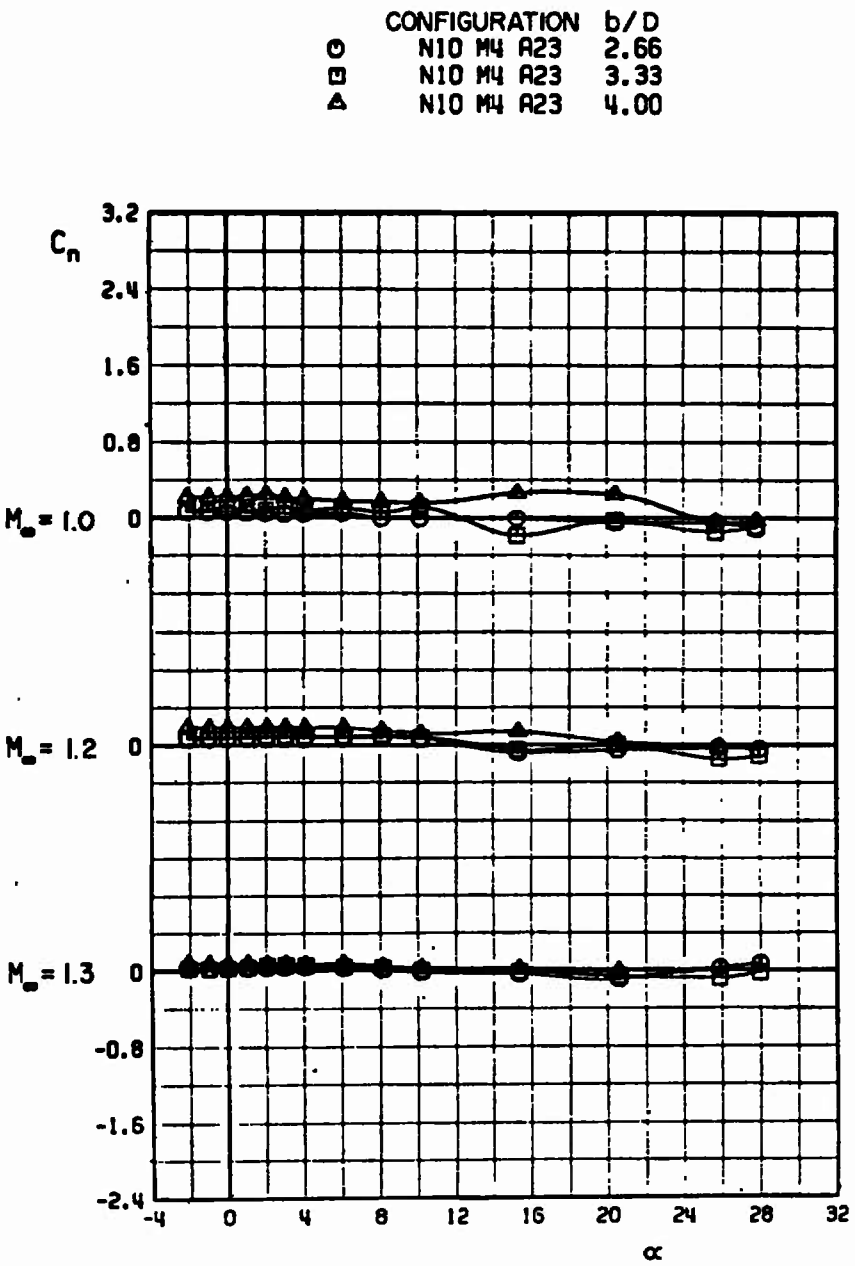

f. Concluded
Fig. 9 Continued

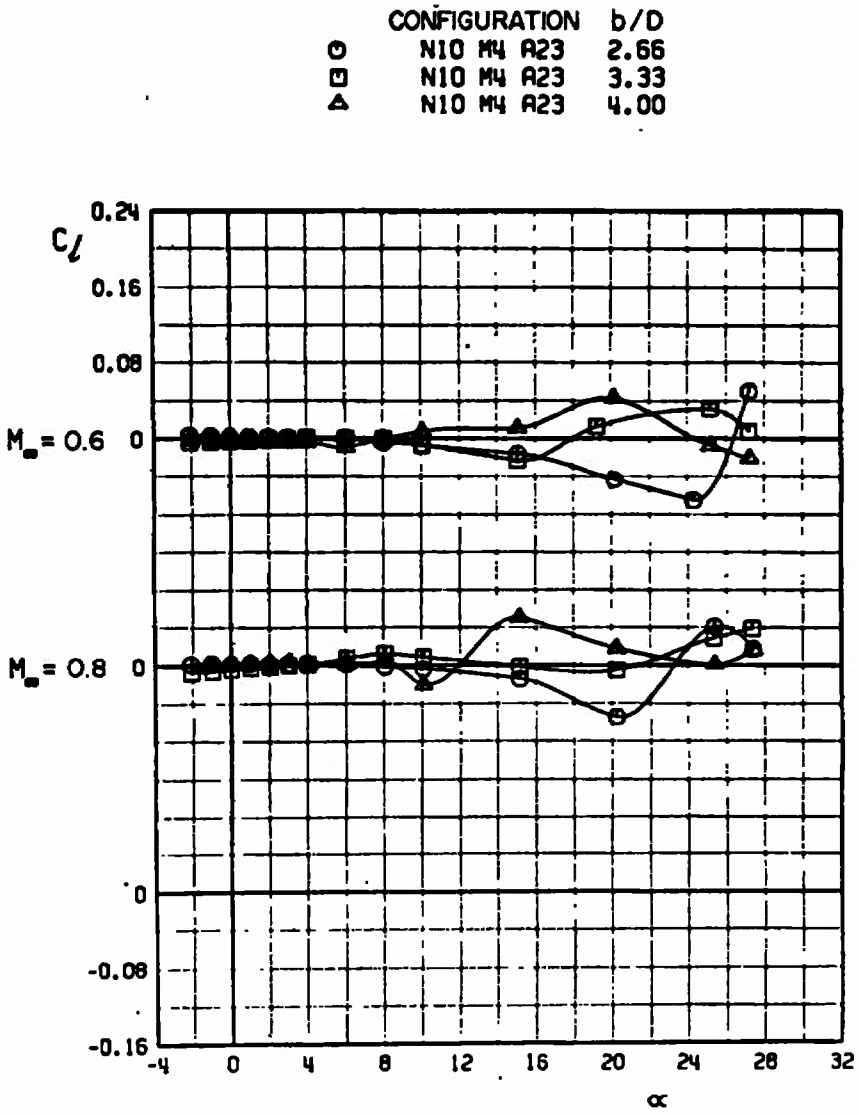

g. C_ℓ versus α

Fig. 9 Continued

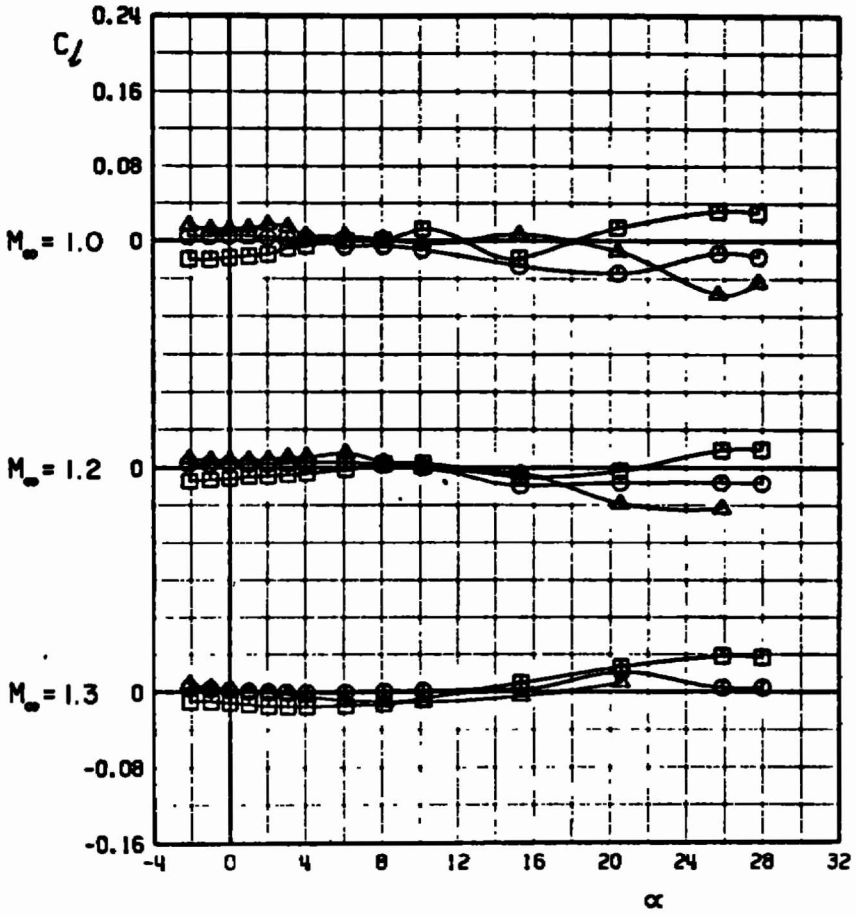

g. Concluded
Fig. 9 Concluded

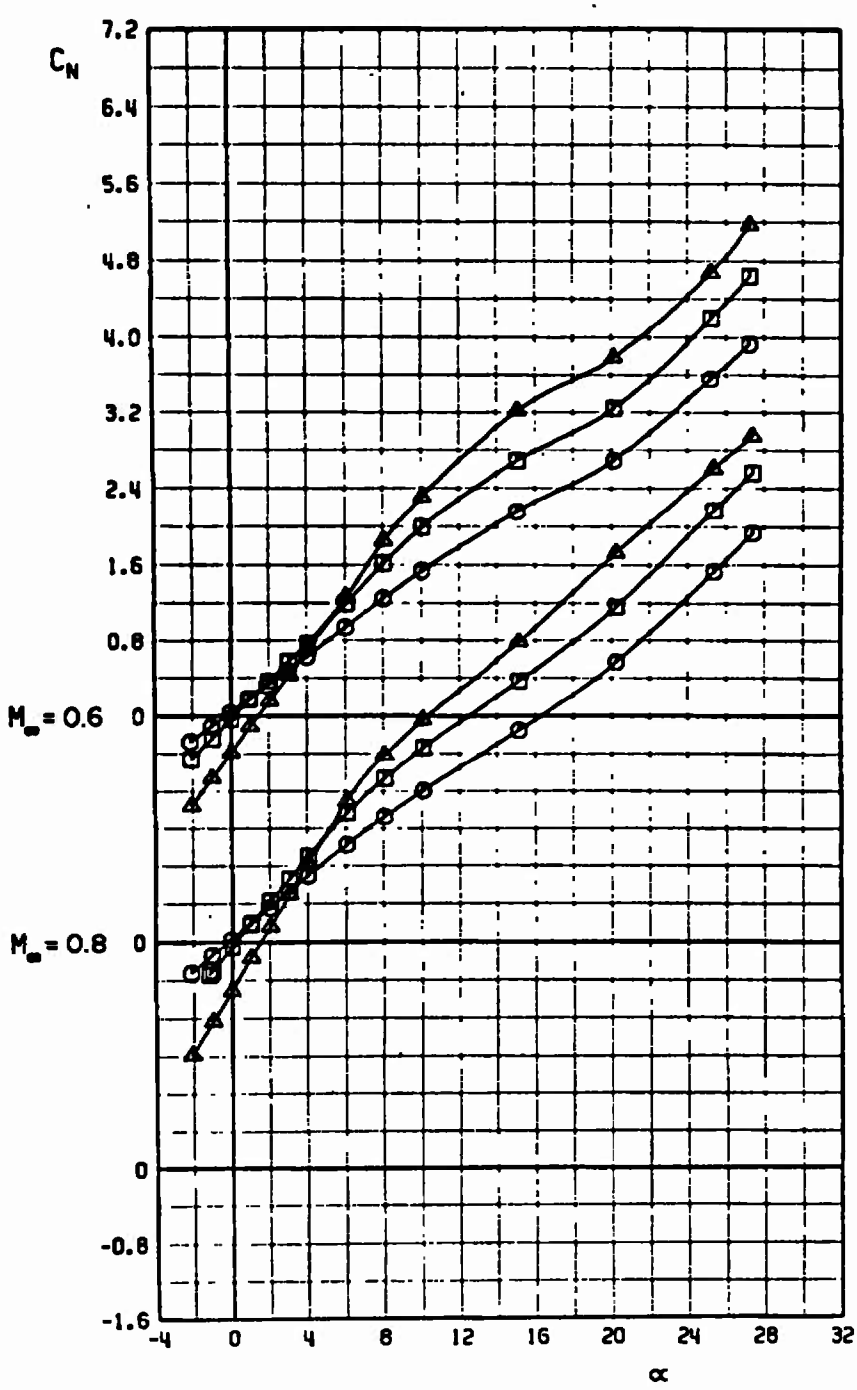

a. C_N versus α

Fig. 10 Aerodynamic Coefficients of Configurations N10M4A24, b/D = 2.66, 3.33, and 4.00

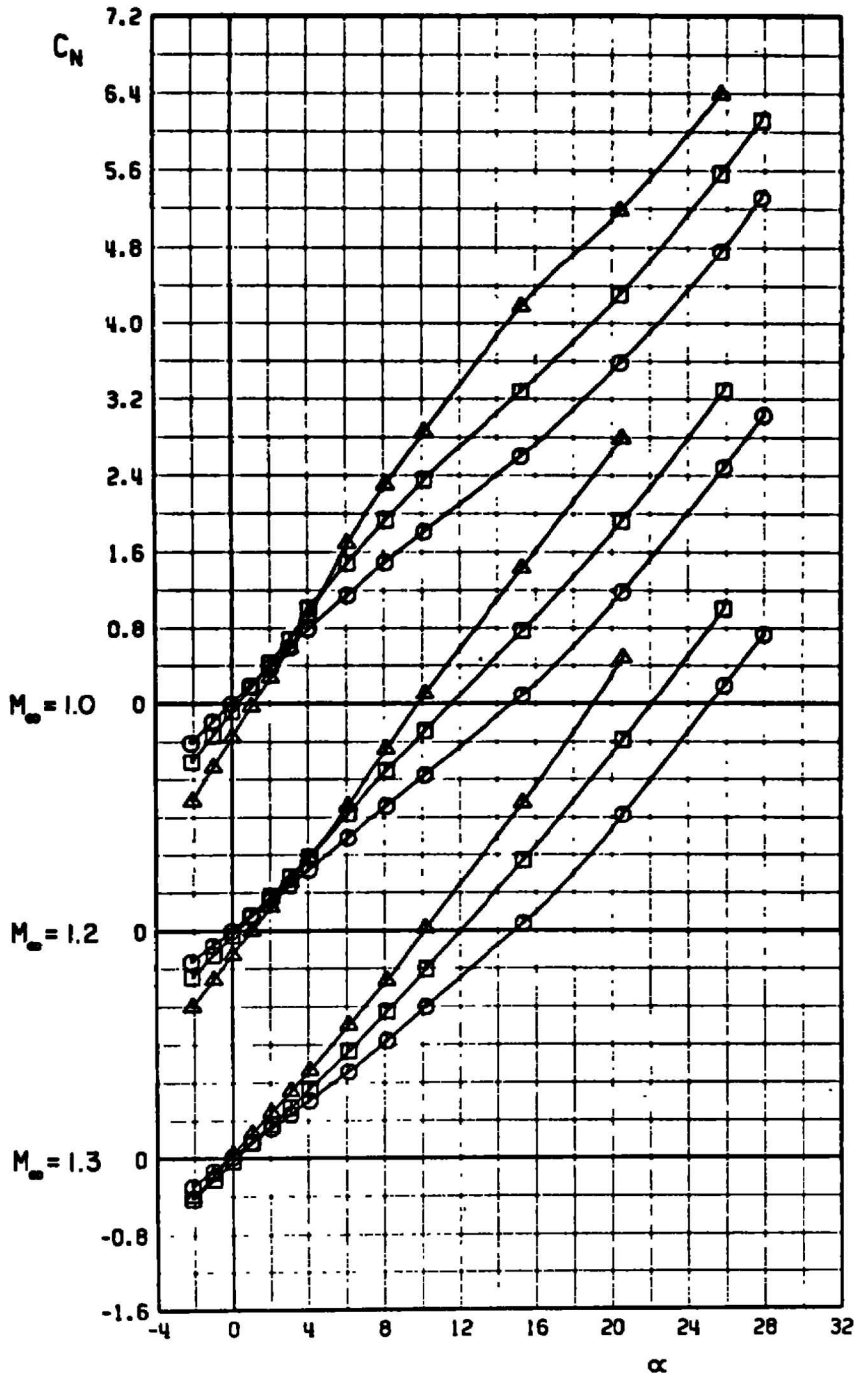

a. Concluded

Fig. 10 Continued

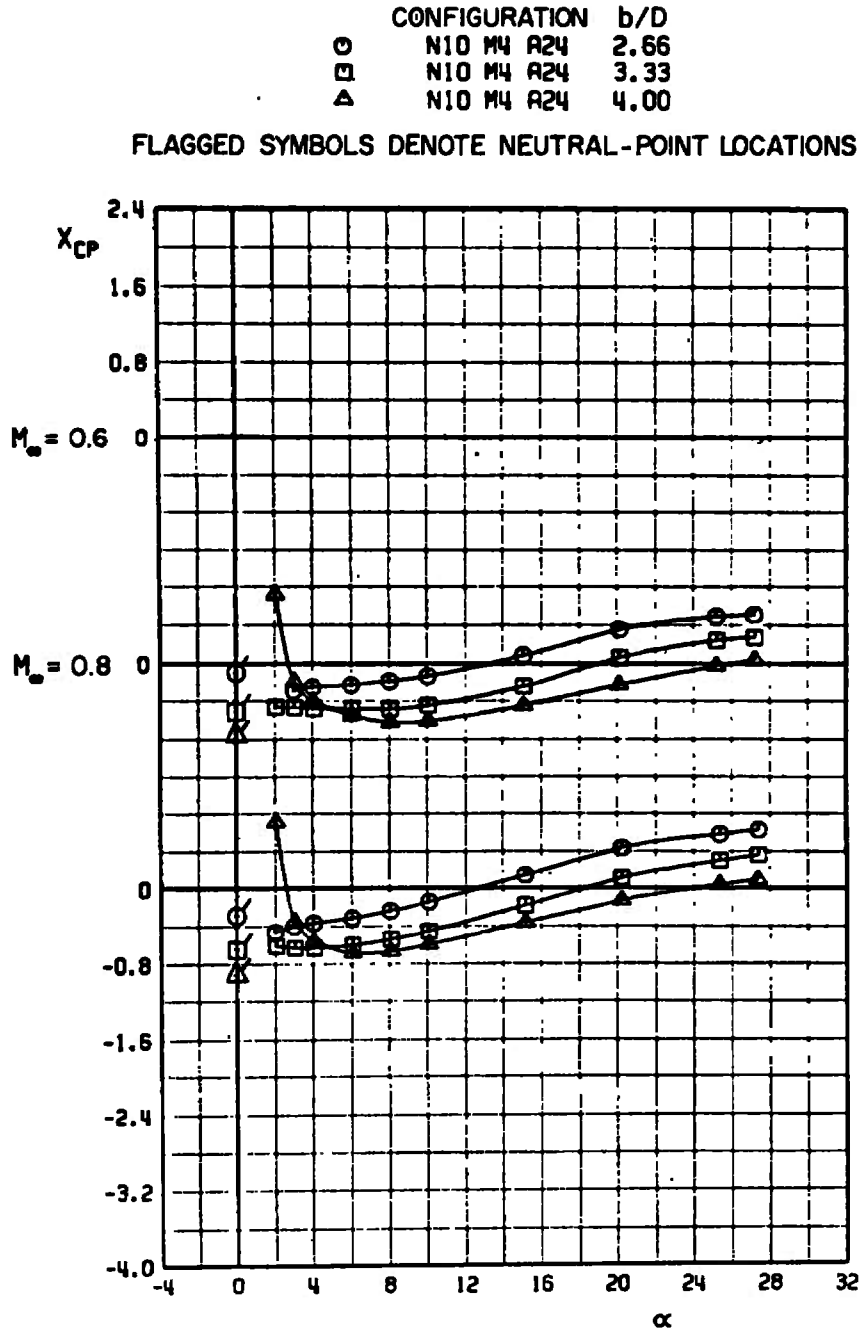

b. X_{cp} versus α

Fig. 10 Continued

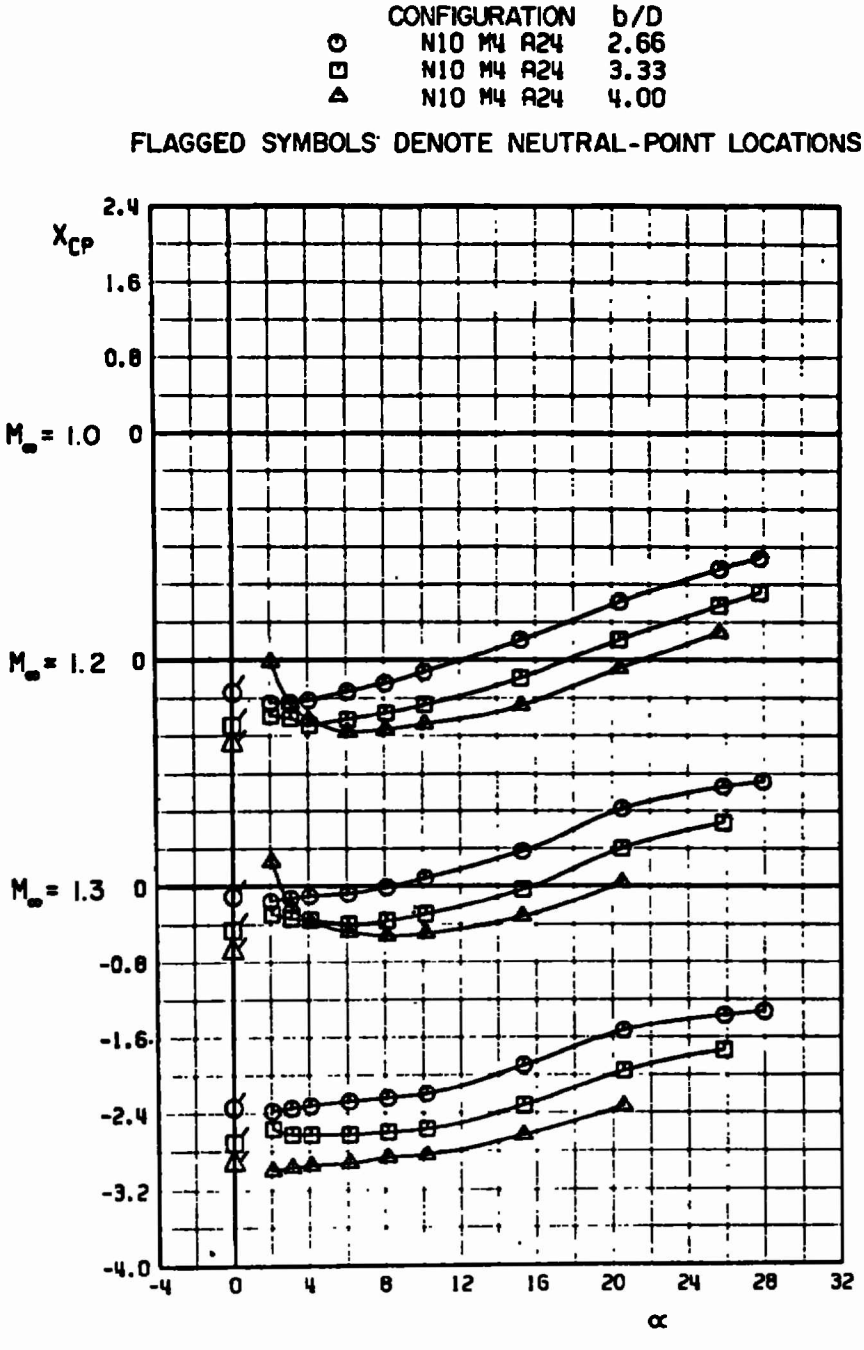

b. Concluded
Fig. 10 Continued

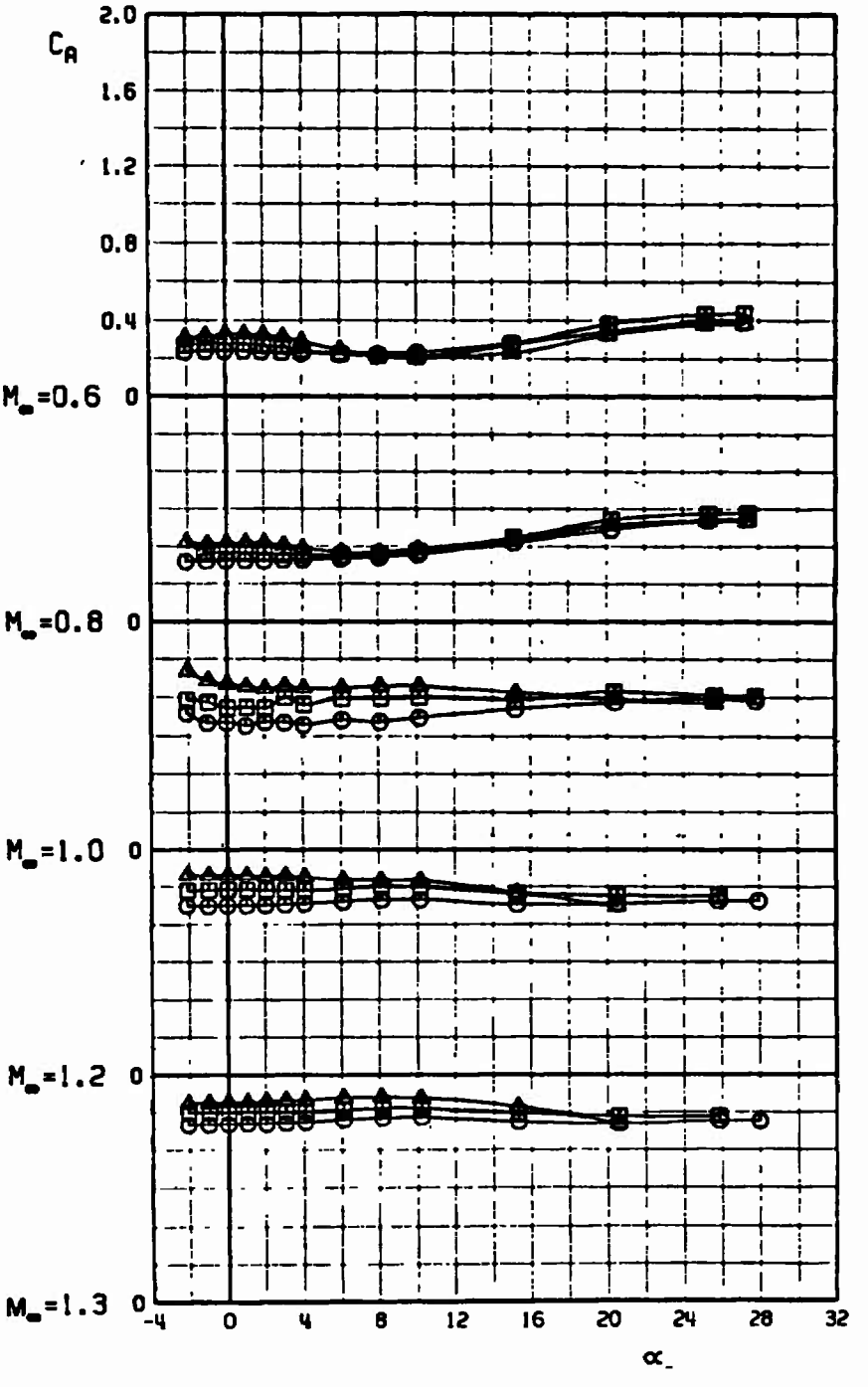

c. C_A versus α

Fig. 10 Continued

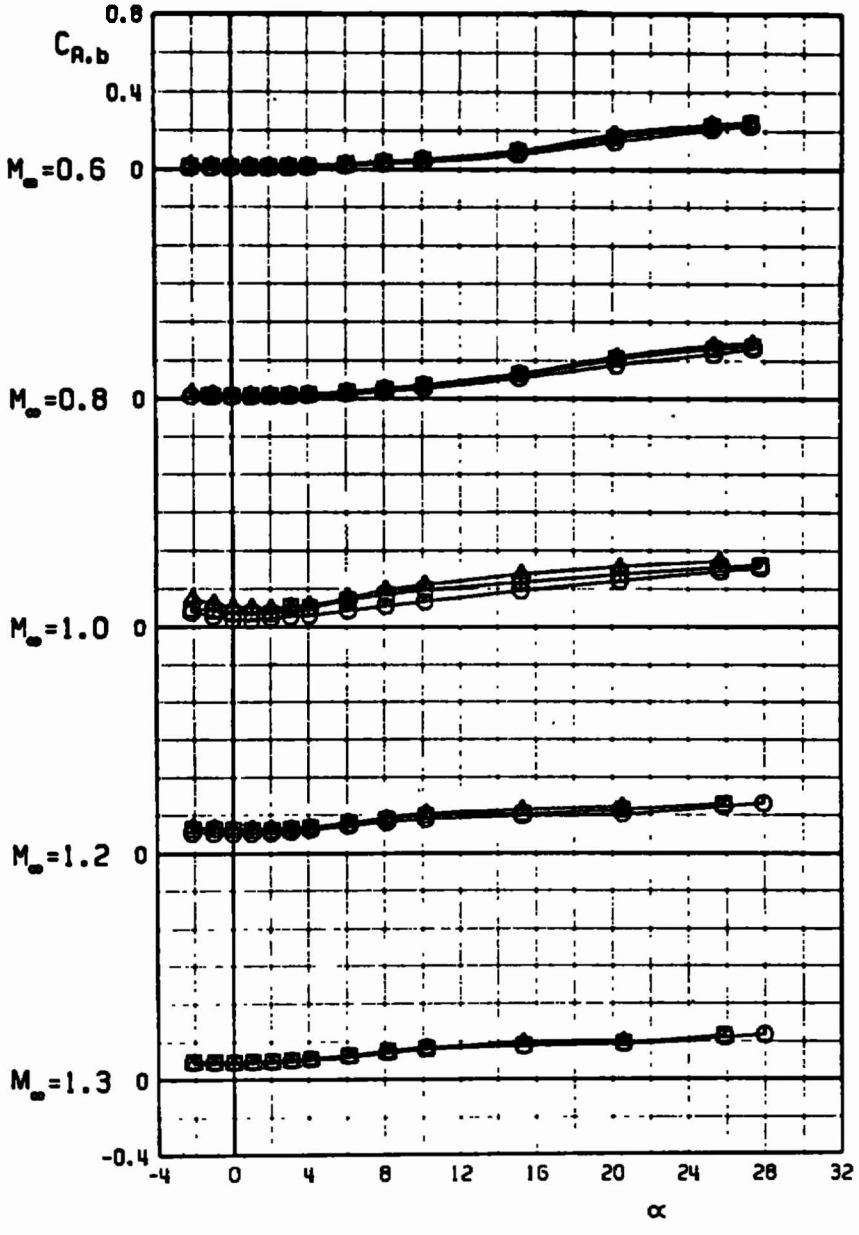

d. $C_{A,b}$ versus α
Fig. 10 Continued

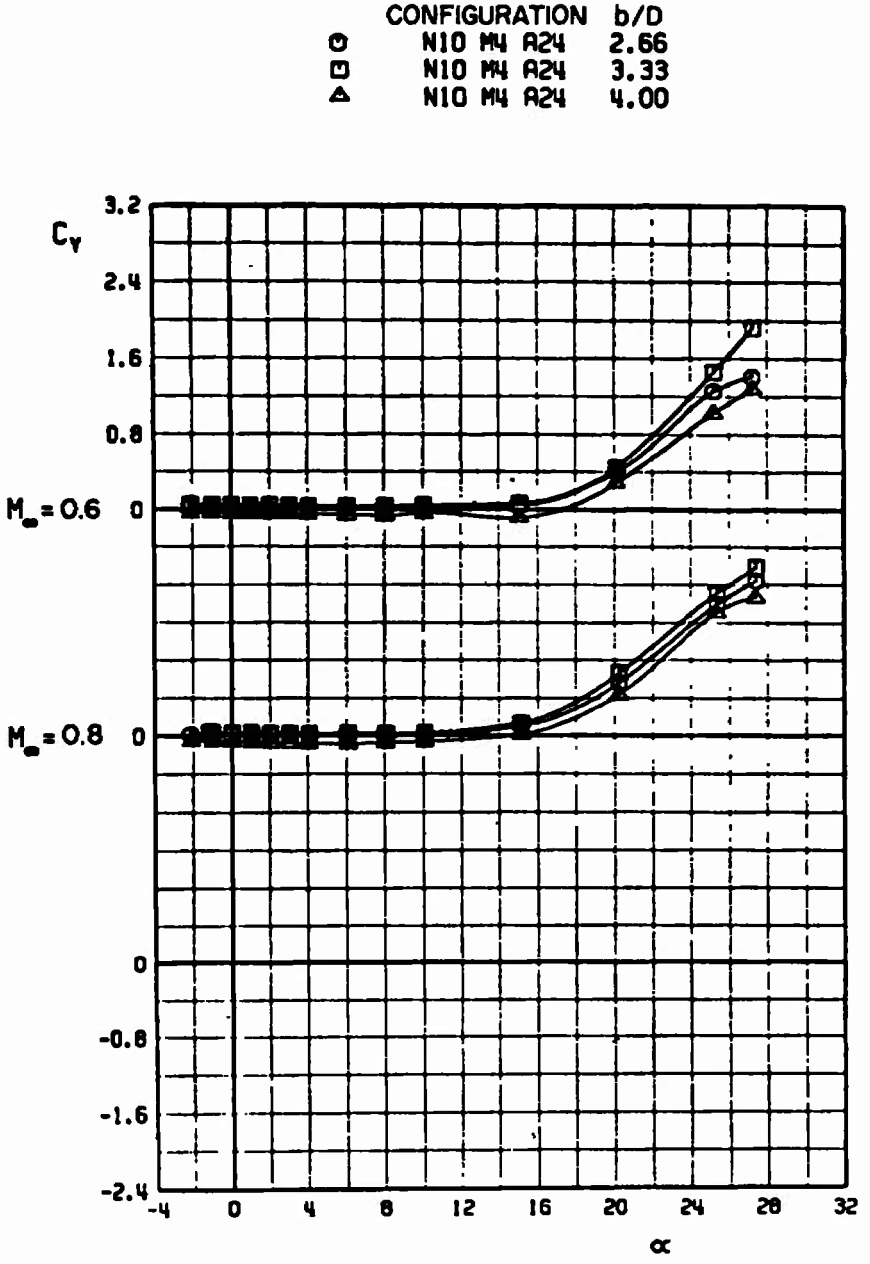

e. C_Y versus α

Fig. 10 Continued

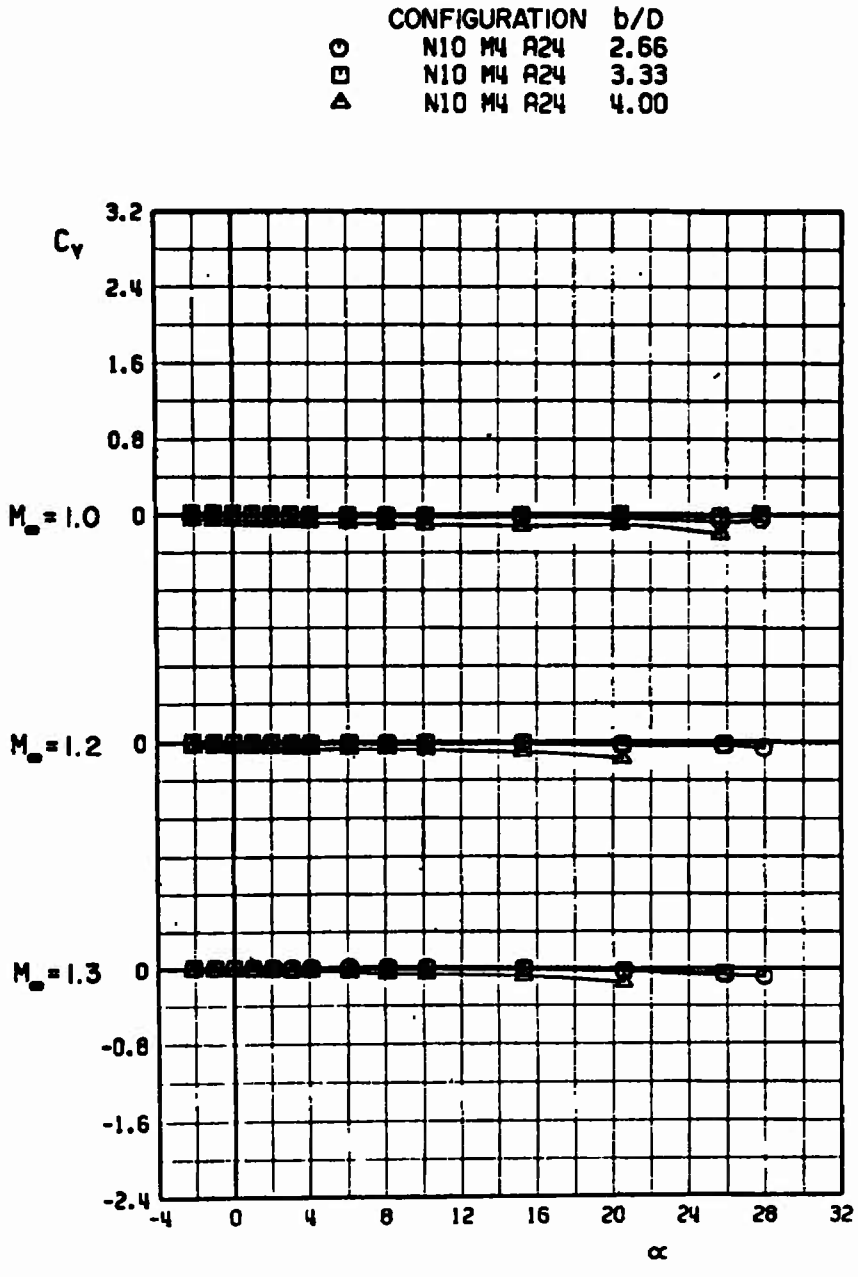

e. Concluded
Fig. 10 Continued

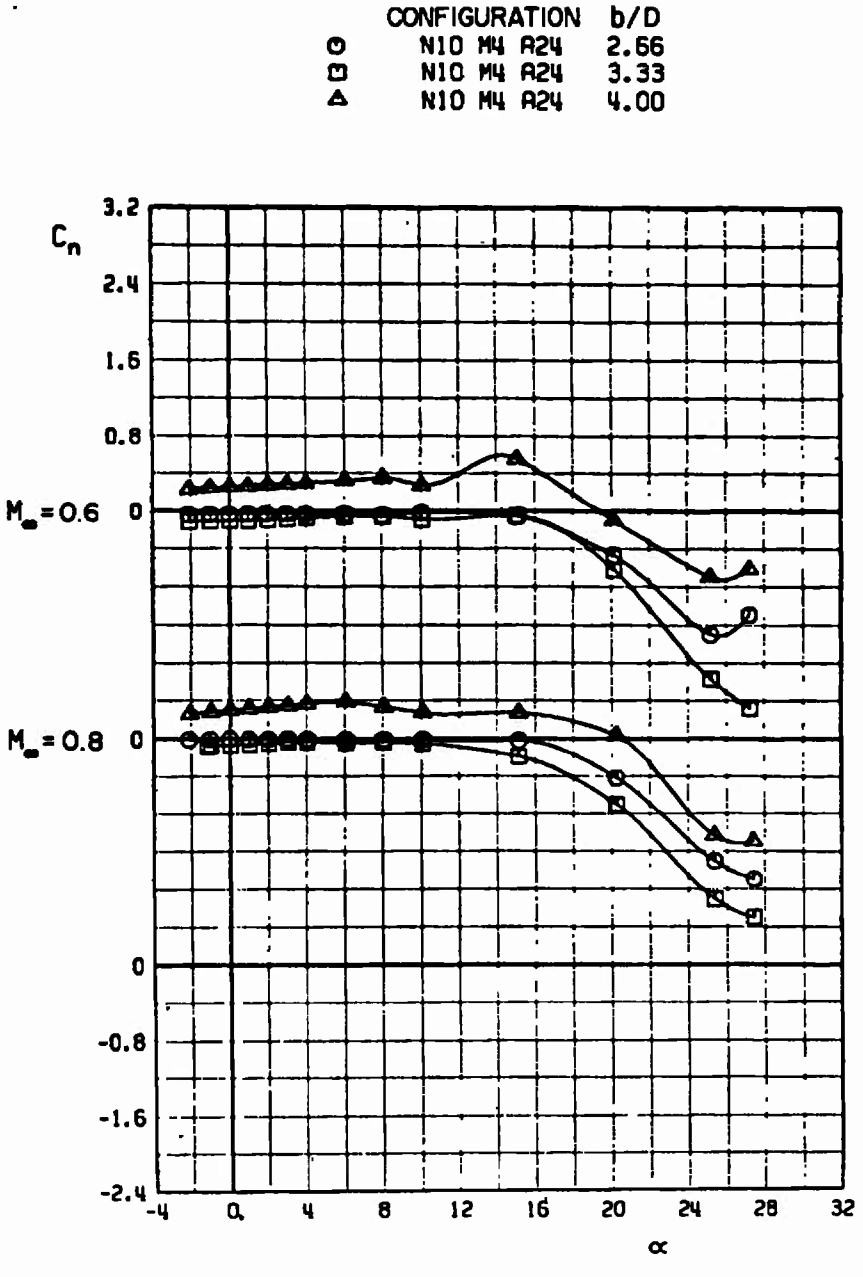

f. C_n versus α
Fig. 10 Continued

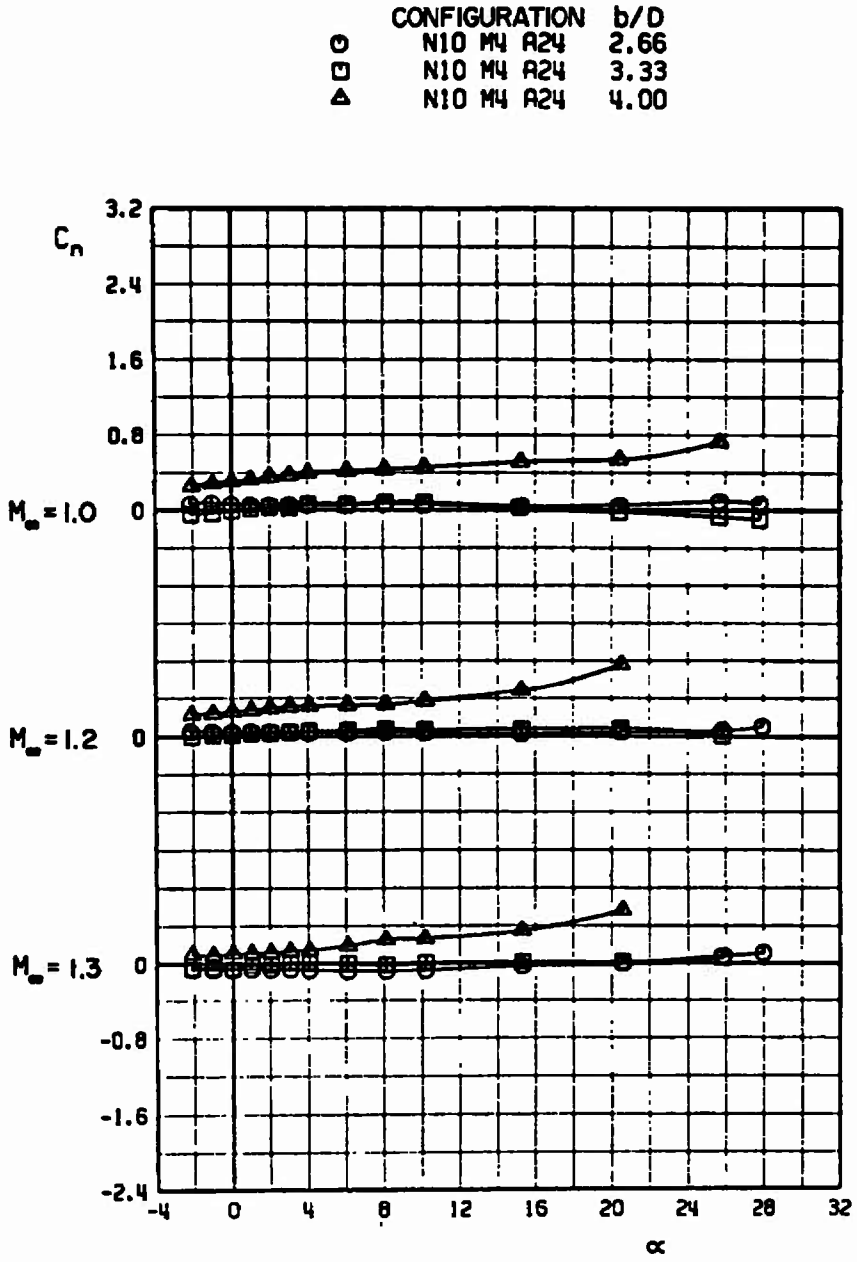

f. Concluded
Fig. 10 Continued

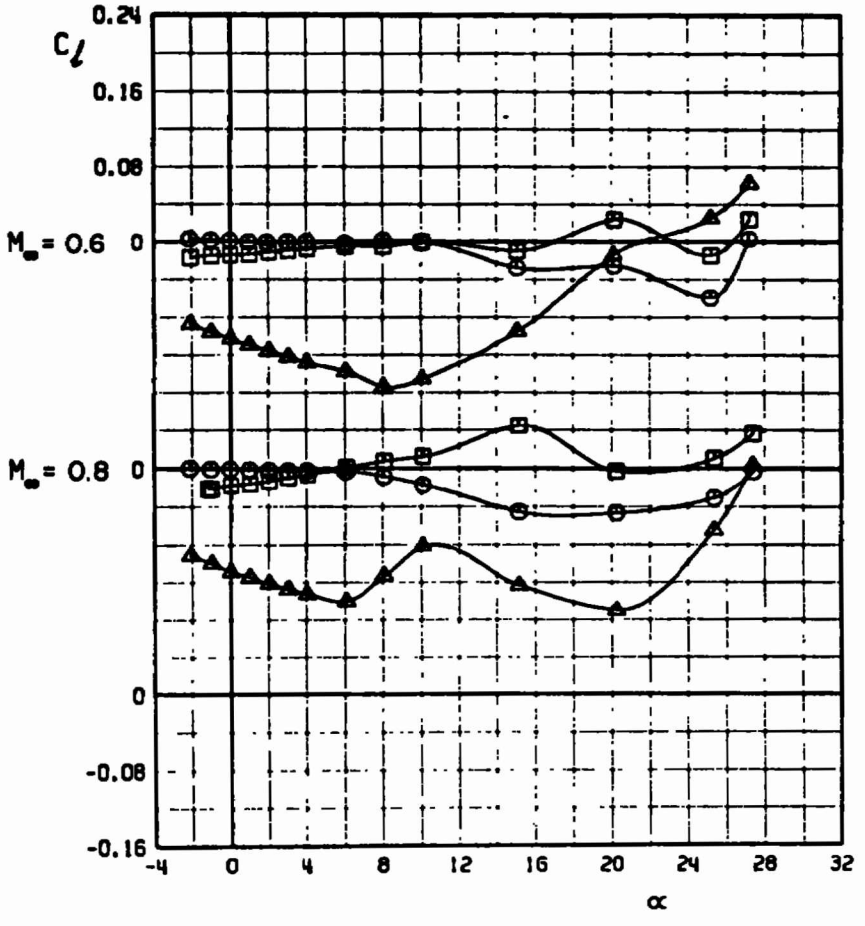

g. C_ℓ versus α
Fig. 10 Continued

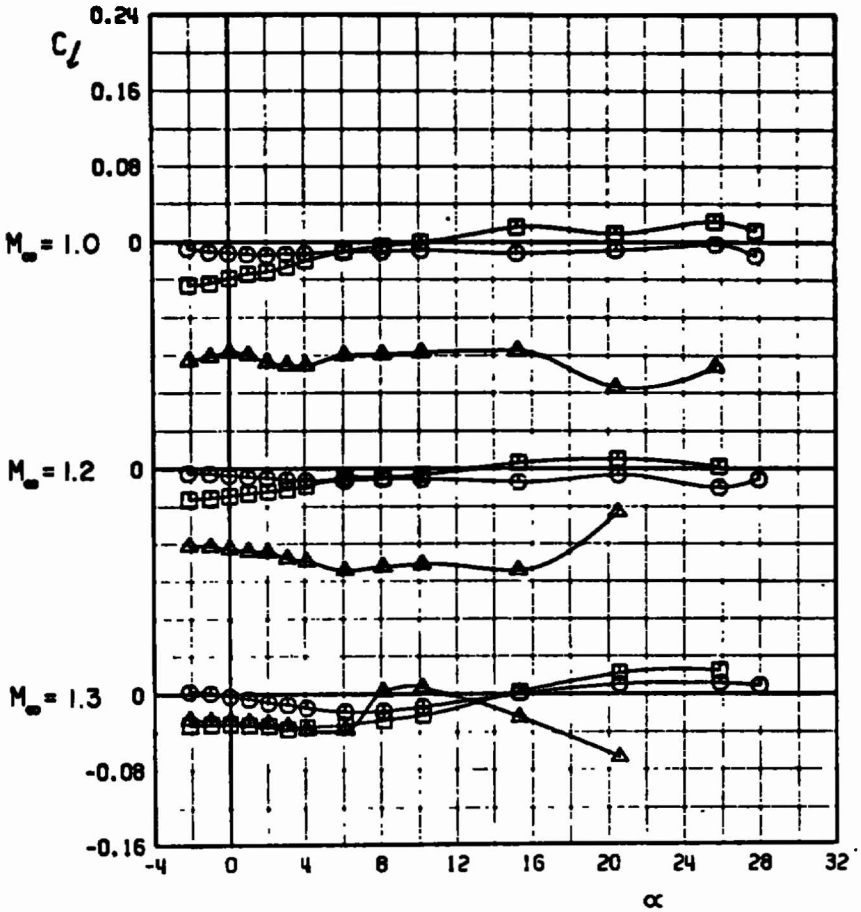

g. Concluded
Fig. 10 Concluded

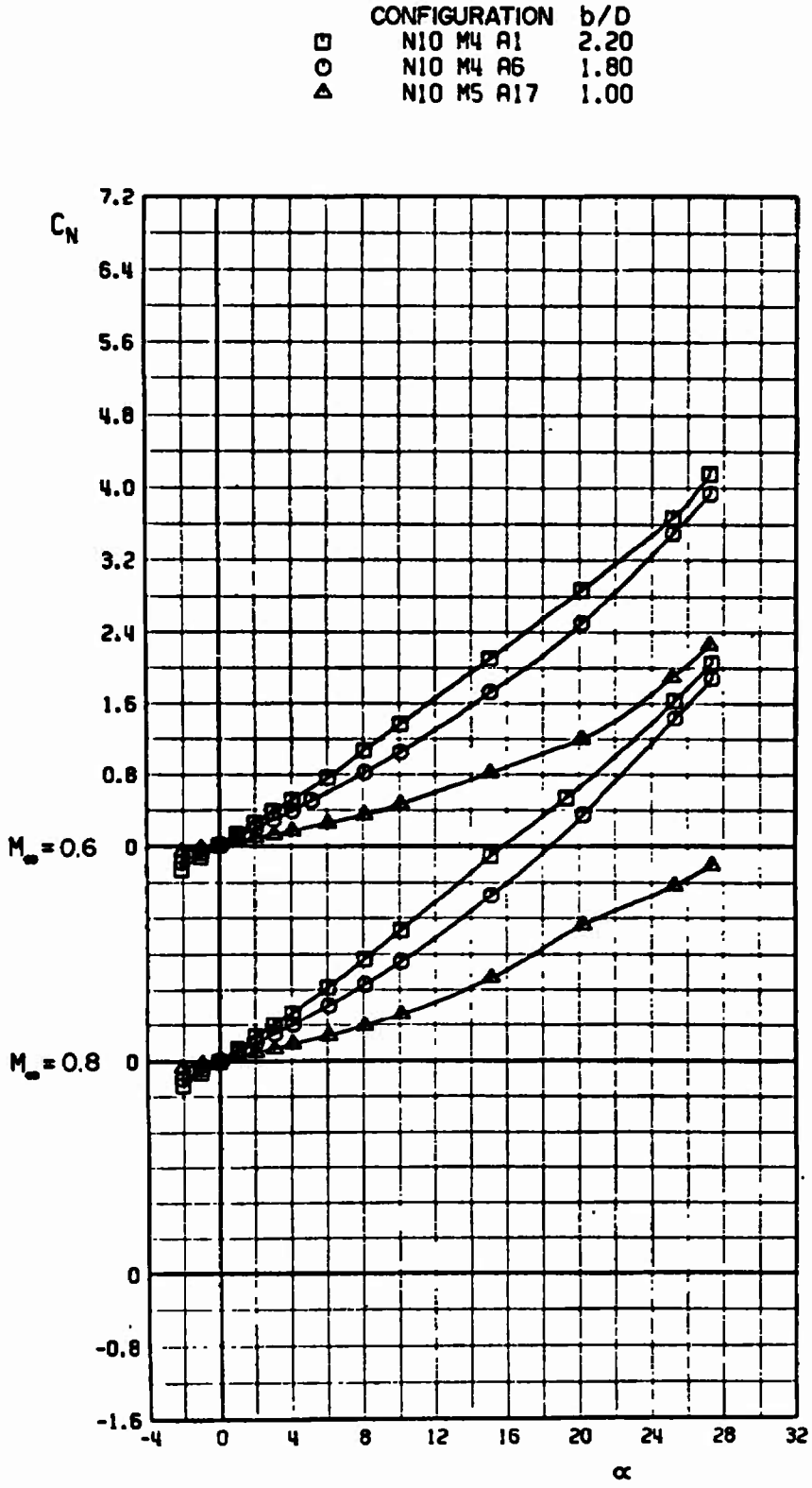

a. C_N versus α

Fig. 11 Aerodynamic Coefficients of Configuration N10M4A1, b/D = 2.20, Configuration N10M4A6, b/D = 1.80, and Configuration N10M5A17, b/D = 1.00

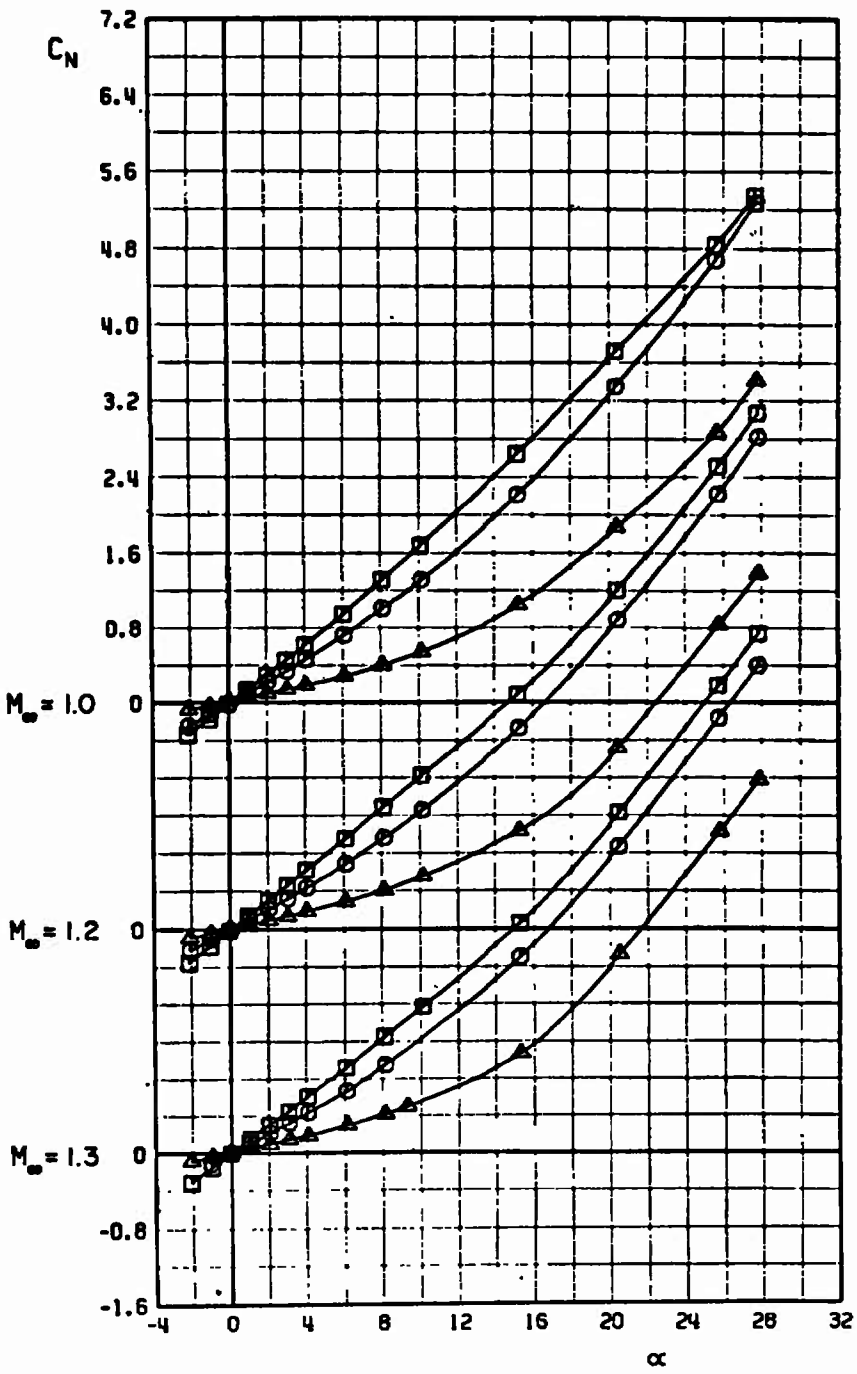

a. Concluded

Fig. 11 Continued

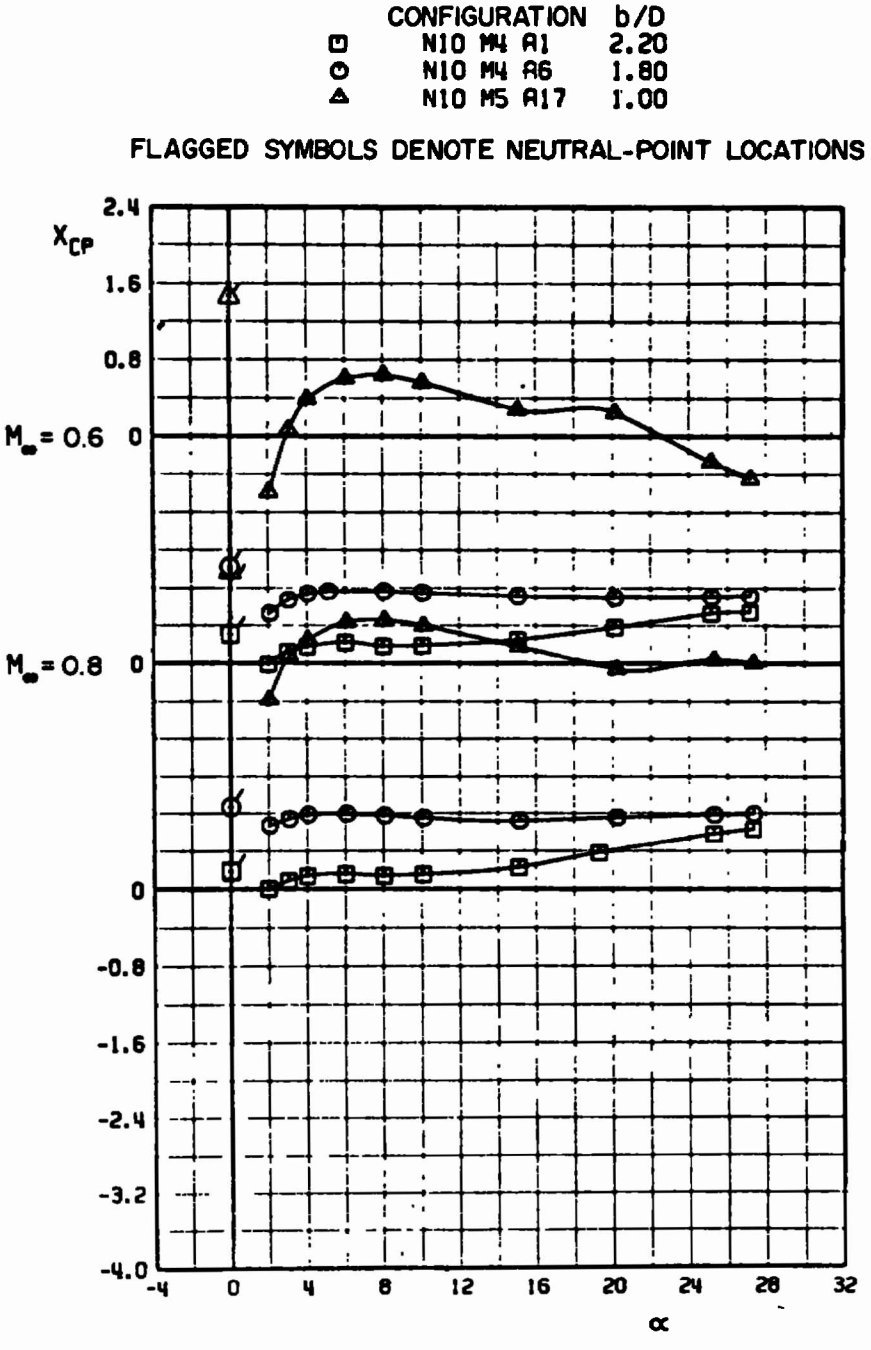

b. X_{cp} versus α

Fig. 11 Continued

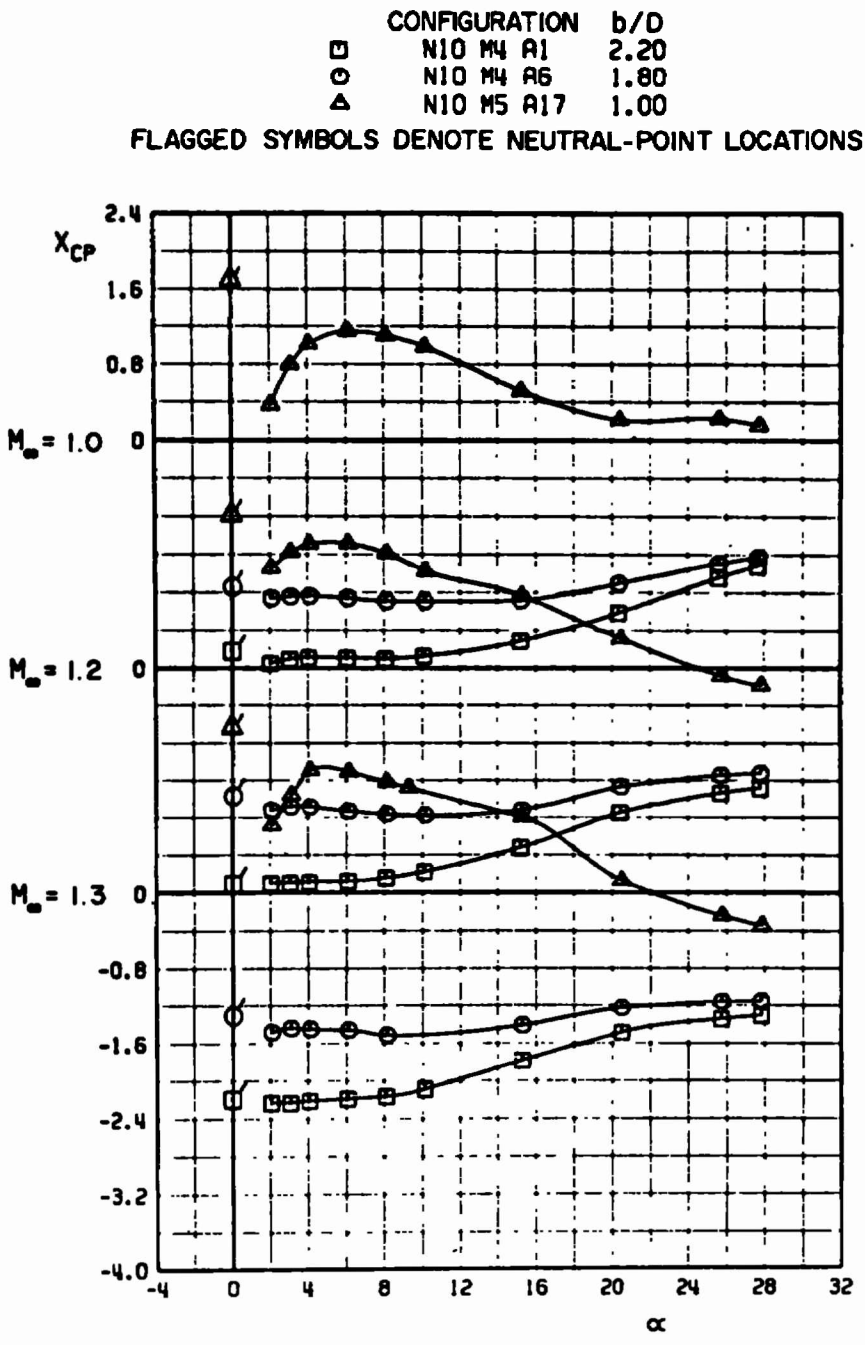

b. Concluded

Fig. 11 Continued

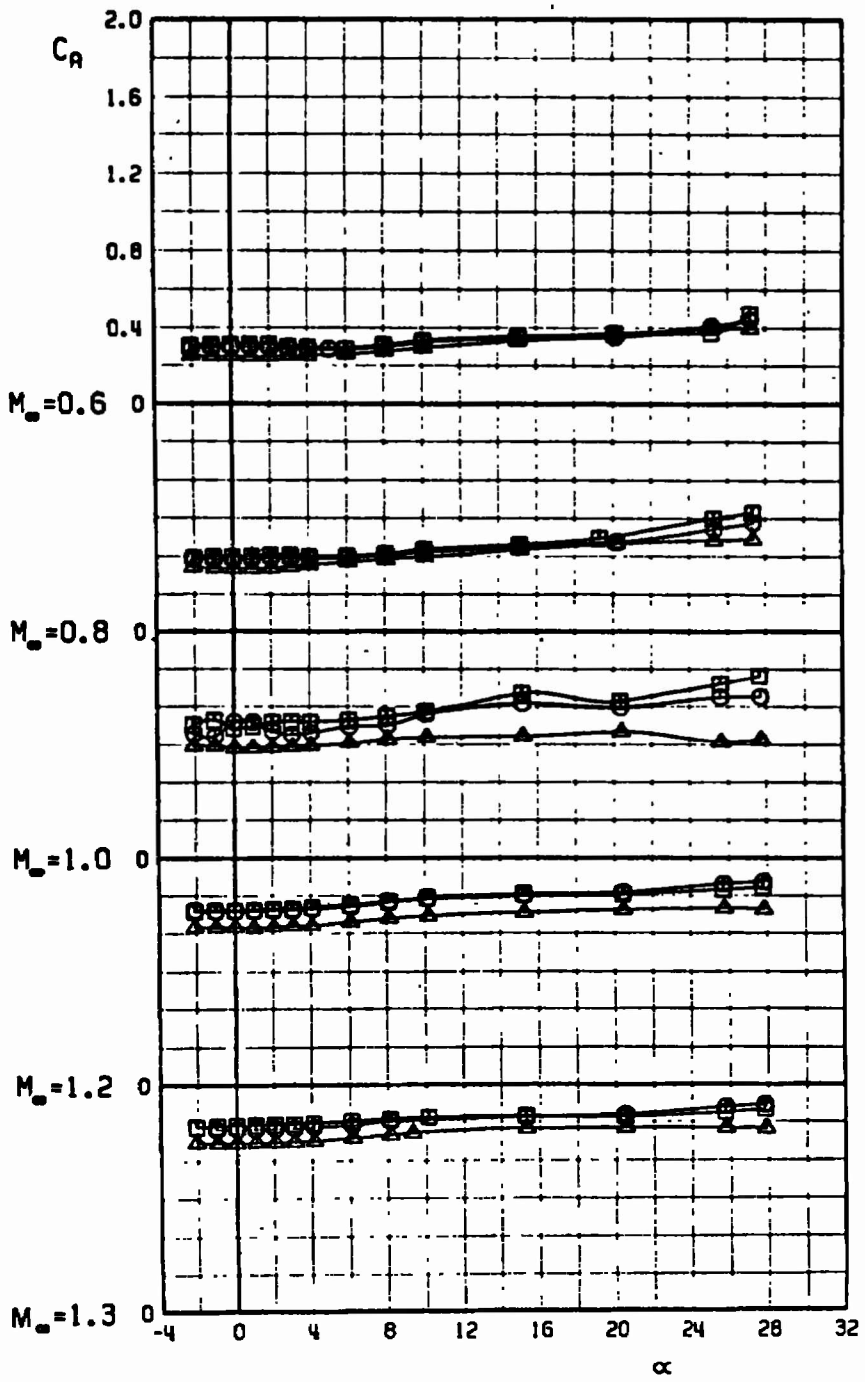

c. C_A versus α

Fig. 11 Continued

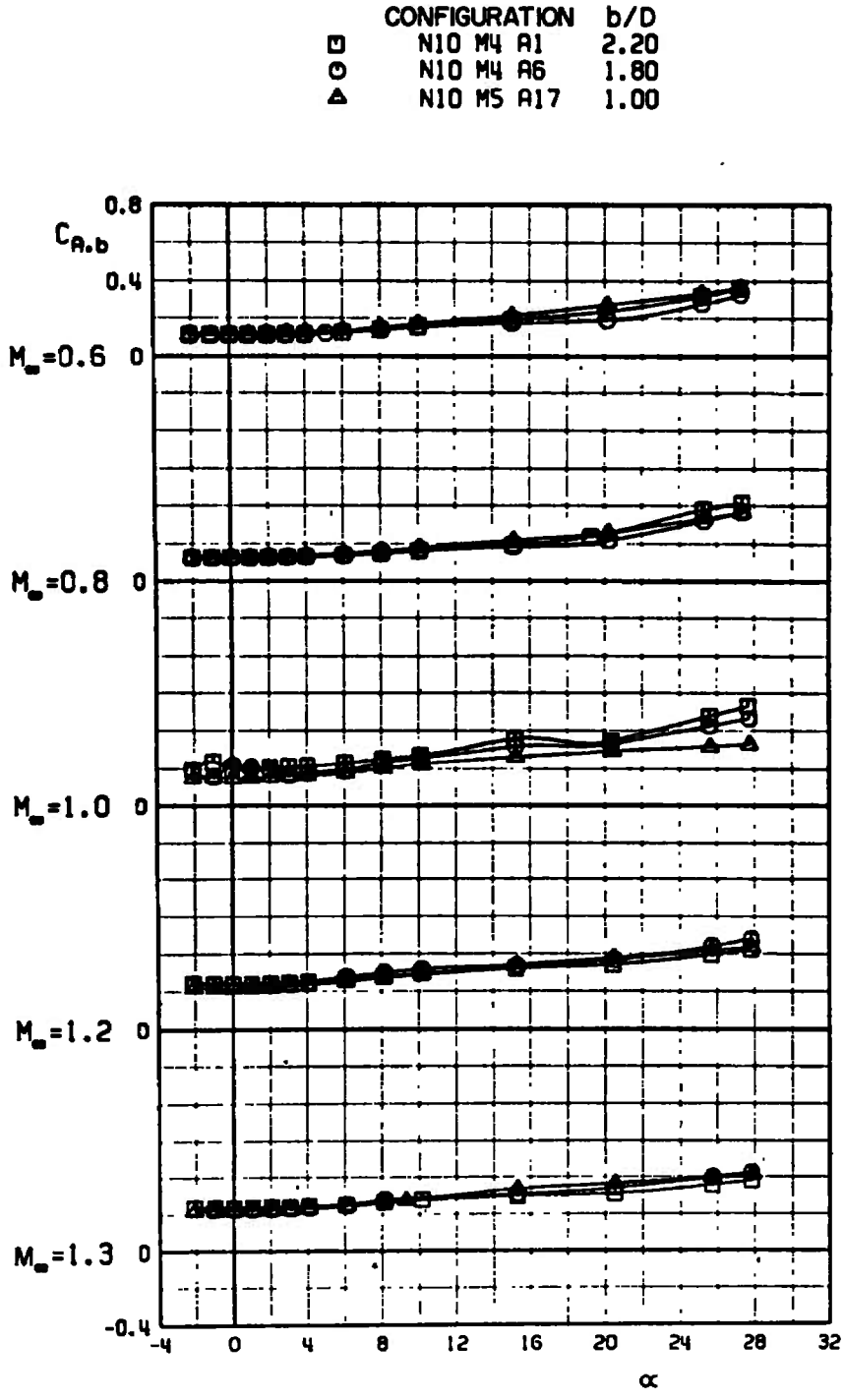

d. $C_{A,b}$ versus α
Fig. 11 Continued

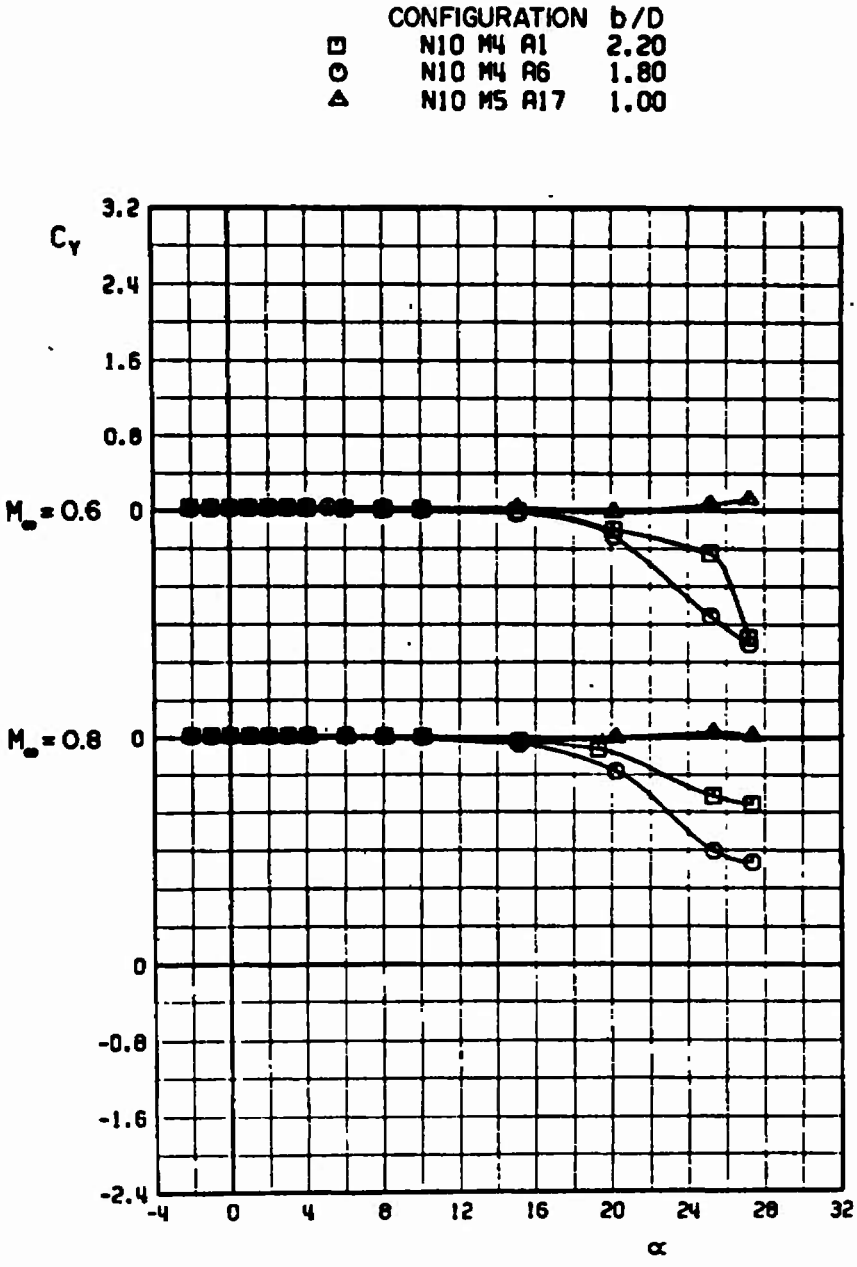

e. C_Y versus α

Fig. 11 Continued

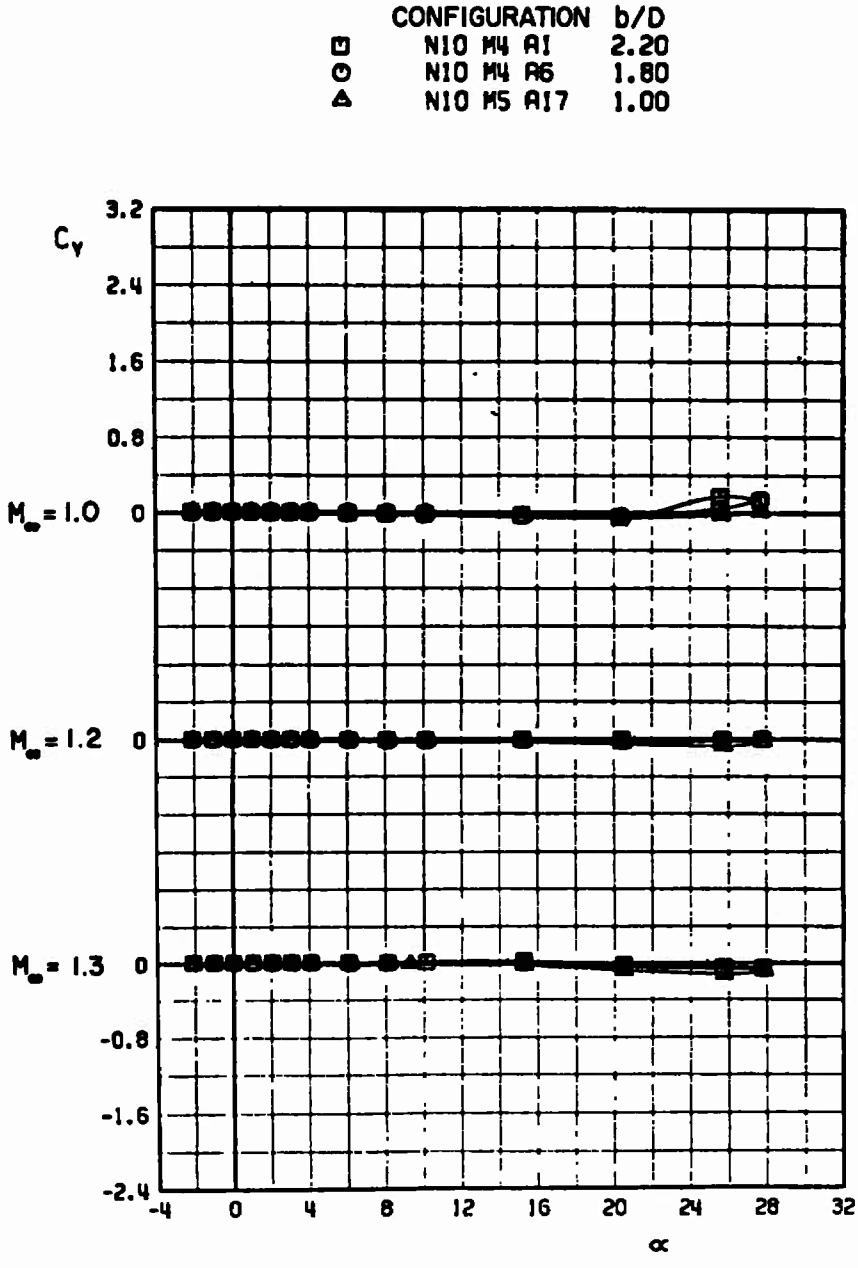

e. Concluded
Fig. 11 Continued

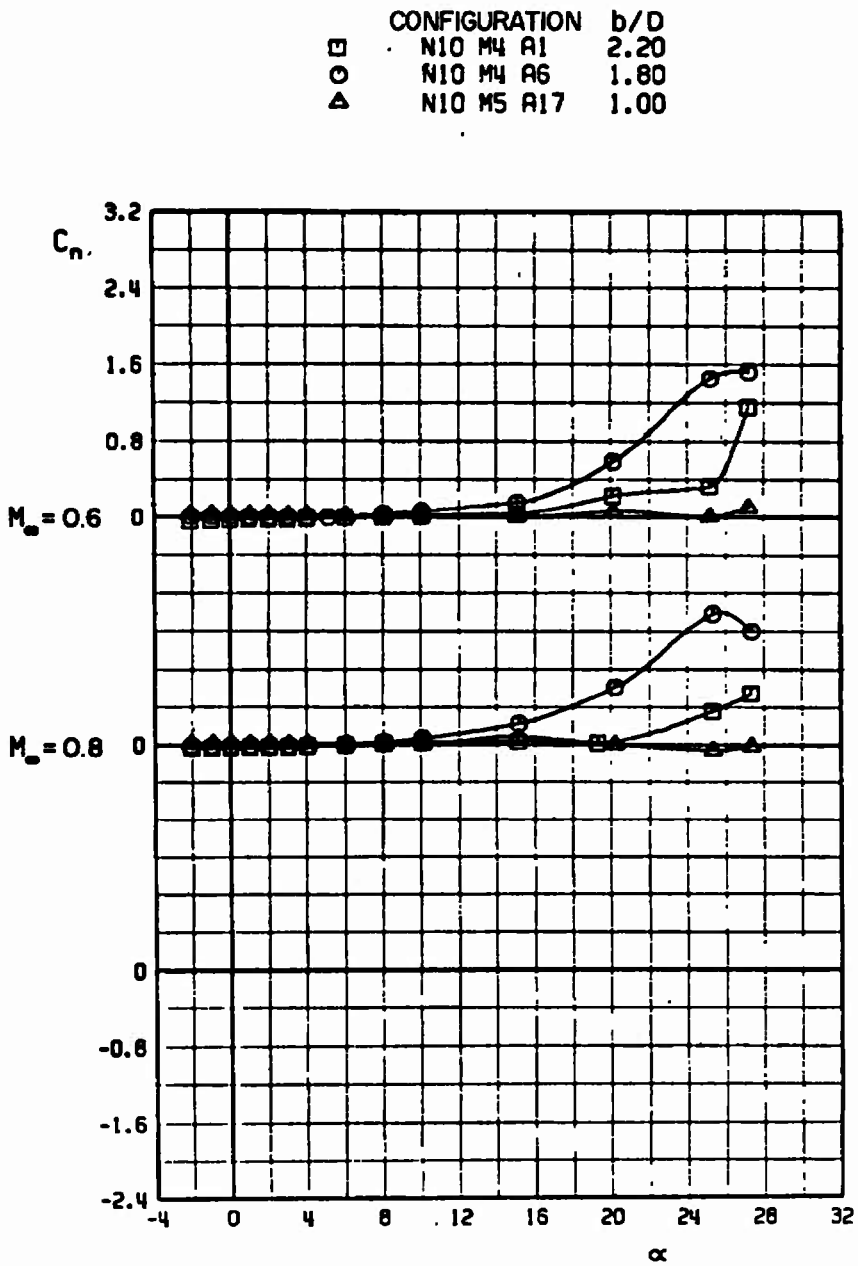

f. C_n versus α

Fig. 11 Continued

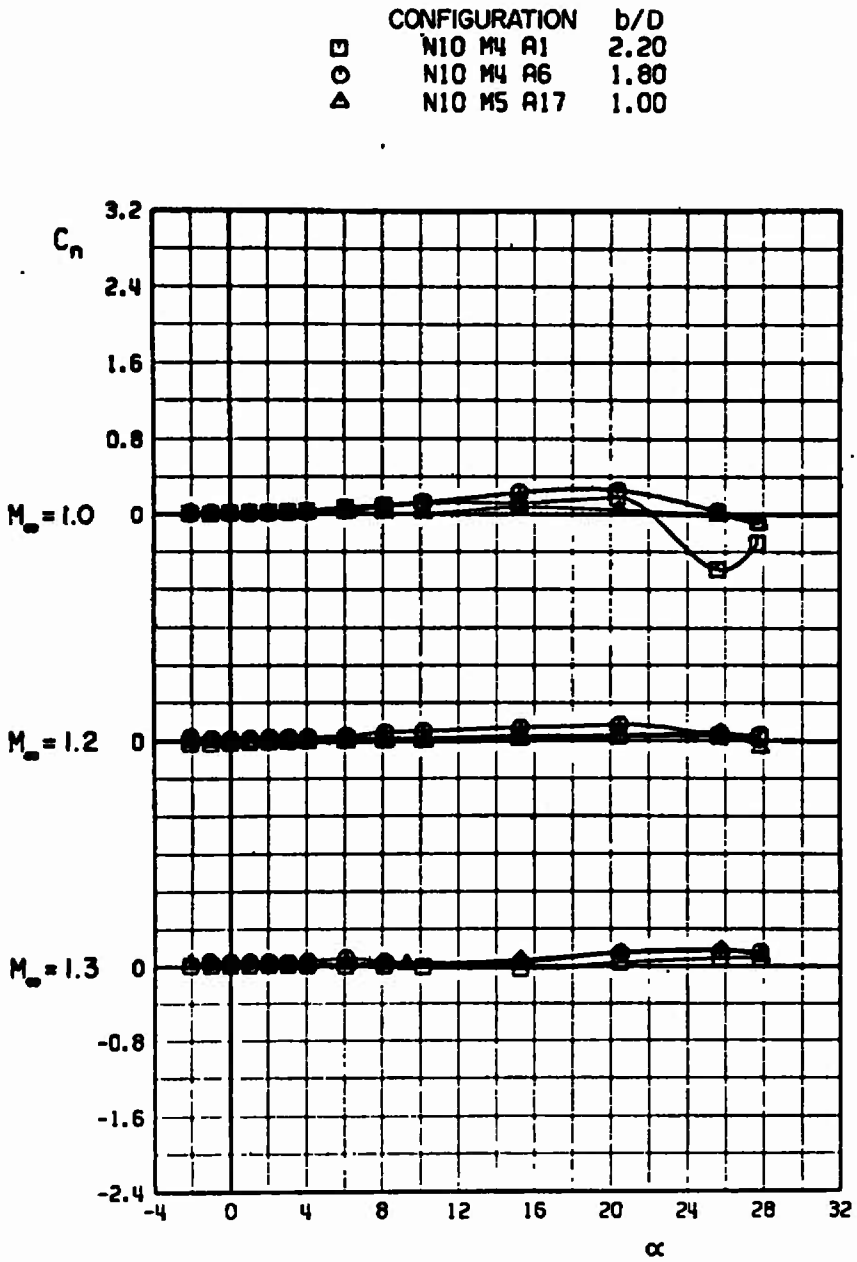

f. Concluded
Fig. 11 Continued

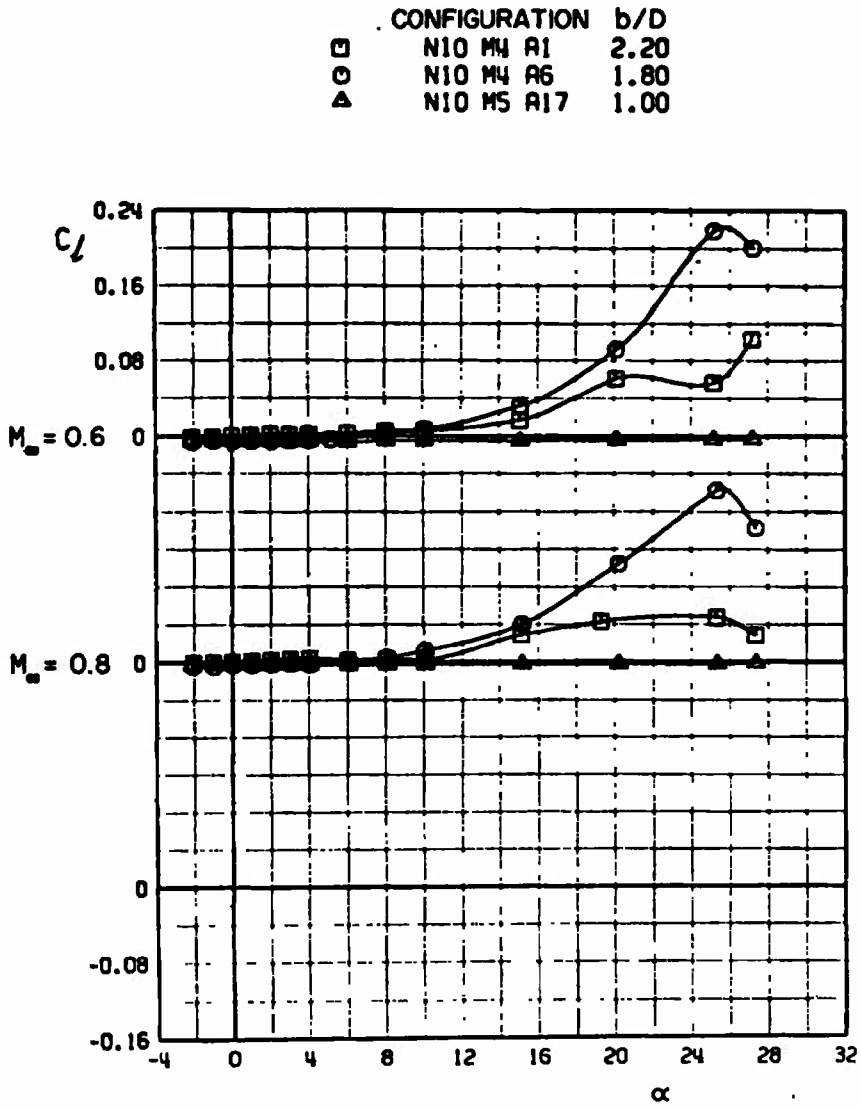

g. C_ℓ versus α

Fig. 11 Continued

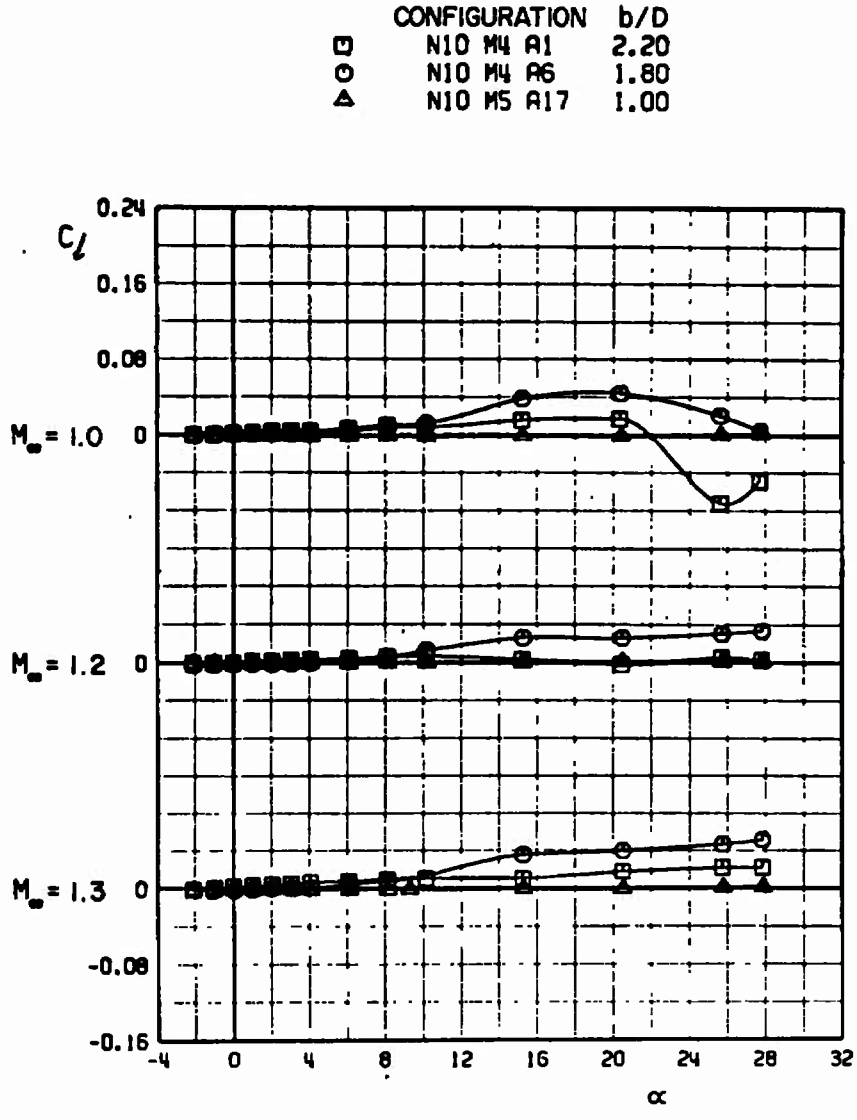

g. Concluded

Fig. 11 Concluded

UNCLASSIFIED

Security Classification

DOCUMENT CONTROL DATA - R & D

(Security classification of title, body of abstract and indexing annotation must be entered when the overall report is classified)

1. ORIGINATING ACTIVITY *(Corporate author)*
Arnold Engineering Development Center
Arnold Air Force Station, Tennessee 37389

2a. REPORT SECURITY CLASSIFICATION
UNCLASSIFIED

2b. GROUP
N/A

3. REPORT TITLE
WIND TUNNEL INVESTIGATION OF THE TRANSONIC STATIC STABILITY CHARACTERISTICS OF A BLUFF BODY SHAPE WITH VARIOUS AFTERBODY-STABILIZER CONFIGURATIONS

4. DESCRIPTIVE NOTES *(Type of report and inclusive dates)*
Final Report - February 16 to 17, 1972

5. AUTHOR(S) *(First name, middle initial, last name)*
G. R. Gomillion, ARO, Inc.

6. REPORT DATE	7a. TOTAL NO. OF PAGES	7b. NO. OF REFS
May 1972	99	4

8a. CONTRACT OR GRANT NO.	9a. ORIGINATOR'S REPORT NUMBER(S)
b. PROJECT NO.	AEDC-TR-72-68 AFATL-TR-72-85
c. Program Element 63601F	9b. OTHER REPORT NO(S) *(Any other numbers that may be assigned this report)*
d. System 670A	ARO-PWT-TR-72-41

10. DISTRIBUTION STATEMENT Distribution limited to U.S. Government agencies only; this report contains information on test and evaluation of military hardware; May 1972; other requests for this document must be referred to Air Force Armament Laboratory(DLGC), Eglin AFB, FL 32542.

11. SUPPLEMENTARY NOTES	12. SPONSORING MILITARY ACTIVITY
Available in DDC.	Air Force Armament Laboratory (DLGC), Eglin AFB, FL 32542

13. ABSTRACT

An investigation was conducted in the Aerodynamic Wind Tunnel (4T) to obtain the static stability characteristics of a bluff body shape with various afterbody-stabilizer configurations. Data are presented for a Mach number range from 0.6 to 1.3 over an angle-of-attack range from -2 to 28 deg. For all configurations tested, it was found that the static margin was greatest for the configurations having the largest span swept and unswept blade-type fins.

Distribution limited to U.S. Government agencies only; this report contains information on test and evaluation of military hardware; May 1972; other requests for this document must be referred to Air Force Armament Laboratory (DLGC), Eglin AFB, FL 32542.

DD FORM 1 NOV 65 1473

UNCLASSIFIED

Security Classification

14. KEY WORDS	LINK A		LINK B		LINK C	
	ROLE	WT	ROLE	WT	ROLE	WT
aircraft external stores						
missiles						
tail assemblies						
bluff body						
static stability						
transonic wind tunnels						